UNESP - Universidade Estadual Paulista
Instituto de Química - Araraquara
Departamento de Química Analítica, Físico-Química e Inorgânica

Doctorate Thesis

"Synthesis and optimization of a selective magnetic molecular imprinted polymer toward quantification of tetracycline in food samples"

Shakeel Zeb

Araraquara, February 2023

“Synthesis and optimization of a selective magnetic molecular imprinted polymer toward quantification of tetracycline in food samples”

Thesis submitted to the Chemistry Institute of the São Paulo State University "Júlio de Mesquita Filho" - Unesp, as part of the requirements for obtaining the title of Doctor in Chemistry

Adviser: Prof.ª Dr.ª Maria Del Pilar Taboada Sotomayor

Co-adviser: Dr. Sabir Khan

Araraquara, February de 2023

Shakeel Zeb

Zeb, Shakeel
Z41s Synthesis and optimization of a selective magnetic molecular imprinted polymer toward quantification of tetracycline in food samples / Shakeel-Zeb – Araraquara: [s.n.], 2023
134 p.: il.

Thesis (doctor) – Universidade Estadual Paulista, Instituto de Química
Advisor: Maria Del Pilar Taboada Sotomayor
Co-adviser: Sabir Khan

1. Nanoparticles. 2. Printed polymers. 3. Electrochemistry. 4. Tetracycline. 5. Biomimetic materials. I. Title.

Sistema de geração automática de fichas catalográficas da Unesp. Biblioteca do Instituto de Química, Araraquara. Dados fornecidos pelo autor(a).

Essa ficha não pode ser modificada

UNIVERSIDADE ESTADUAL PAULISTA

Câmpus de Araraquara

CERTIFICADO DE APROVAÇÃO

TÍTULO DA TESE: "Synthesis and optimization of a selective magnetic molecular imprinted polymer toward quantification of tetracycline in food samples"

AUTOR: SHAKEEL ZEB
ORIENTADORA: MARIA DEL PILAR TABOADA SOTOMAYOR
COORIENTADOR: SABIR KHAN

Aprovado como parte das exigências para obtenção do Título de Doutor em Química, pela Comissão Examinadora:

gov.br Documento assinado digitalmente
MARIA DEL PILAR TABOADA SOTOMAYOR
Data: 15/02/2023 12:24:56-0300
Verifique em https://verificador.iti.br

Prof.ª Dr.ª MARIA DEL PILAR TABOADA SOTOMAYOR (Participaçao Virtual)
Departamento de Quimica Analitica, Fisico-Quimica e Inorganica / Instituto de Quimica - UNESP - Araraquara

Prof. Dr. SAJJAD HUSSAIN (Participaçao Virtual)
Faculty of Materials and Chemical Engineering / Ghulam Ishaq Khan - GIK - Paquistão

Profa. Dra. SAIMA GUL (Participaçao Virtual)
Department of Chemistry / Islamia College Peshawar - ICP - Paquistão

Prof. Dr. MARCOS VINICIUS FOGUEL (Participaçao Virtual)
Departamento de Química Fundamental / Centro de Ciências Exatas e da Natureza - UFPE - Recife

Prof.ª Dr.ª JULIANA FERREIRA DE BRITO (Participaçao Virtual)
Departamento de Química Analítica, Físico-Química e Inorgânica / Instituto de Quimica - UNESP - Araraquara

Araraquara, 13 de fevereiro de 2023

I dedicate it to my father **Aurangzeb Khan** and my mother **Balqees Zeb**, and also to all my family and friends who supported me during these years. And to my advisors and teachers who guided me on this journey.

ACKNOWLEDGEMENTS

I owe a great debt of gratitude to **God**, who has put me in this position and given me the strength to continue forward.

To my father, **Aurangzeb Khan**, for all of the support and affection throughout the years of study and throughout every single day of my existence, including the challenging times. Dedicated to my mother, **Balqees Zeb**, for instilling in me the value of persistence and hard work in the pursuit of one's dreams. Sincere gratitude to my siblings, **Waqas Zeb**, **Awais Zeb**, and **Kalsoom Zeb**, for their encouragement and assistance in my pursuit of higher education.

Gratitude to my brother-in-law **Arshad Khan** and the rest of my family for all their help and encouragement on this journey. **Iqtidar Ahmed** my cousin, gave me good times and companionship.

Thank you to my mentor, Professor **Dr. Maria del Pilar Taboada Sotomayor**, for everything you've taught me, advised me on, helped me get, and been patient with me throughout the years. Because without our teachers, we would not be who we are today.

Thank you to my co-advisor, **Dr. Sabir Khan**, for the time and effort he put into helping me succeed academically and professionally. For the good and the bad times, for the companionship and the help.

I would like to thank my master's supervisor Prof. **Dr. Sajjad Hussain** for his encouragement and guidance in my Ph.D. I have been very lucky to have such a great mentor who cares a lot about my future career.

Thank you to my research friend Dr. **Ademar Wong** for his scientific guidance throughout this Project, and to **Bianca** for her HPLC analysis.

To members and friends of GEAr for friendship, collaboration, discussions, and relaxation. Especially: **Neres**, **Bianca, Douglas**, **Gilberto**, and **Javier**. Thank you to everyone who works at the Instituto de Química, especially those in the Analytical Chemistry department, the library, and the Undergraduate and Graduate Technical Section.

Finally, thanks to **CAPES** for the financial support and to the **UNESP Institute of Chemistry, Araraquara** for the infrastructure, for the studies, and knowledge, for the experience acquired, and for the welcome during these years. And to all those who contributed directly or indirectly to the realization of my work. This study was financed in part by the Coordenação de Aperfeiçoamento de Pessoal de Nível Superior - Brasil (CAPES)- Finance Code 001"

Abstract

Tetracycline is an exceptionally important antibiotic that is frequently utilized for the treatment of bacterial disorders and respiratory conditions in both humans and animals. Both the prevention of bacterial infections and the treatment of advanced stages of bacterial growth are common applications for this antibiotic in the poultry farming industry. In order to detect tetracycline antibiotics in food samples, magnetic molecularly imprinted polymers (mag-MIP) were synthesized and tested in this work. High-performance liquid chromatography (HPLC), and fluorescence spectroscopy analysis were applied to investigate the adsorption experiments. Moreover, the tetracycline antibiotic was identified using an alternate electrochemical sensor technique. In order to make magnetic nanoparticles, iron salts like $FeCl_3.6H_2O$ and $FeCl_2.4H_2O$ were used; they were then modified using methacryloxypropyltrimethoxysilane (MPS). Initially, part of the research was based on HPLC and Spectro-fluorometer analysis: Magnetic nanoparticles, methacrylic acid (functional monomer), ethylene-glycol-dimethacrylate (cross-linker), and benzoyl peroxide (radical initiator) were all used in calculated proportions to synthesize the mag-imprinted polymer. In the second segment, which deals with electrochemical investigation, the mag-imprinted polymer was prepared by mixing the appropriate amount of magnetic nanoparticles, acrylic acid (functional monomer), ethylene-glycol-dimethacrylate (cross-linker), and 2,2 azo-*bis*-isobutyronitrile (radical initiator). The techniques of field emission scanning electron microscopy (FESEM), high-resolution transmission electron microscopy (HRTEM), and Fourier transform infrared (FTIR) were utilized in order to explore the morphological, and chemical characteristics of synthesized materials. The analytical curve was produced using the range from 1.0×10^{-5} mol L^{-1} to 8.0×10^{-5} mol L^{-1}. The adsorption capacity of mag-MIP at equilibrium was 4.123 mg g^{-1} and adsorption process followed the Langmuir isotherm, and Temkin model and pseudo-2nd-order reaction kinetic. The proposed mag-polymer materials were applying in food samples using two different concentrations of tetracycline (1.7×10^{-5} and 2.5×10^{-5} mol L^{-1}) obtaining recoveries ranging from 73.2-87.3% (HPLC) and 90.53–103.7% (Spectro-fluorometer), respectively. In electrochemical sensor: Tetracycline detection was carried out under optimal conditions utilizing square wave voltammetry, 15 mg of mag-MIP (on carbon paste), and the time is 80 seconds. Using this method, well-defined peaks ranging from 0.5 to 1.0 V vs. Ag/AgCl (KCl_{sat}) were produced. Analytical curves were constructed using the second peak at 0.83 V, yielding the following results: linear range of 5.0×10^{-7} to 4.0×10^{-5} mol L^{-1} (R^2 of 0.9993), the limit of detection (LOD) of 1.5×10^{-7} µmol L^{-1}, and repeatability of 2.82%. The results of the selectivity analysis showed that the suggested electrochemical sensor is highly efficient for tetracycline determination. The sensor was effectively used to identify tetracycline in commercial and raw milk samples, with recovery rates ranging from 93 to 103%.

Keywords: Magnetic nanoparticles (mag-NPs), molecularly imprinted polymers (MIPs), biomimetic sensor, electrochemical sensor, tetracycline.

Resumo

A tetraciclina é um antibiótico excepcionalmente importante que é frequentemente utilizado para o tratamento de distúrbios bacterianos e condições respiratórias em humanos e animais. Tanto a prevenção de infecções bacterianas quanto o tratamento de estágios avançados de crescimento bacteriano são aplicações comuns desse antibiótico na indústria avícola. Para detectar antibióticos tetraciclinas em amostras de alimentos, polímeros magnéticos de impressão molecular (mag-MIP) foram sintetizados e testados neste trabalho. Cromatografia líquida de alta eficiência (HPLC) e análise de espectroscopia de fluorescência foram aplicadas para investigar os experimentos de adsorção. Além disso, o antibiótico tetraciclina foi identificado usando uma técnica de sensor eletroquímico alternativo. Para fazer nanopartículas magnéticas, foram utilizados sais de ferro como $FeCl_3.6H_2O$ e $FeCl_2.4H_2O$; eles foram então modificados usando metacriloxipropiltrimetoxisilano (MPS). Inicialmente, parte da pesquisa foi baseada em HPLC e análise de espectrofluorímetro: nanopartículas magnéticas, ácido metacrílico (monômero funcional), etileno-glicol-dimetacrilato (reticulador) e peróxido de benzoíla (iniciador radical) foram todos usados em proporções calculadas para sintetizar o polímero impresso em mag. No segundo segmento, que trata da investigação eletroquímica, o polímero impresso em mag foi preparado misturando a quantidade apropriada de nanopartículas magnéticas, ácido acrílico (monômero funcional), etileno-glicol-dimetacrilato (reticulador) e 2,2 azo-*bis*-isobutironitrila (iniciador radical). As técnicas de microscopia eletrônica de varredura de emissão de campo (FESEM), microscopia eletrônica de transmissão de alta resolução (HRTEM) e infravermelho por transformada de Fourier (FTIR) foram utilizadas para explorar as características morfológicas e químicas dos materiais sintetizados. A curva analítica foi produzida utilizando o intervalo de $1,0 \times 10^{-5}$ mol L^{-1} a $8,0 \times 10^{-5}$ mol L^{-1}. A capacidade de adsorção do mag-MIP no equilíbrio foi de 4,123 mg g^{-1} e o processo de adsorção seguiu o modelo de isoterma de Langmuir e Temkin cinética de reação de pseudo-2ª ordem. Os materiais mag-polímeros propostos foram aplicados em amostras de alimentos usando duas concentrações diferentes de tetraciclina ($1,7 \times 10^{-5}$ e $2,5 \times 10^{-5}$ mol L^{-1}) obtendo recuperações variando de 73,2-87,3% (HPLC) e 90,53-103,17% (Espectrofluorímetro), respectivamente. No sensor eletroquímico: A detecção de tetraciclina foi realizada em condições ideais utilizando voltametria de onda quadrada, 15 mg de mag-MIP (em pasta de carbono) e o tempo é de 80 segundos. Usando este método, picos bem definidos variando de 0,5 a 1,0 V vs. Ag/AgCl (KCl_{sat}) foram produzidos. As curvas analíticas foram construídas usando o segundo pico em 0,83 V, produzindo os seguintes resultados: faixa linear de $5,0 \times 10^{-7}$ a $4,0 \times 10^{-5}$ mol L^{-1} (R^2 de 0,9993), o limite de detecção (LOD) de $1,5 \times 10^{-7}$ mol L^{-1} e repetibilidade de 2,82%. Os resultados da análise de seletividade mostraram que o sensor eletroquímico sugerido é altamente eficiente para determinação de tetraciclina. O sensor foi efetivamente utilizado para identificar tetraciclina em amostras de leite comercial e cru, com taxas de recuperação variando de 93 a 103%.

Palavras-chave: Nanopartículas magnéticas (mag-NPs), polímeros molecularmente impressos (MIPs), sensor biomimético, sensor eletroquímico, tetraciclina.s

List of Figures

List of Tables

Table of Contents

CURRICULUM VITAE

Name: Shakeel Zeb

Date of Birth: 06-04-1992

RNE: F009990-V

CPF: 241-908-888-80

Nationality: Pakistani

Present Adress: Av: Luiz de Camões, 142 – Fundos, Bairro Quitandinha, Araraquara-SP

Email: shakeelzeb41785@gmail.com

Academic formation:

M.Phil. (Chemistry), Hazara University Manshera, Pakistan (2017).

B. Science (Honours) Chemistry, Hazara University Manshera, Pakistan (2015).

Publications of articles:

[1] S. Zeb, Electrochemical Oxidation of Acid Brown 98 using Ti/Ru0.3Ti0.7O2 Composite Anode, Int. J. Electrochem. Sci. (2018) 9428–9440. https://doi.org/10.20964/2018.10.06.

[2] S. Zeb, N. Ali, Z. Ali, M. Bilal, B. Adalat, S. Hussain, S. Gul, F. Ali, R. Ahmad, S. Khan, H.M.N. Iqbal, Silica-based nanomaterials as designer adsorbents to mitigate emerging organic contaminants from water matrices, J. Water Process Eng. 38 (2020) 101675. https://doi.org/10.1016/j.jwpe.2020.101675.

[3] S. Hussain, H. Khan, N. Khan, S. Gul, F. Wahab, K.I. Khan, S. Zeb, S. Khan, A. Baddouh, S. Mehdi, A.F. Maldonado, M. Campos, Process modeling toward higher degradation and minimum energy consumption of an electrochemical decontamination of food dye wastewater, Environ. Technol. Innov. 22 (2021) 101509. https://doi.org/10.1016/j.eti.2021.101509.

[4] I. Ahmad, I. Shahid, A. Ali, S. Zeb, L. Gao, J. Cai, The van der Waals CdO/PtS 2 heterostructures for photocatalytic water splitting with excellent carrier separation and light absorption, New J. Chem. 45 (2021) 17699–17708. https://doi.org/10.1039/D1NJ03232A.

[5] S. Zeb, A. Wong, S. Khan, S. Hussain, M.D.P.T. Sotomayor, Using magnetic nanoparticles/MIP-based electrochemical sensor for quantification of tetracycline in milk samples, J. Electroanal. Chem. 900 (2021) 115713. https://doi.org/10.1016/j.jelechem.2021.115713.

[6] S. Zeb, J.E.L. Villa, A. Wong, S. Khan, S. Hussain, M.D.P.T. Sotomayor, Combining fluorescent quantum dots with molecularly imprinted polymers for the screening of both emerging and classical environmental pollutants: a review", Journal of the Brazilian

Chemical Society, Accepted in December 2022 (ID JBCHS-2022-0228).

Book Chapter Publications

[1] B. Mortari, S. Zeb, R.R. Pupin, S. Khan, A. Wong, M.D.P.T. Sotomayor, Molecularly imprinted polymer composites as sensor, in: Mol. Imprinted Polym. Compos., Elsevier, 2021: pp. 227–265. https://doi.org/10.1016/B978-0-12-819952-7.00012-3.

[2] S. Khan, S. Zeb, J. Vega-Chacón, S.E. Torres, S.Q. Martínez, R. López, I.M.M. Mejía, C.R.J. Hernández, J.L. Vila, E.J. Cornejo, C.P. Aquino, B. Mortari, L.F.T. Borges, G.A. Ruiz-Córdova, F.L.R. Carhuas, M.D.P.T. Sotomayor, G. Picasso, Non-toxic nature of nano-biosorbents as a positive approach toward green environment, in: Nano-Biosorbents Decontam. Water, Air, Soil Pollut., Elsevier, 2022: pp. 187–226. https://doi.org/10.1016/B978-0-323-90912-9.00009-5.

Most recent works presented at scientific conferences

Poster Presentation: III Workshop INCT DATREM

Shakeel Zeb, Sabir Khan, Ademar Wong e Maria Del Pilar Taboada Sotomayor. “Construction and Development of a Biomimetic Sensor towards Tetracycline Quantification”

Teaching Internship:

Supervisora: Drª. Prof.ª Drª. Mirian Cristina dos Santos

UNESP - Universidade Estadual Paulista, Araraquara/SP

Curso: Química Analítica Qualitativa:

Período: 2º semestre de 2022

Chapter 1

1. Introduction

Due to the rising global population, the demand for poultry, eggs, and related goods has skyrocketed, making the poultry business one of the most successful in the world[1-2]. The rapid rate of expansion has led to a number of environmental problems, including contamination of the water and soil [3-4]. Antibiotics are used on a global scale at a rate of around 100,000 to 200,000 tons per year[5] . Antibiotics developed specifically for use in veterinary medicine are frequently prescribed to animals in order to prevent and cure illness. Livestock farming is one of the most common applications for these pharmaceuticals, as farmers frequently utilize them to enhance and keep their businesses profitable. A growing number of countries are turning to antibiotics for use in cattle agriculture[6].

Due to its rich micro- and macronutrient composition, animal milk is an excellent source of nourishment for new-born, children, and adults. Milk is an excellent source of several essential nutrients, including those listed below: calcium, magnesium, selenium, riboflavin, zinc, and vitamin B12[7]. Milk fat is the most complicated type of all naturally occurring fats since it contains roughly 400 distinct kinds of fatty acids and is the most complex form of fat overall[8].

An ever-increasing population means there will be greater demand for milk and other dairy products, putting more on producers to keep their bulk quantities of these goods at a consistently high standard. For example, a wide variety of medications are often given to all female dairy cattle (cows, buffalo, goats, and sheep) in order to maximize the amount of milk that may be produced by each animal. As a result, ruminants are vulnerable to contamination from a wide range of human-made sources, and it's probable that some of these toxins make

their way into the animals' milk. Therefore, the scope of this investigation is limited to identifying the presence of the antibiotic tetracycline in foods associated with agricultural production.

1.2. Antibiotics

Chemical substances that are utilized against bacterial illnesses, stop or avoid the development of bacteria in a living life form and upgrade the life quality are known as antibiotics. The first evidence about antibiotics has been found in the literature about the accidental utilization of antibiotics in alternate medicines, Salvarsan drug or Organoarsenic compound was first introduced at the beginning of 1910, and was used to treat syphilis[9]. In 1928, Alexander Fleming, was the first scientist to introduce penicillin antibiotics[10]. This discovery leads him to earn the noble price in 1945, and helped to fabricate a vital antibiotic to have saved the lives of living organisms. Onward 1945, was the golden era to recognize the various sort of antibiotics. Latterly, teixobactin was introduced which may be a modern class of antibiotics using a culture-free method[11]. Due to the current decline in novel antibiotic discoveries, culture-free detection promises future discoveries.

Old evidence has been found in the reported literature that people of old civilizations utilized different natural items comprising herbs, honey, and animal excrement for the cure of viral diseases[12]. Rotten bread applied topically was a popular remedy in ancient Egypt, China, Serbia, Greece, and Rome. Indeed a few more-modern antibiotics may have been presented in old times. The tetracycline have been recognized in human skeletons at times of digging in the Nubia region and during the Roman occupation of Egypt[13].

The initiation of antibiotics into clinical use changed into likely the maximum noteworthy clinical strength of the twentieth (20^{th}) century[14]. Antibiotics created several medical strategies possible as well as cancer treatment, organ transplants, and open-heart

surgery. The skipping of proper doses of antibiotics causes rapid antimicrobial resistance as result the infection would be rise[15]. In light of the potential risks of a post-antibiotic era, lawmakers have pledged to provide additional allowance funding, which is becoming increasingly crucial to the continued development and research of antibiotics. The official of the UK government detailed that without urgent action 10 million individuals will die from medicating resistance disease by 2050 [16]. The great desire for growing a brand new technology of anti-infective drugs is to find out new microbial herbal products due to the fact those compounds are unrivalled in their chemical range and efficiency as antibiotics. Clinically utilized antibiotics their classes and sources **(Table.1)** [17].

Table 1 Antibiotics their class, discovery date, and examples.

S.Nº	Class	Discovery	Examples
1	Actinomycetes	1944	Kanamycin A
2	Tetracyclines	1948	Tetracycline
3	Amphenicols	1947	Chloramphenicol
4	Macrolides	1952	Erythromycin
5	Tuberactinomycins	1951	Viomycin
6	Lincosamides	1962	Clindamycin Protein Semi-synthetic derivative of lincomycin
7	Ansamycins	1959	Rifamycin SV Semi-synthetic derivative of rifamycin
8	Cycloserines	1955	Seromycin
9	Streptogramins	1953	Pristinamycin
10	Phosphonates	1969	Fosfomycin
11	Carbapenems	1979	Meropenem Synthetic molecule based on thienamycin
12	Lipopeptides	1987	Daptomycin
13	Lipiarmycins	1975	Fidaxomicin

Source: (Antibiotics: past, present and future. **Curr. Opin. Microbiol. 51**, 72–80 (2019)), No need permission because open access

1.3. Role of pharma industries in emerging environmental challenges

Within the rising era, pharmaceutical and chemical industries become a serious environmental challenge[18]. As of now, one of the foremost noteworthy environmental concerns is declining the quality of freshwater. Pharmaceutical items are utilized to make strides in the resistance quality of human health against various infections, due to which their life quality is upgraded. During the manufacturing process, the pharmaceutical industries discharge high concentrated antibiotics wastewater into the environment, contaminating the water[19]. The reported literature demonstrates, that pharmaceutical wastewater treatment plant (WWTP) from the pharmaceutical industry isn't satisfactorily successful sufficient to eliminate traces of antibiotics from wastewater[20]. The mismanagement causes serious environmental pollution which leads to bringing serious infection in human and marine organisms[21].

Aside from water, antibiotics also are often observed in various environments, which include, soil and sludge[22], which will increase the spread and accelerate antibiotic resistance growth with inside the environment, this leads to increase risk in human life[23]. Subsequently, it should be imperative to treat profoundly concentrated antibiotics wastewater before the release. Worldwide, the use of antibiotics has increased over the past decade[24]. After being eaten by animals and humans, most antibiotics are only incompletely metabolized, providing that 25% –75% of antibiotics may be excreted unchanged from the body after use[25-26]. Antibiotics have been studied extensively, and many reports have been published on their effects[27-28].

The foremost causes for the bacteria resistance growth are injudicious and unselective to employ antibiotics in ecosystems. The extensive usage of antibiotics in human beings and animals has been shown to surge antibiotic resistance[29-30]. The sharing of the same surroundings, the extensive usage of antibiotics for poultry, also leads to the growth of antibiotic resistance, which may influence humans as well. This is often since; antibiotic

resistance is the connection between animals and humans within the common environment. Consequently, the bacteria that was resisted from antibiotics could be grown and extended from animals to the surroundings[31]. Thousand tons of pharmaceutical items might be getting used around the world each year. Presently, highly concentrated antibiotics have been found in wastewater[32-33]. Even less concentrated antibiotics are biologically active, cause severe damage to vital organs of living organisms in the ecosystem, lead to extend the resistance among natural populations of bacteria and hence, generate a negative impact on living health[34]. Antibiotics in drinking water lead to trigger the allergic problem in living organisms [35]. The antibiotic that is contained in wastewater contributes to the development of antibiotic resistance as well as the proliferation of superbugs[36]. Antibiotics can also affect aquatic organisms such as plants, animals, and microorganisms. The growth of green alga in freshwater may be the effect due to the member of the antibiotics class named chlortetracycline[37]. The quantity of antibiotics in the ecological community is frequently little. In natural surroundings, the small concentrations of antibiotics are substantial for the maintenance and improvement of resistance in bacterial populations[38]. Present-day medication has done awesome work in accomplishing antibiotics against the sickness that resulted from bacteria.

In any case, when it is truly required, the bacteria are getting to be less responsive and resistant to antibiotic treatment[39-40]. Antibiotic resistance is the ability of bacteria to grow resistant to a specific antibiotic to which they were once sensitive [41,42,43]. The rise of resistant antibiotics to bacteria is the key subject in community health is the infections instigated by resisted bacteria have become hard and expensive for treatment [44,45,46,47]. Since the seriousness of the issue, it has gotten to be a worldwide concern, as marked by WHO “Antimicrobial resistance” the World Health Day subject in 2011.

1.3.1. Structure and mechanism of action of tetracycline

In 1945, Benjamin Duggar exposed the world to aureomycin (chlortetracycline), the first member of the tetracycline group, and a byproduct of the natural fermentation of Streptomyces aureofaciens bacteria. Just two years later, in 1948, terramycin (oxytetracycline) was introduced as the second member of this class of antibiotics, the product of streptomyces. In 1953, scientists revealed the discovery of the antibiotic tetracycline and its simple structure.The tetracycline antibiotic was synthesized through a biological process. Many members of the tetracycline family were synthesized artificially and naturally during the duration from 1950 to 1970. During this period tetracycline was used as a common antibiotic in the United States of America Tetracycline product consists of broad-spectrum antibiotics. Tetracycline consists of four rings which are attached with many groups like alkyl, hydroxyl, and amine. An upper and a lower periphery can be found in the structure of tetracyclines, several different kinds of functional groups can be found in these regions. When changes are made to the top part of the tetracycline's periphery, its properties as an attacker on biological targets are bolstered, while when changes are made to the lower part, the antibiotic and non-antibiotic nature of the drug are reduced. The spectrum and action mechanism of tetracycline derivatives are consistent. It is crucially essential for pharmacological action that these compounds retain the full configuration of the natural carbon atom (C-4). The amide group at carbon 2 is responsible for tetracycline's biological activity, while the lack of methyl groups and hydroxyl at carbon 6 increases the drug's enzyme inhibitory power. Antibiotics, whether taken orally or intravenously, spend most of their time in the stomach and first portion of the small intestine. Antibiotics in the tetracycline family, for example, are poorly metabolized (less than 20% of the prescribed dose is eliminated in the urine), and the remaining 80% or so are eliminated basically unaltered in the stool. The section about tetracycline antibiotics was adapted with material from reference[48]. All these descriptions are shown in **Figure 1**[48]**.**

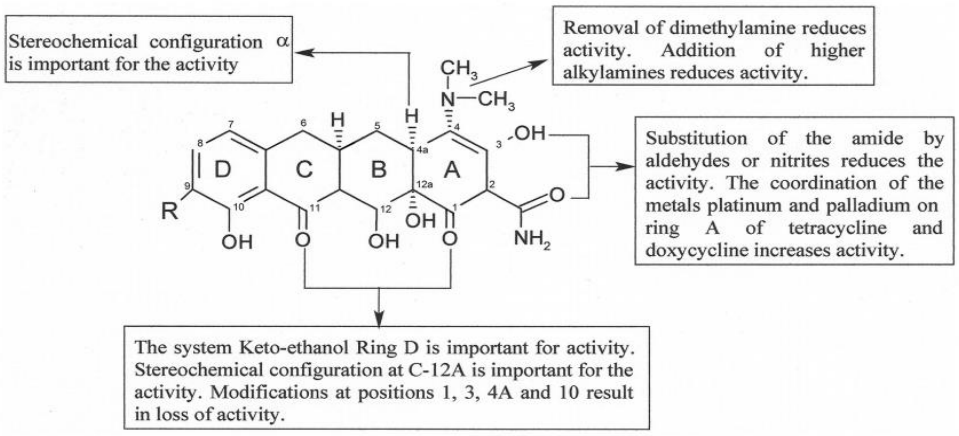

Figure 1. Relationship between structure and activity of the molecule of Tetracycline[48]. Source no need permission because of open Access

1.3.2. Techniques for identifying the harmful antibiotics

It is now very necessary to define and evaluate the dangerous contaminants that may be found in the environment, food products, wastewater and biological samples. Antibiotic identification in samples has been achieved by a number of different analytical approaches[49,50,51]. Toxic compound identification in a wide variety of samples has been accomplished using a number of alternative methods[52,53]. However, traditional methods have drawbacks such as expensive, requiring a particularly trained person, limited sensitivity, and most of them being utilized only in laboratory circumstances[54]. In recent years, there has been an increase in the use of alternative methods such as nano-sensors for the detection of effluents as a means of compensating for the drawbacks of conventional technologies. The benefits of this method include high selectivity and high specificity, as well as low cost, and convenience of use[55]. The term "nano-sensor" refers to a sensing device that collects data at the nanoscale, often having at least one dimension of 100 nm. The study of the physicochemical properties of materials at the nanoscale, which are often distinct from the characteristics of the substance in its bulk form, is what is referred to as nanotechnology. These remarkable properties of nano-

sensors may be enhanced in contrast to those of traditionally constructed sensors with just fewer sensing components[56]. As a consequence of this, nano-sensors are not necessarily tiny enough to detect and measure reaction occurring at the nanoscale; rather, they may be bigger devices that make use of the characteristics of nanomaterials in order to detect and measure events occurring at the nanoscale.

1.4. Electrochemical Sensors

Electrochemical sensor is considered to be a powerful recognition technique in analytical chemistry, because of their high accuracy, precision, sensitivity, and as well as low-cost for their arrangement as compared with other analytical instrumental methods[57]. An electrochemical sensor may be defined as, a fabricated device that provides information (signal) about any chemical species which is present in its surrounding[58]. A transducer is the unified part of the sensor which is used to detect the physical quantity (concentration of analyte) and translate it into useful analytical signals. Additionally, transducers are based on two types such as, passive and self-generating transducer, passive required outside power source to function, and self-generating doesn't require any external power source. **Figure 2,** shows the general representation of an electrochemical sensor. The electrochemical sensor has a foremost position between at the moment existing sensors, also has a huge range of applications in the field of clinical, environmental, and agriculture. An electrochemical sensor is available in three types of sensors, for instance, potentiometric, amperometric, and conductometric. Potentiometric sensor, which detects the electrical potential of an electrode as results provide useful information about a component (analyte) in gas or solution. An amperometric sensor is a device that works on the phenomena of oxidation and reduction, as a result, a current is

measured and changed into useful analytical signals. On the other hand, conductometric sensor measures conductivity at a range of frequencies[58].

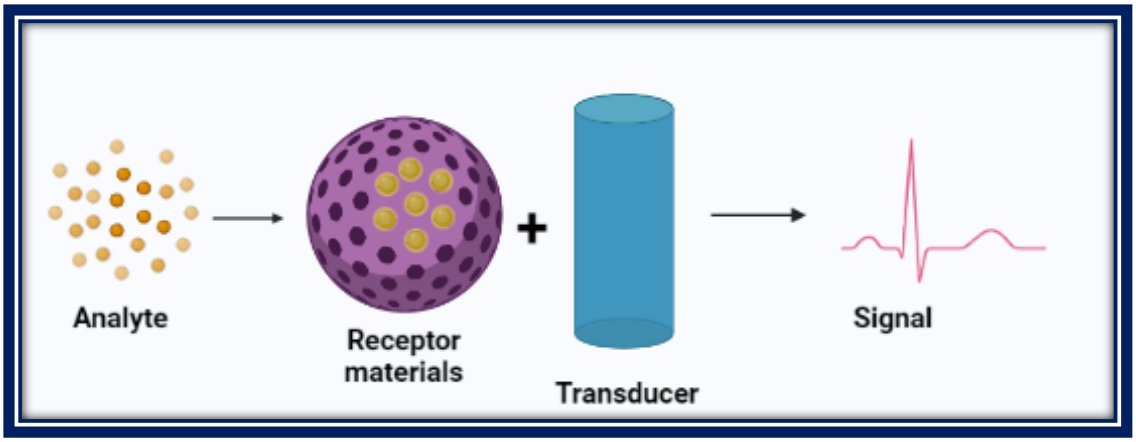

Figure 2. Graphically representation of an electrochemical sensor. Source: Author

Chemically modified electrodes are those with chemicals added to their surface[59-60]. Modification of electrodes with various sorts of materials and chemical enhance the physicochemical nature of electrodes, and, also increases the detection ability in the field of tracing compounds such as antibiotics, drugs, pesticides, heavy metals, and dyes [61]. The most interests to analytical applications comprise; the increasing speed of electron exchange responses, special accumulation, or selective membrane saturation, and interferent exclusion. These kinds of modifications are able to convey greater selectivity, tracing, stability, and reproducibility of an electrochemical sensor[62,63,64]. Several types of electrodes have to get the leading position in electroanalytical chemistry, most of them are carbon paste electrode, gold, platinum, glassy carbon, and diamond doped with born. Various immobilization methods are used to get the electrode modified, such as; adsorption, covalent binding, and occlusion[65-66].

In the adsorption immobilization method: To perform adsorption immobilization, the modifying agent is dissolved in a suitable solvent, and the electrode is then immersed in the solution for a predetermined amount of time. Graphite electrodes are more favourable for

adsorption immobilization such as pyrolytic and carbon paste. In any case, it presents the drawback of not being exceptionally strong due to desorption of the modifier that finds on the surface of the electrode. This reality winds up conceding the feedback of the sensor and its lifetime[65-66].

Immobilization by covalent bonding: manipulates the reactivity of the modifier agents containing functional groups and electrodes, as a result, modifier materials attach with substrate surface via covalent binding. Suitable substrates such as carbon and metal oxides have more ability to initiate a covalent bond with esters, ethers, amides, among other functional groups. The strategy for modification via covalent bond is exceptionally stable in comparison to other strategies, be that as it may, it needs more time to carry out [65-66].

Immobilization of polymeric films via occlusion: comprising of a coating of the electrode surface with conductive or penetrable polymeric films to the supporting electrolyte and the species of interest. The modification with membranes polymeric permits the immobilization of the active species on the modified surface, significantly magnifying the electrochemical response. In this way, polymers have been utilized in chemically modified electrodes and used in the construction of sensors to protect the surface of electrodes from impurities, block interferers, immobilize bio-components, incorporate mediators, and provide bio-compatibility[65-66]

Immobilization of composite materials via occlusion: when two or more than two materials are combined, as result, new material is established called composite, the properties of this material are unique from its original individual materials. The combination of organic-inorganic, inorganic-inorganic, and organic-organic materials generates a composite material or hybrid material. This method of modification has been highly appreciated in carbon paste electrodes, and graphite-epoxy electrodes, holding the paste together frequently applied the

inert binder like mineral oil [65-66]. **Figure 3.** displays the various types of immobilization techniques [67-68]

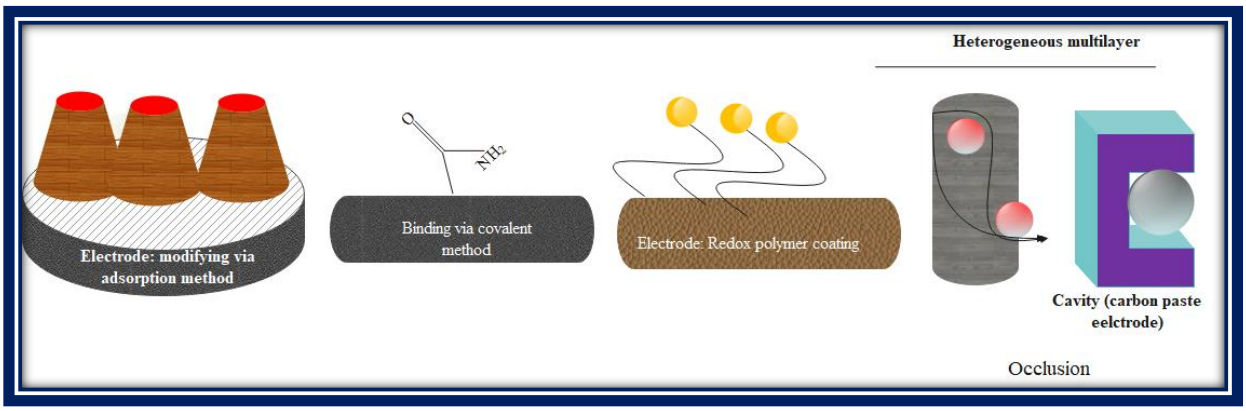

Figure 3. Graphically representation of modified electrodes using various methods. Source: Author

1.4.1. Electroanalytical sensor techniques

To quantify the interaction between chemical parameters and electrical variables like current, potential, or charge is the focus of electroanalytical sensors. The majority of the electrochemical devices that are used for monitoring systems fall into three categories. These categories are ultimately determined by the type of analyte being monitored, the nature of the sample matrix, and the degree of sensitivity and selectivity that is actually needed. In order to identify desire toxic compounds at low concentrations, the electrochemical method of differential pulse voltammetry (DPV) is used.

The DPV method includes superimposing an increasing potential ramp on a series of pulses of a constant amplitude applied to the electrode. The current is then monitored both before and after the pulse, which permits a reduction in capacitor current. When compared to the current measured using cyclic voltammetry, the capacitive current measured with DPV is thus noticeably lower. Differential pulse voltammetry was used by W. S. Fernandes-Junior et

al[69]. to explore the electrochemical behaviour of tetracycline using a nano-diamond and manioc starch biofilm-modified glassy carbon electrode.

Researchers working in the area of compound identification have shown a desire for employing analytical voltammetry techniques due to the superior efficiency, rapid response, and exceptional sensitivity of these approaches[70]. Cyclic voltammetry has been shown to be appropriate for screening analyte of interest in wastewater, in addition to its other features, which include simplicity of operation, excellent sensitivity (limited), and cheap operating costs. Screening wastewater for target analytes using cyclic voltammetry has also been demonstrated to be feasible [71]. Cyclic voltammetry was utilized by Guo et al[72]. to improve the detection efficiency of a glassy carbon electrode that had been treated with ionic liquid multi-carbon nanotubes. As a result, they were able to reach a detection limit of 30 nmol L^{-1}. The analytical efficacy of square wave voltammetry (SWV) has been shown to be superior to that of other voltammetric techniques in a number of reports that have been published in the scientific literature[73].

When compared to traditional voltammetric methods, SWV analysis takes less time and yields more accurate results in a shorter period of time. As a result, it's particularly applicable to identifying target molecules at extremely dilute concentrations, such as ppb (parts per billion) and ppt (parts per trillion). An analyte's electrochemical kinetics may be either slow or rapid, and this difference is readily apparent when using a pulse approach, which can effectively provide either good results with outstanding reproducibility and high stability or

negative results[73]. Considering these merits, we have agreed on this method for the screening of the target molecule.

1.4.2. Modification of electrodes

A) Carbon paste electrode

The interest of the primary portion of the project is the modified carbon paste electrode. Consequently, ought to have to talk about the procedures reasonably utilized for the modification of carbon paste. Two strategies were briefly discussed for the modification of carbon paste electrodes [74]. The use of conductive powder and liquid binders in the modification of carbon paste electrodes may affect the sensor signal. Two methods have been reported in the previous literature [74]. In the first strategy, the uses of conductive powder such as multi-wall carbon nanotubes, single-wall carbon nanotubes, graphene, and metal oxide nano-powders have been utilized[75,75,76,77]. This question comes to mind first, why can't all be graphite powder replaced with conductive materials such as multi-wall carbon? A large proportion of the nanomaterials have the ability to expend the result of the non-faradic current, and also lead the semiconductor behaviour of electroactive compounds which cause to reduce the signal of the sensor. So, it is important to optimize the ratio of graphite and other nanomaterials in the modification of carbon paste electrodes. To obtain modified working electrodes, the use of carbon paste electrodes with electrically active compounds is a rare choice. The electro-catalytic properties of the nanomaterials include, ferrocene and their derivatives, catechol derivatives, and inorganic complexes have the capability of improving the selective recognition of an electrochemical sensor. The literature reported getting the synthesis of this type of electrode is easy as compared to solid electrodes[78-79].

In the second strategy, an electrical active liquid binder is used as a modifier for the carbon paste electrodes. Normally, paraffin and nujol® oil are utilized as a binder to get the

carbon paste electrode, but it is not electrical active because of their aliphatic hydrocarbons chain. In the present time, most of the researchers utilized the conductive ionic liquid binder in the modification of the carbon paste electrodes [80, 81,82,83]. Because of its ionic structure and high viscosity got more attention, and also has high efficiency to enhance conductive behaviour in voltammetric studies. The room temperature, ionic liquids at a high level can insurance the electrode surface and interchange electrons of a redox system with the electro-active site of the electrode surface (carbon) will be rigid. It's important to optimize the ratio of conductive ionic liquid binder in the carbon paste electrode before getting the analysis. The carbon paste electrode has considered as a promising electrode as compared to Au (Gold) electrode, Pt (platinum) electrode, mercury electrode, glassy carbon electrode, pencil graphite electrode, Ni (Nickel), quartz crystal microbalance electrode, boron-doped diamond paste electrode) because of, low background currents, easy renewability, easy modification, and exact reaction kinetics[84-85].

1.4.3. Modified carbon paste electrode for analysis of drugs

The over-use of drugs in daily life produces side effects upon the human body. In addition, most antibiotics are prescribed by doctors for the treatment of various diseases. The overdose or skipping of prescriptions of the doctor, as result these drugs or antibiotics cause an adverse impact on human vital organs. The fast and selective recognition of these drugs is a key problem in human bodies or in environmental samples. So, the researchers introduced a fast, easily operational, selective, and inexpensive electrochemical approach towards the identification of hazardous and toxic compounds in wastewater[86]. The carbon paste electrode is the most easily prepared electrode that is utilized in the electrochemical monitoring of drugs and antibiotics. The signal of the analyte is achieved because of oxidation and reduction, depending on the structure of the target compound. For instance, the oxidized electron of adrenaline can be detected on the surface electrode. The involve electron of the reaction, the

shift from the working electrode (carbon paste) to counter electrode can be recognized by an electrochemical system. Basically, the modification of the electrode enhances the mobility of electrons, which is a key factor in the electrochemical sensor system, and helps to increase the limited detection of the sensor. The modification of carbon paste electrode with $CuFe_2O_4$ nanoparticles and 1, 3-dipropylimidazolium bromide was used to monitor the adrenaline in the real samples such as injections and urine. The fabricated modified electrode was used to construct the analytical curve in the range of 0.1-400 µmol L^{-1}.[87]

The same technique was extended by Maleh et al., to synthesize a carbon paste electrode in the presence of modified agents like ZnO nanoparticles and n-hexyl-3-methylimidazolium hexafluorophosphate for the analysis of isoprenaline[88]. The modified electrode was utilized in the concentration range of 0.3-320 µmol L^{-1} with a limit detection of 0.09 µmol L^{-1}.[88] Ferancová et al[89]., enhanced the detection ability of carbon paste electrodes with β-cyclodextrin. The constructed electrode was used for the determination of tricyclic antidepressants–imipramine, trimipramine, and thioridazine. Differential pulse voltammetric techniques were employed for the electrochemical analysis. The same technique was employed by Gupta et al[90]., who fabricated ZnO/CNTs nanocomposite and n-hexyl-3-methylimidazolium hexafluoro-phosphate and combined with carbon paste electrode to increase the sensor detection efficiency towards carbidopa. The cyclic voltammetric technique was employed to investigate the interaction of electro-active agents and drugs.

1.5. Transducer and recognition system (selective materials)

Transducer belongs to the part of the sensor device which holds the recognition materials and converts the tracing information about the concentration of the analyte into a physical measurable signal. Transducers have four main types includes: Electrochemical, optical, piezoelectric and thermal.

Among, the various above-mentioned transducer electrochemical has got more popularity because of its high sensitivity, specificity, fast and accurate analysis[91]. These profitable highlights have permitted the advancement of new investigation devices, such as biosensors that utilize biological (natural) components such as cells, tissues, antibodies, antigen, protein, DNA or proteins, which are immobilized on the surface of electrodes[92]. Another crucial component that plays an imperative part in the detection of the sensor is known as the recognition material/layer. The function of the recognition layer provides better selectivity and also can stop the interference of other analytes[93]. Various nanomaterials have been employed as a recognition layer in an electrochemical sensor, for instance, enzymes and antibodies (these biological recognition materials utilised in biosensors), while artificially made materials like, organic and inorganic are used in others.

1.5.1. Core@shell nanomaterials applied in electrochemical sensor

Nanotechnology is a fastly emergent class of science with prospective applications in various research areas, including, sensor[94-95], energy storage[96-97], nanomedicine[98-99] and wastewater treatment[100-101]. Nanoscale materials got profound interest because of their commendable properties like electrical, magnetic, and optical[95], hence nanoscale materials based determination provides noteworthy leading roles over conventional analysis approaches, because of its great sensitivities, excellent performance, and simplicity of analysis. Core@shell materials are composite nanoscale materials and their structures consist of two components such as core (innermost portion of one material), and shell (outer layer of another material) which makes core-shell structure[102]. The modern era has modified the definition, class of nanoscale-based materials having an inner material enclosed partly or entirely through the external layer provided both can be recognised individually. By increasing the range of shells,

the unique properties of the centre (core) and the shell (outer) may be combined in solo material advertising exceptional applications. These core@shell nanomaterials increase the analytical signals and provide many benefits such as larger surface area, great catalytic activities, and biocompatibilities towards the target compound. Because of these benefits, the core@shell materials got a leading role in the area of the sensor device. In the current years, science has viewed extensive developments in sensing specifically. Durable sensing platforms, tracing of target compounds in low concentration, multicomponent detection, miniaturized tools, detection in multiplex matrices, etc[103]. So far, engineered materials (inorganic and organic), natural materials (nucleic acid, micro-organism, chemical, proteins, antibody, and tissue), and certain biomimetic materials have been utilized for the improvement of distinctive sorts of detecting devices.

1.5.2. Types of core@shell based on materials

Core@shell has been divided into two main groups, including, organic and inorganic. Organic core@shell materials nano-scale materials consist of carbon-based materials while inorganic belongs to metals, metal salts, and metal oxides. Recently, a new class of material has been introduced like metal-organic frameworks (MOFs) based core@shell structure[104].

The organic core@shell nano-materials has gotten more attention because of its stability and biocompatibility. Organic core, shell, or both may be introduced by polymerization methods. Basically, in this type of approach, the three-dimension structure has been synthesized in the existence of functional monomers, cross-linker, and radical initiator used to initiate the polymerization process. For instance, fabrication of a metal-free electro-catalyst by an *in situ* polymerization of aniline monomers within the channel pores of mesoporous silica (SBA-15)[105]. The massive synthesis of charged (conductive) polymer leads to poor properties, for example, small surface area, low porosity, and low contact area to

interact with solutions. However, in this case, PANI is controllably fabricated using persulfate as an oxidizing agent on the channel walls of SBA-15 foremost to unvarying and high surface area polymeric structure with high contact area to interact with solutions. Moreover, Mesoporous carbon was also made by the carbonization of PANI/SBA-15 followed by etching away the silica framework[106].

The inorganic core@shell, belongs to two classes, (i) silica-based, and (ii) metal-based, most of the silica-based core@shell is fabricated via sol-gel or Stober method[107]. These methods have gotten a leading position because of easy control, reproducibility, and flexibility. The strategy includes the formation of hydroxides followed by condensation of silicon halides, or alkoxides in a liquid solution with the assistance of base a catalyst like ammonia to form unchanging colloidal microspheres. Though, nanoparticles generated from this technique are non-porous or solid; therefore, in the present era, new techniques had been planned to created porous nanoscale materials including template-assisted techniques or post-synthetic modifications. The porous core@shell-based nanomaterials display high surface area, and cores along with shells may be gotten to beneficially, which gives multifunctional application conceivable outcomes. Also, these porous materials can more be altered with appropriate functional groups permitting applications in wide sectors of science and industries. Metal-based core@shell comprise metallic, metal salts, and metal oxides nanoparticles. The reduction method has been employed for the production of metallic core@shell nanomaterials. In this method, different reducing agents are used such as $NaBH_4$, ascorbic acid, and hydrazine. Temperature, time, and type of reducing agents cause a key role in the reaction while any variation in these reaction parameters created changes in size, shape, particle growth, and consequently variation in physical, optical, and chemical properties. Metal oxide core@shell nanomaterials are also synthesized via thermal decomposition or co-precipitation methods. In thermal decomposition, the organometallic precursors are treated with high heating in the

presence of oxygen or air to get the desired products, while precipitation in a basic medium is named the co-precipitation method. Gaseous precursors are also used in the synthesis of metal oxides but this synthesis is applied in chemical vapour deposition (CVD) and pulse laser deposition (PLD). The core@shell-like metal salt can be synthesized by the precipitation of metal salts. Other methods such as microwave-irradiation and ultrasound have been used effectively for the preparation of various core@shell nanoscale materials.

The core@shell based on **metal-organic framework (MOFs)**, inorganic nanoparticles act as a core while MOFs are used as a shell. Basically, MOFs consist of three structures, including, crystalline, porous and hybrid materials, having a cage structure of metal ions or clusters coordinated to organic ligands to form one, two, and three-dimensional structures. In this kind of core@shell materials, the metals, metal oxides, and nanorods nanoparticles act as core, which may be implanted in the MOFs materials[108]. The combination of nanomaterials with MOFs (NP@MOFs) introduced a new hybrid material with excellent properties, such as, physical and chemical, as a result, can be utilized in versatile applications. The use of MOFs shell layer around the core nanomaterials (NP) avoids the aggregation of core nanoparticles, and also enhance the high surface area which leads to enhancing the performance of the desired application. The synthesized hybrid nanomaterials (NP@MOFs) have been utilized in many filed, including catalysis[109], sensor [110-111] and drugs delivery[112]. Core@shell MOFs may be fabricated using three methods (i) creating cavities inside MOFs structure and introducing the nanoparticles in cavities. (ii) Synthesis of the nanoparticles separately and then embedded into MOFs structures. (iii) Using the one-pot method. The core@shell hybrid material (Au@MOF-5) was synthesized via a one-pot approach, and then applied for the detection of CO_2 in gas mixtures [105]. The fabricated sensor showed good potential against other interferents such as N_2, O_2, and CO while also having a good selectivity towards the target element. Although the remarkable properties of hybrid core@shell composites (NP@MOFS), there are numerous

challenges to overcome in order to fabricate an excellent hybrid core@shell structure like control over the size and the morphology of the composite together with the dispersibility of nanoparticles in MOF structure. Hence, more basic engineered strategies are required for huge scale generation and far-reaching utilization.

1.5.3. Core@shell nanoscale materials as a recognition layer in the sensor development

The modification of electrodes is a fascinating area in materials science due to new challenges faced by industries, clinics, automotive, and the environment. These sectors facing these challenges in the form of analysis of multi-matrices, homogeneity matters, multicomponent tracing, low concentration of bio-fluid samples, etc. The electrochemical sensor needs better modifier nanomaterials that can speed up the electron transferring between the electrode surfaces and target analyte. To improve the detection efficiency, various nanoscale materials are employed as modifiers in an electrochemical sensor like noble metals, carbonaceous materials, metal oxides, metal nitride nanomaterials, different conducting polymers, and their nanocomposites[113].

Core@shell nanoparticles provide a good sensing platform due to high surface area, avoiding aggregation, and high electron exchange between surface and analyte. Metallic nanomaterials have bad aggregation properties which makes them limited in sensor applications. Thus, a reasonable support material is suggested to avoid the conglomeration of nanoparticles. For example, Kalambate et al[114], fabricated a hybrid material sensor (Pd@Pt/MWCNT) for the simultaneous monitoring of doxorubicin and dasatinib. In this hybrid material, MWCNT was used as support material to improve the sensing efficiency of the electrode, high surface area and to stop the aggregation. To get the efficient sensing platform fabrication or modification is an important phase. The selection of proper modifier agents introduces a good selectivity, sensitivity, and also enhance the conductivity of the

working electrode, as, result enhancing the electron transferring kinetics. Numerous types of conductive electrodes have been applied in electrochemical sensors, comprising, carbon-based electrodes such as glassy carbon electrodes (GCE), boron-doped diamond electrodes, pencil graphite electrodes, screen-printed carbon electrodes to metal-based electrodes including gold, silver, platinum, and copper electrode[115]. These electrodes could be altered with appropriate modifiers. Many developed methods have been successfully employed for the alteration of sensing electrodes based on the nature of materials to be placed including electrochemical polymerization, electrochemical deposition, self-assembled layers, irreversible adsorption, covalent bonding, and others. The modified sensing electrode display the advantages, such as, good catalytic activity, selectivity, speed up the oxidation and reduction response, and improve the quality of detection.

1.6. Biomimetic Sensors

A biomimetic material may be defined as, the development of a human-made system that emulates nature or mimics a biological system. That a manufactured enzyme makes the same forms done by the natural catalyst, but does not fundamentally follow the same way.[116]

Biomimetic sensors based on these artificial recognition materials are more strong and longer life, because, these materials are not denaturation as biological materials. Biomimetic sensors can analyse the target analyte in the different matrices in the presence of opposing circumstances such as extreme pH, high temperature and organic solvents [117-118]. That's why a biomimetic sensor has been successfully employed in this work to investigate the analysis of tetracycline antibiotics, exhibited a good quality of characteristics such as stability, and durability. Especially the uses of the biomimetic sensor for the detection of pesticides provide additional benefits like selectivity while biological recognition materials i.e, enzymes applied for the detection of pesticides[119,120,121], are not selective for a specific target analyte (for

example peroxidase, tyrosinase, etc). Moreover, using electrochemical tools in the biomimetic sensors can offer a direct signal, which may be increased with the concentration of the only one pesticide.

1.7. Molecularly Imprinted or biomimetic polymers

Before going into the explanation of molecularly imprinted polymer it is important to know how the molecularly imprinted polymer was introduced. The first time the molecularly imprinted technique was introduced was in the 1930s. The first idea about molecular imprinting was provided by Pauling in 1940 which consist of protein antibodies[122]. The first report was published in the current field in 1972 regarding organic polymers by reversible chemical bonds[123]. In the early 1980s, molecular imprinting technology had been come into practice and was prepared molecularly imprinted polymer using the non-covalent approach. Based on this approach the imprinted technique was rapidly mature[124]. The polymer which possesses a selective cavity according to the memory of the template molecule is known as molecularly imprinted polymer, while synthesized via polymerization process in the presence of monomer, template, radical initiator and cross-linker. **Figure 4.** Shows the general representation of molecularly imprinted polymer.

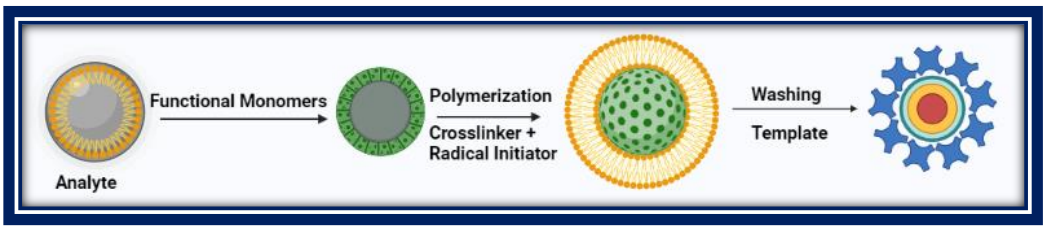

Figure 4. Illustration of molecularly imprinted polymer. Source: Author

Commonly, three kinds of interaction have been reported between template and monomer in the literature. The non-covalent (hydrogen bonding, Vander wall and Colombic force) interaction between the template and monomer in the designing of the polymer[125]. The

methacrylic acid is considered to be a monomer for this approach. The formation of the complex with multiple template monomer stoichiometries makes it challengeable and this complex has to create an effect on the selective binding sites. The advantages comprise the effortlessness of operation, strength and flexibility of the non-covalent methodology made it more mainstream in the recent past. In contrast[123], the reversible covalent interaction was introduced in between functional monomer and template by Wulff et al. The stable contact of monomer and template makes its binding sites are more homogenous[126], while a similar bonding accomplished between the template and polymer on rebinding. The applications of this strategy in the designing of the molecularly imprinted polymer are limited because of the less availability of functional monomers and less flexibility. In comparison with the covalent approach, the non-covalent strategy has to be assumed superior because of easily operational and produces higher affinity binding sites. The short of durability and additional sensitivity to the external environment causes an interruption in the result of monomer-template complexes and makes the non-covalent approach is not sympathetic. The integration of both strategy covalent and non-covalent lead to a semi-covalent approach for the designing of the molecularly imprinted polymer. Monomer interacts with template via the covalent while the analyte ensnares by mean of non-covalent approach. Some common functional monomers, cross-linker and initiators are exhibited in **Table 2**[62]**.**

Table 2. Various Functional monomers, radical initiators and Cross-linkers

Functional monomers		
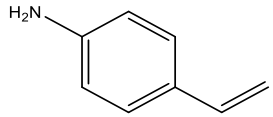	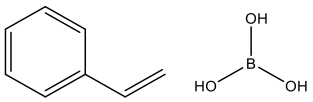	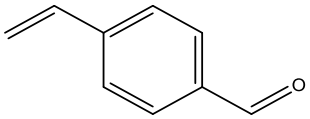
4-vinyl benzaldehyde	4-vinyl aniline	4-vinyl benzene boric acid
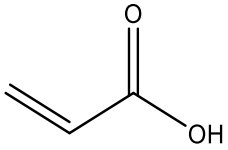	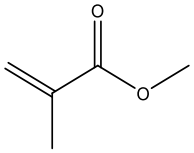	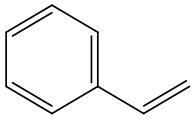
Acrylic acid	Methyl methacrylate	Styrene
Initiators		
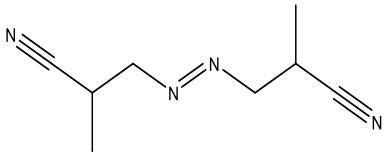	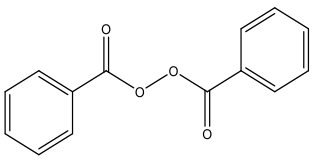	
Azobis-isobutyronitrile	Benzyol peroxide	
Cross-linker		
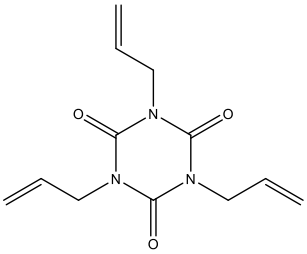	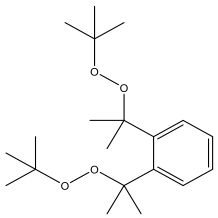	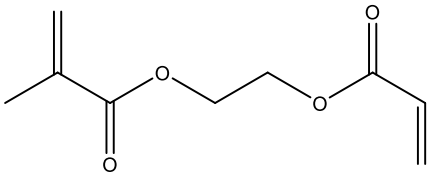
triallyl isocyanurate	N-N/-methylenediacrylamide	Ethylene glycol-dimethacrylate

Source: (Molecular imprinting: perspectives and applications. **Chem. Soc. Rev**. **45**, 2137–2211 (2016).

Cross-linking agent is used to fix the functional monomer around the template molecule. The cross-linker agent is used as a shield to protect the structure of the polymer from demolition after washing the template molecule. An optimized amount of cross-linker is required to synthesize the imprinting polymer. The high measure of cross-linker prompts the

decrease of the number of cavities in the polymer matrix while the low amount causes insecure mechanical strength. The limited number of conceivable cross-linkers ruins the advancement in MIP innovation; hence cross-linker agents may be divided on based on their synthesis methods are triallyl isocyanurate (TAIC), bis-(1-(tert butylperoxy)-1-methylethyl)-benzene (BIBP) (covalent procedure); tetramethoxysilane (TMOS), diphenyldiethoxysilane (DPDES) (sol-gel procedure); and ethylene glycol dimethacrylate (EGDMA), divinylbenzene (DVB), N-N/-methylenediacrylamide (MDAA), and 3,5-bis(acrylolamido).Solvent plays a vital role as a dispersion medium and provide the way which controls the pore and porosity of the MIP. Solvent assists to reduce the side reaction and heat effects which is associated with the synthesis of molecular imprinting polymer. Therefore, healthy optimization of MIP needs an appropriate selection of porogen solvent (also known like porogen). As a result of the use of polar solvent, favourable interaction among template and functional monomer is badly affected. Usually, the non-covalent approach is used to synthesis the MIP in the presence of low polarity organic solvent while the solvent has high polarity involved in the covalent approach.

Here is some common porogen that is used in the synthesis of MIP methanol, tetrahydrofuran, 2-methoxyethanol, chloroform, dichloromethane, acetonitrile, toluene, and N,Ndimethylformamide. The competence to extract the MIP is influenced by the porogen. The aprotic solvent with low hydrogen and have the ability of donor/acceptor is an example of an ideal porogen and these capabilities are counted in their distinctive feature. Many researchers conducted density functional theory/ simulation studies to choose the appropriate solvent medium for the polymerization process. Such a kind of theoretical approach is used to stay away from the repetitive experimental system for porogen choice. For example, the influence consequences of porogen have been investigated on the determination of 4-nitrophenol[127]. An initiator is a chemical source that generates free radical upon heat and light while the consequential radical gets to start the polymerization process. Various kind of polymerization

methods is used to manage the synthesis of molecular imprinting polymer for instance: free radical, photo and electro-polymerization. The synthesis of MIP via free-radical polymerization is achieved by azo and peroxy chemical compounds initiator. The extensively used initiator like Azo-bis-isobutyronitrile (AIBN) plays a vital function in the synthesis of MIP. The significant results of radical polymerization are attained by an inert environment, providing bubbling inert gas like nitrogen and argon.

1.7.1. Mechanism involved in the polymerization technique in the MIPs

Polymerization is a process in which huge numbers of monomers react to produce polymers. Polymerization process may involve in three steps such an (i) initiations, (ii) propagation, and (iii) termination

A) INITIATION

In the 1st step of the polymerization, initiator start the formation of free radicals proceed by several ways. The several ways due to which free radical is generated described below and showed in Scheme 1:

Thermal initiation: By applying heat, the monomer is transformed into a polymer. But this method has dis-benefit and lead to unwanted polymerization monomer. Because of this reason, inhibitors are frequently added to the monomers' earlier storage. This causes the existence of a non-reproducible initiation period when such monomers are polymerized.

Initiation by radiation: This type of polymerization can be initiated via a light or additional source of energy. This is a very expensive technique because it can be controlled under very low temperatures[128].

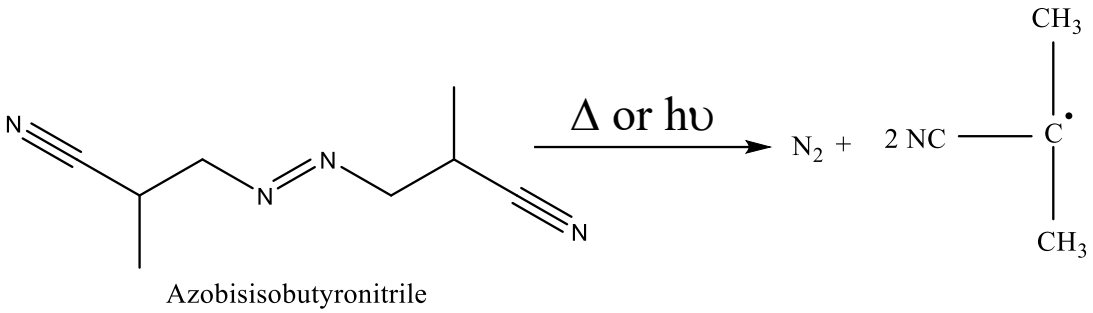

Scheme 1. Reaction exhibits the decomposition of initiator (AIBN). Source: Author

B) PROPAGATION

Step involved, the adding of monomer to a radical chain, in turn, produces a long polymer chain. In the case of substituted vinyl monomers or 1, 3 dienes, the repeat unit usually follows a head-to-tail arrangement which leads to disturbing the normality of the polymer chain. This severely affects the crystallinity of the chain, and also strongly influence the mechanical strength of the final chain.

The chain transfer polymerization approach consists of a chain agent which has a weak chemical bond that provides abilities to the polymer chain. Common chain transfer mediators comprise thiols, especially dodecyl mercaptan (DDM), and halocarbons, like carbon tetrachloride[129].

C) TERMINATION

Two different mechanisms are involved in the termination step, termination occurs by combination leads to form a single polymer chain, while termination via disproportion. When two radical chains with varying degrees of polymerization meet at their free radical ends, a process known as termination by combination. The disproportional termination results in two

terminated chains. In this case one terminated chain will having a saturated and the other an unsaturated carbon.

1.7.2. Core@shell magnetic molecular imprinted polymer (MIP)

Magnetic nanomaterials used as a core in the MIP provides magnetic and special properties. The materials which possess magnetic properties, including, iron, cobalt, nickel and their oxidizing material or alloy [130-131]. The uses of cobalt and nickel are restricted in many applications such as biologicals and pharmaceuticals because of their toxicity. Fe_3O_4 offers extensive advantages, comprising, less toxicity, low cost, easy to prepare, and easily separated from solution with help of external magnetic[132]. The magnetic MIP shown in **Figure 5.**

That is why magnetic-MIP composite provided more simplicity over the traditional MIP because traditional MIP needs centrifuge and filtration for the separation**.** This magnetic-MIP composite is broadly used as a potential candidate in biological area, separation[133], for protein and nuclear acids[134], standard analytical method (HPLC): biotin in food sample[135], and ametryn in fruits[136], sensors: folic acid[137] and tetracycline[138].

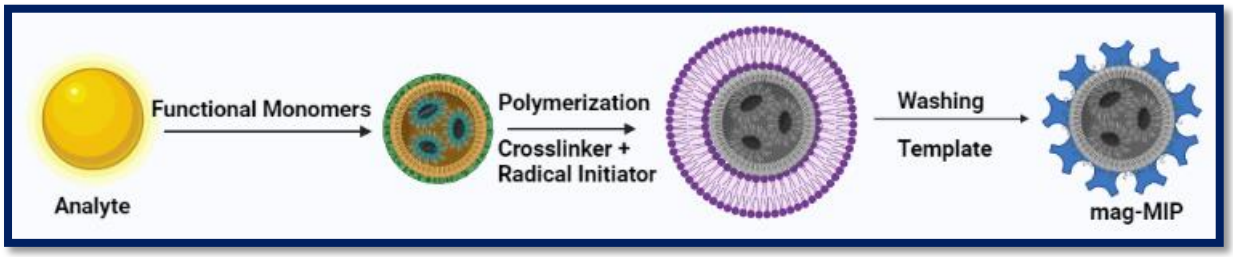

Figure 5. Schematic representation of magnetic MIP Source: Author

The magnetic nanoscale materials (Fe_3O_4) are synthesized using solvo-thermal and co-precipitation methods. Due to its simple process, simple glassware, and mild reaction conditions, co-precipitation is the first broadly utilized strategy[139]. The solvo-thermal method required high temperature and pressure due to which it is difficult to control it, thus these

advantages make it complicated. Xiao et al[140]., synthesized the magnetic nanoparticles via a hydrothermal approach while this method provides uniform nanoparticles and less aggregation. Thus, the embedded magnetic nanomaterials in the MIP (Fe_3O_4-MIP) offers improved analytical performance in term of selectivity, sensitivity, increase tracing efficiency, and reduce the interference effect because of a bulky number of recognition sites positioned on the surface of the nanomaterials.

1.8. Adsorption in the MIPs: Performance and Optimization

Adsorption is the process by which a molecule moves from a fluid bulk to a solid surface. Adsorbate refers to the substance that collects on the surface, whereas adsorbent refers to the substance that adsorb[141]. The solid support either chemically or physically adsorb the component that is transported from one phase to another during the process. The vast majority of solid adsorbents are porous and have a significant amount of surface area. Adsorption is a surface phenomenon that can take place on the surfaces of the adsorbents [142]. Because the pores are often quite small, differences in size or polarity might allow certain molecules to be imprisoned more securely than others, which in turn can cause selective separation of desirable species. Accumulation of substances by adsorption is an important operational technology in petrochemical, biotechnology, water purification and pre-concentration for analysis. As an important part of the adsorption process, the adsorbent, such as magnetic molecular imprinted polymer (mag-MIP), should be economical, easy to process, highly selective (cavities according to template memory), wide in surface area, and long-life time. In theoretically, the data on adsorption can be quantitatively represented by mathematical models that rely on the kinetics and equilibrium of the adsorption process. Adsorption models such as the Langmuir and Freundlich models are the most commonly utilized for analysing experimental results. Predicting the capacity and rate of equilibrium adsorption can be done using these models.

1.8.1. Kinetic studies of molecularly imprinted polymer

Adsorption studies of the template in MIP at specified intervals of time are used in kinetic studies, which are one method for evaluating kinetic physicochemical constant (k_1, k_2). This technique involves exposing a constant volume of MIP to solutions containing various concentrations of tetracycline for a predetermined amount of time prior to analysis. After adsorption time, the target template solution is isolated from the mixture (polymer + solution) via way of means of filtration. The remaining concentration of the target template is measured using standard instrumental analytical techniques, including, chromatographic and fluorimetric measurements, and by difference, the amount adsorbed is calculated.

1.8.2. Isotherms obtained from the interaction of magnetic-MIP and template

The isotherm experiments are performed to obtain the maximum adsorption capacity of magnetic-MIP and magnetic-NIP (Non-Imprinted polymer), or another adsorbent material (in a generic way). The experiments are commonly performed at room temperature.

In order to obtain the isotherms profile, several mathematical models for experimental data have been reported in the literature for example **linear**[143]; Quite a few useful isotherms can have their first stages described by the linear isotherm. Adsorption energy (lowering energy while adsorbing two materials) is widely considered to be coverage-independent, hence this theory is accepted for use at low surface coverages. **Temkin**[144]; model implies that when surface coverage of an adsorbent increases, the adsorption heat of all molecules reduces linearly, as well as the fact that binding energies in adsorption tend to be distributed uniformly up to a maximum value. **Dubinin-Radushkevich (D-R)**[145]: isotherm model assumes that the micropore size of the adsorbent is similar, and that the adsorption equilibrium relation for a certain adsorbate-adsorbent pair can be stated in terms of the adsorption potential, which is independent of temperature.

But here, we only describe only of them, Langmuir and Freundlich models. Freundlich's model suggested the multilayer formation on the adsorbent material (magnetic-MIP and NIP), and also guesses an exponential scattering of more than one adsorption site with unique energies. The equation is given below equation (1.1)[146]

$$Qe = K_f \times C_e b \ldots\ldots\ldots\ldots\ldots\ldots (1.1)$$

Where above in equation (1.1) Q_e represents the adsorption equilibrium (amount of adsorbate/template adsorbed at equilibrium) unit: mg g^{-1}, C_e is the amount of concentration at equilibrium, K_F and b_F are factors belong to the Freundlich isotherm.

The Langmuir isotherm involves the production of a monolayer on the adsorbent substrate (magnetic-MIP and NIP) and an estimation of the adsorption maximum amount. The mathematical expression is shown below in equation (1.2)

$$Qe = K_L \times \frac{C_e}{1} + A_L \times C_e \ldots\ldots\ldots\ldots (1.2)$$

Where Q_e is the quantity of adsorbed substance (template) at equilibrium (mg g^{-1}), C_e is the template concentration at equilibrium (mg L^{-1}), and K_L and A_L are Langmuir isotherm constants. The linear form of Langmuir isotherm exhibits below in equation (1.3)[147]

$$\frac{C_e}{q_e} = \frac{1}{K_L} + \frac{A_L}{K_L} Ce \ldots\ldots\ldots\ldots\ldots\ldots\ldots (1.3)$$

1.8.3. Analytical methodologies used to the adsorption of the analyte

Many researchers employed various analytical approaches to measure toxic compounds in an aqueous medium. This section will consist of only standard analytical methods such as HPLC and Fluorometric.

A) High-performance liquid chromatography (HPLC)

HPLC is a kind of column chromatography used in analytical-chemistry and analysis to separate, identify, and quantify hazardous compounds. In high-performance liquid chromatography (HPLC), the packing material (stationary phase), mobile phase(s), and detector. The retention period is affected by the interactions that take place between the stationary phase, the molecules that are being examined, and the solvent(s) that are being used [139]. A minor volume of the sample to be studied is added to the flow of mobile phase, and the sample's movement through the system is slowed down as a result of certain chemical or interaction with the stationary phase. The characteristics of the analyte as well as the make-up of the stationary and mobile phases are factors that determine the degree of retardation. The amount of time that passes until a particular analyte elutes is referred to as the retention time. The term "solvent" refers to any combination of water or organic liquid that is miscible with other liquids (the most common are methanol and acetonitrile)[148]. Gradient elution is a technique wherein the mobile phase composition is separated and then recombined during the study. Affinity of the analyte for the present mobile phase determines how the gradient separates the analyte mixtures. For example, the synthesis was done by Li et al[149], to determine the concentration of tetracycline antibiotic employing porous polythiophene materials as an adsorbent, the HPLC technique was used to conduct the analysis on the target component. A novel ultra-fast micro-extraction process has been developed using acetonitrile, which was then followed by a gradient reversed-phase HPLC–UV approach in order to determine six tetracycline concurrently in a variety of milk products[150]. This study extended the standard analytical approach, which is called HPLC, to monitor the tetracycline component in real food samples.

B) Fluorometric measures

Fluorometry refers to the process of measuring fluorescence. Fluorometers and fluorimeters are the names given to the instruments that are used to measure fluorescence. A fluorometer works by producing the specific light wavelength needed to ignite the target analyte, selectively transmitting that wavelength, and then measuring the intensity of the emitted light. The amount of light that is given out is directly proportional to the concentration of the analyte that is being measured (up to a maximum concentration). Fluorometers select the excitation and emission wavelengths by utilizing monochromators (in the case of a spectrofluorometer), optical filters (in the case of a filter fluorometer), or narrow band light sources such as LEDs or lasers. When compared to other analytical methods, fluorometry is chosen because of its exceptionally high sensitivity as well as its high specificity, its ease of use, and its low cost.

Certain compounds (usually polyaromatic hydrocarbons or heterocycles) known as fluorophores or fluorescent dyes undergo a three-stage process that results in fluorescence.

Stage 1 – Excitation: A photon $h\upsilon_{ex}$ energy is delivered to the fluorophore from an external source such a lamp or a laser, and the fluorophore absorbs it, resulting in an excited singlet electronic state (S1′). This technique differentiates fluorescence from chemiluminescence, in which the excited state is produced by a chemical reaction.

Stage 2 – Excited-State life time: There is a limit to how long an excited state can persist (usually between 1 and 10×10^{-9} seconds). During this time, Fluorophore undergoes conformational changes and engages with its surroundings molecules. These mechanisms have two significant repercussions as a result. First, the energy of S1′ is partly released, producing a relaxed singlet excited state (S1). For the second, by fluorescence emission, not all molecules that were stimulated by absorption (Stage 1) return to their initial ground state (S_0). Collision quenching, fluorescence energy transfer, and intersystem crossover may also depopulate S1.

Fluorescence's efficiency in comparison to these other processes is measured by the fluorescence quantum yield, which is the ratio of fluorescence photons released (Stage 3) to photons absorbed (Stage 1).

Stage 3 – Fluorescence Emission: Fluorophore returns to its ground state S_0 after emitting $h\upsilon_{em}$ energy. Because of energy dissipation during the excited state lifespan, this photon has a lower energy and thus a longer wavelength than the excitation photon $h\upsilon_{ex}$. This energy ($h\upsilon_{ex}$–$h\upsilon_{em}$) is known as Stokes shift. Fluorescence techniques rely on the Stokes shift to achieve their high sensitivity because it separates emission photons from excitation photons and allows them to be detected against a low background. Tetracycline is a fluorescent compound, a metal particularly divalent metals, which may lead to enhance the fluorescence spectra of tetracycline. [151-152]

1.9. Application of Molecular imprinted polymer

When analyte is present at low concentration levels, the solid phase extraction method (SPE) is a frequently used method for extraction, clean-up, and concentration. It is possible to quantify the analyte of interest from complicated matrices using this technology, isolating it from interfering chemicals[153-154]. When compared to other materials such as modified silica, ion exchange resins, and immunosorbents, the use of MIP as an adsorbent material in the solid phase extraction technique has shown to have high selectivity, chemical, and thermal stability, as well as reproducibility in the polymer preparation[155-156]. The method is known as solid phase extraction with molecular imprinting (MISPE). The only difference between MISPE and a traditional SPE process is that the printed polymer is replaced with common stationary phases instead of the printed polymer. The stages of conditioning, loading, washing, and eluting the cartridges are included in this process. To sure that the analyte is retained to the greatest extent feasible, the solvent in which the samples are to be percolated should not interfere with the

contacts created between the polymer and the analyte. The properties of the analyte employed as a template are critical for selecting the optimal washing solvent. Low polar solvents such as dichloromethane, toluene, and chloroform are commonly utilized, as are high polar solvents such as methanol. Thus, in this form of analysis, the pH, polarity, and volume of solvent must be tuned in order to achieve template separation of the interfering substances. The efficiency of this method, as well as its applicability in diverse matrices, will be determined by several aspects, including the amount of MIP employed, MIP efficiency in adsorption, template interaction with the active site, and analytical method.

Integration of MIPs as selective recognition layers in sensing devices and assays was initially proposed in the 1990s[157]. This involved connecting MIPs to standard biosensor readout technologies, which act as transducers by translating chemical binding into a quantifiable signal[158].This shift has been accelerated by developments in MIP synthesis processes, microelectronics, and computing over the past two decades, leading to the emergence of a variety of novel sensor and assay platforms[159-160]. Urine, blood, wastewater, soil samples, etc., can now be analysed for a wide variety of analytes because to MIPs and the associated output platforms [161-162]. As a result, there is a possibility that the sensitivity and limit of detection (LOD) of a device will change depending on the method and MIP employed. This diversity in sensing capacities has led to the inability to establish a single MIP output combination as ideal, with some techniques being preferred in specific contexts[163-164]. In spite of the fact that all MIP-based systems offer the advantage of easy, cheap receptor manufacture and enhanced physical and chemical stability, commercialization still appears to be a barrier. Researchers have looked into a variety of different ways to include MIPs into electrochemical sensor platforms, such as those that use field-effect transistors, chemiresistors, or the readout principles of amperometry, voltammetry, impedancemetry, capacitancemetry, and

conductometry[165]. Carbon nanotubes, conductive polymers, and metallic nanoparticles are some of the often used approaches to employed in MIP to improve he sensing properties[166-167].

1.10 Literature review

Zhang *et al*[168]., fabricated molecularly imprinted polymer (MIP) modified with mesoporous silica covered magnetic graphene oxide (MGO@MS@MIP) for the selective removal of tetracycline. The developed mag-materials showed promising results for tetracycline removal and separation from water.

Wang *et al*[169]., employed Zein to prepare biocompatible magnetic molecularly imprinted polymers for the removal of tetracycline compound. A high adsorption capacity of 236.40 mg/g was obtained through synthesized materials, and followed pseudo-second-order kinetic model.

Gao *et al*[170]., synthesized the core-shell magnetic molecularly imprinted polymer nanoparticles for tetracycline adsorption and separation from food matrices. Maximum adsorption capacities of 40.48 mg/g were measured for magnetic materials, and recoveries in the range of 91.14–104.52 % were found to be quite excellent.

Song *et al*[171]., synthesized Fe-based MOFs materials for the selective detection of tetracycline antibiotics. Electrochemical sensor demonstrated high selectivity and stability with a lowest detection limit of 0.01 nM. In addition, the detection of tetracycline in real water samples was made possible.

Guo *et al*[172]., measured the concentration of tetracycline using a glassy Carbon electrode modified with iron cation exchanged montmorillonite. The electrode exhibited the high current density as compare to traditional electrodes. For the detection of the antibiotic tetracycline hydrochloride, montmorillonite has been proposed as a viable electrochemical sensor material due to its low cost and ease of production.

Liu et al[173]., 3D-framework of functionalized multi-walled carbon nanotubes (fMWCNTs) coated with molecularly imprinted polymer (MIP) has been fabricated in order to enable rapid and ultrasensitive electrochemical molecular sensing. The electrochemical sensor was utilized well for the purpose of the quantification of norfloxacin in pharmaceutical formulations. The recoveries that were achieved by the use of pharmaceutical formulations ranged from 97.36 to 109.58%.

Wang et al[174]., prepared ased on a carbon paste electrode (CPE) modified with multi-walled carbon nanotubes (MWCNTs) and boron-embedded molecularly imprinted composite membranes, a novel electrochemical sensor was developed for the sensitive and selective detection of tinidazole. Pharmaceutical and biological samples were analyzed to show the sensor's practicality, with recoveries range of 82.40–104.00%.

Wang et al[175]., demonstrated a new electrochemical sensor based on CuCo2O4/N-CNTs loaded molecularly imprinted polymer (MIP) modified glassy carbon electrode (GCE) is presented, for determination of detection of metronidazole. The electrochemical sensing system is stable, repeatable, and reproducible with a high degree of sensitivity and selectivity. The designed sensor demonstrates satisfactory recovery (95.9–100.9%).

Feier et al[176]., examined molecularly imprinted polymer (MIP) obtained by electropolymerization in an aqueous medium of indole-3-acetic acid (I3AA) on a glassy carbon electrode (GCE) and on boron-doped diamond electrode for detection of cefalexin. The BDDE and GCE had a detection limit of 3.2 nM and 4.9 nM, respectively.

Chapter 2

2. Aims and objectives of a research project

The suggested study's primary goals and objectives are as follows:

2.1. Synthesis of a hybrid magnetic-MIP to:

2.1.1. Synthesis and optimization of a hybrid magnetic nanoparticle modified with molecularly imprinted polymer.

2.1.2. Mass, time, concentration kinetic and isotherms parameters have all been examined.

2.1.3. Detection of tetracycline in actual samples such as honey, raw milk, and egg.

2.2. Development of an electrochemical sensor

2.2.1. Synthesis of another molecular imprinted polymer-modified magnetic nanoparticles.

2.2.2. The electrochemical sensor's performance was optimized by studing pH, tetracycline concentration, and mag-MIP mass.

2.2.3. The effectiveness of sensors for tetracycline quantification in both raw and commercial milk samples has been studied.

2.3. Characterization techniques

Scanning electron microscopy (SEM) was used to examine the surface morphologies of synthesized polymer materials. The different functional groups of reagents utilized in the synthesis of polymer materials were confirmed using Fourier transform infrared spectroscopy (FTIR). Magnetic nanoparticles with a spherical shape were investigated using a transmission electron microscope (TEM).

Chapter 3

3. Experimental Procedure

In the experimental procedure section, I will discuss about the reagents, working solutions, synthesis, and preparation of real samples.

3.1 Reagents and solutions

Analytical grade or HPLC-grade reagents were employed, and all solutions were made using deionized water from a Milli-Q Direct-0.3 (Millipore) purification system (resistivity 18 MΩ). The reagents used in this thesis are listed in **Table 3.**

Table 3. Identification and origin of each chemical reagent used in this study.

Reagent	Company	Reagent	Company
Tetracycline chloride or tetracycline	Sigma-Aldrich	Methanol	Sigma-Aldrich
Iron(II) chloride tetrahydrate	Sigma-Aldrich	Ethanol	Sigma-Aldrich
Iron(III) chloride hexahydrate	Sigma-Aldrich	Acrylic acid	Sigma-Aldrich
Tetraethoxysilane (TEOS)	Sigma-Aldrich	Ethylene-glycol dimethacrylate (EDGMA)	Sigma-Aldrich
3-(methacryloyloxy) propyl]trimethoxysilane (MPS)	Sigma-Aldrich	2,2′-azobisiso butyronitrile (AIBN)	Sigma-Aldrich
Toluene	Sigma-Aldrich	Acetic acid	Sigma-Aldrich
Ammonia	Sigma-Aldrich	Sodium hydroxide	Sigma-Aldrich
Methacrylic acid	Sigma-Aldrich	Hydrochloride	Sigma-Aldrich
Benzoyl Peroxide	Sigma-Aldrich	Acetonitrile	Sigma-Aldrich

The stock solution of tetracycline, a concentration of 1.0×10^{-3} mol L^{-1} was prepared in deionized water and used to make the working solutions in the range of 1.0×10^{-5} to

8.0×10^{-5} mol L^{-1} in a 25.00 mL volumetric flask using 0.01 mol L^{-1} phosphate buffer (pH = 7) as a solvent.

3.2 Analytical method

This section will be only focus on the HPLC and fluorescence spectroscopy analysis for the determination of tetracycline antibiotic in order to investigate the efficiency of the magnetic-MIP (in comparison with the corresponding magnetic-NIP).

3.2.1. HPLC Analysis

The chromatograms obtained at different concentrations of tetracycline chloride were obtained using a Shimadzu model 20A, an SPD-20A UV/Vis detector, a SIL-20A autosampler, and a DGU-20A5 degasser and using a C18 column (250 mm × 4.6 m). The flow rate of 1.0 mL per minute was used for the mobile phase, which included 0.01 moles of oxalic acid, acetonitrile and methanol (70:20:10 v/v). The sample was injected in a volume of 20 µL, and the detection of the sample is carried out at a wavelength of 350 nm (tetracycline chloride).

3.2.2. Fluorescence Analysis

In order to evaluate the selective adsorption of tetracycline using the synthetized materials, the fluorescence spectroscopic also was used, since through this technique is possible to improve the sensibility toward quantitative application using MIP for recognition of tetracycline antibiotic[177]. For a maxima emission at a wavelength of 350 nm, the corresponding spectra were recorded in the region from 400 to 650 nm, using a spectrofluorometric (Model: LUMAX FLUORAT®-02-PANORAMA). This equipment has two monochromators with a resolution of a 900-l/mm concave diffraction gratings with a curvature radius of 100 mm. The spectrofluorometer also has a Xenon flash lamp as a light source with a spectral range of 210 - 690 nm.

In the fluorescence experiment, tetracycline (TC) stock solution with a concentration of 1.0×10^{-3} mol L^{-1} was utilized. A concentration of 0.01 mol L^{-1} of phosphate buffer (pH =7) was utilized to record the fluorescence spectra of TC.

When used mag-MIP and mag-NIP the fluorescence experiments were carried out using the same mass (10mg) as the HPLC analysis, in order to comparison of techniques.

3.3. Synthesis of magnetic molecular imprinted polymer

Firstly, magnetic nanoparticles (mag) were synthesized in accordance with a protocol of co-precipitation synthesis that is devised in the research laboratory[178], such as procedure described to follow. Specifically, 80 mL of deionized water was added to a vessel, along with known volumes of $FeCl_2.4H_2O$ and $FeCl_3.6H_2O$, and the mixture was stirred vigorously (with a high and mechanical stirrer) in an anaerobic (N_2) atmosphere. Afterward, drop by drop, NH_4OH was added to the reaction solution and allowed to react for 30 minutes. Another external magnet was used to recover the black magnetic nanoparticles (Fe_3O_4), which were then cleaned with deionized water and dehydrated in a 60 ºC oven.

Then, the magnetic nanoparticles were modified with SiO_2 to obtain the $Fe_3O_4@SiO_2$ nanomaterial, that were synthesized by ultrasonically dispersing 300 mg of black magnetic nanoparticles (Fe_3O_4) in 40 mL of ethanol (C_2H_5OH) and 4 mL of pure water. The reaction system was then filled with 5 mL of NH_4OH and 2.0 mL of TEOS ($SiC_8H_{20}O_4$). It took 12 hours to finish the reaction system. After the reaction was completed, the modified $Fe_3O_4@SiO_2$ nanoparticles were collected with an external magnet and rinsed many times with deionized water.

Consequently, methacryloxypropyltrimethoxysilane (MPS) was used to modify the surface of the $Fe_3O_4@SiO_2$ nanoparticles, which was accomplished by combining 250 mg of

Fe_3O_4@SiO_2 nanoparticles with 50 mL of toluene (C_7H_8) and 5 mL of MPS in an anaerobic (N2) atmosphere. After an interval of response time of 12 hours, the resulting modified Fe_3O_4@SiO_2–C=C- (also named Fe_3O_4@SiO_2-MPS) nanoparticles were washed numerous times with deionized water to remove any remaining reaction products.

After the obtain of modified magnetite (Fe_3O_4@SiO_2–C=C-) the shell of MIP was obtained used acetonitrile (30 mL) to dissolve the functional monomer methacrylic acid (4 mmol) and the tetracycline (178 mg). The solution was mixed for a total of 2 hours. In the next step, 200 mg of the modified magnetic nanoparticles (Fe_3O_4@SiO_2-MPS) were added and stirred for 3 hours. An additional 20 mmol of EGDMA (crosslinking reagent) and 82.5 mg benzoyl peroxide (radical initiator) were added to the reaction, which was then heated in a nitrogen atmosphere while being mixed.

The analyte had to be removed by a washing step after polymerization. In addition, with this procedure, the extra monomer and any other remaining or contaminants in the reaction mixture were also eliminated from the reaction mixture. A Soxhlet technique was used to extract the template using a solution of methanol and acetic acid (9:1 v/v) to remove the leftover analyte.

3.3.1. Binding experiments

In order to evaluate the material described in the previous section, the adsorption assays were performed using HPLC-UV and fluorescence spectroscopy experiments[179]. For this, 10 mg of prepared mag-MIPs and mag-NIPs to 2 mL of tetracycline solution, a working solution of tetracycline was obtained from a stock solution with a concentration of 10^{-3} mol L^{-1}. After agitating the mixture in shaker for 120 minutes, the materials were then separated with the help of a magnetic bar and passed through a polyester membrane with a pore size of 0.45 μm. After separating the remaining solution from the polymers, the concentration of adsorbed tetracycline in the supernatant solution was calculated. Fluorescence tests were conducted using the same

method. The fluorescence spectroscopy and the HPLC-UV methods were utilized in order to ascertain the amount of tetracycline that had been adsorbed

In the process of the adsorption studies, the percentage (%) of TC that were removed to initial solution (standard or sample) was calculated using the expression that is presented below[180]:

$$\text{Removal } (\%) = \frac{Co-Ce}{Co} \times 100 \ldots\ldots\ldots\ldots (3.1)$$

Where: C_e is the tetracycline antibiotic concentration after adsorption equilibrium time "t_e" at the maximum wavelength of remaining solution, and C_0 is the initial tetracycline antibiotic concentration.

The following equation was used to get the adsorption capacity Qe (mg g^{-1}) of the synthesized polymers.

$$Qe = \frac{(Ci-Ce)V}{m} \ldots\ldots\ldots\ldots\ldots (3.2)$$

In equation (3.2) of the equilibrium adsorption amount Q_e (mg g^{-1}), C_i represents the initial different concentrations of tetracycline (mol L^{-1}) before the adsorption experiments, C_e is the final concentration (mol L^{-1}) of TC solution after to attain the equilibrium time, V (mL) is the volume of tetracycline solution, and m (mg) is the weight of mag-MIP and mag-NIP. The binding experiment allowed to found the parameters to optimization of the tetracycline on the mag-MIP, such as Mass, equilibration time and concentration of analyte and while the pH parameter has been already defined in the literature[181].

The determination of the adsorption isotherm plays such an important role in the process of developing the nature of an adsorption system, thus, the implementation of one

isotherm model has been done. The Langmuir analysis was performed in order to analyse the data and Eq. (6) was utilized for the linearized Langmuir model[182]:

$$\frac{Ce}{qe} = \frac{1}{K1Qm} + \frac{Ce}{Qm} \dots\dots\dots\dots\dots\dots\dots (3.3)$$

Where: C_e is the equilibrium concentration of tetracycline (mg L^{-1}), q_e is the quantity (mg g^{-1}) of TC adsorbed, Q_m (mg g^{-1}) is adsorption capacity, and K_1 is Langmuir constants, reflecting adsorption capacity (mg g^{-1}).

In order to estimate the adsorption mechanism of the TC on the magnetic material, was used the pseudo-second-order equation, shown in Eq. (3.4).

$$\frac{t}{Qt} = \frac{1}{k2Qe2} + \frac{1}{Qe}\, t \dots\dots\dots\dots\dots\dots (3.4)$$

The value of Q_e (mg g^{-1}) or $Q_{120\ min}$ is the maximum amount of TC adsorbed on the mag-MIP and time (min) respectively, 1.0×10^{-5} mol L^{-1} concentration was used to investigate the adsorption of TC. k_2 is the pseudo-second-order adsorption equilibrium rate constant (mg g^{-1} min^{-1}). The plot of t/Q_t against t was used to determine the values of k_2 and Q_e. The rate constant (k_2), and correlation coefficients (R^2) values were calculated for the mag-MIP and mag–NIP, while the theoretical value of maximum adsorption capacity Q_e was calculated using the pseudo 2nd order kinetic equation.

3.3.2. Preparation of food samples

Honey was prepared a solution with a 30 mL of 0.01 mol L^{-1} phosphate buffer (pH 7) contained 1 grams of honey sample. After that, they were heated in a water bath at 50 °C for 10 min and then centrifuged at 4,000 rpm for 15 minutes, and filtered with filter paper. After heating the honey, a 1 mL sample was taken from the treated honey using a micro-pipette. In order to simplify the honey matrix prior to the dispersive solid phase extraction of tetracycline

residues, an ethanol wash is required. This is done in order to reduce the honey matrix's complexity[183-184]. Then added two different concentration levels (1.7×10^{-5}, and 2.5×10^{-5} mol L^{-1}) of tetracycline to honey sample.

To evaluate the mag-MIP adsorption capability, was used raw milk samples (cow) collected from a dairy in Araraquara. To prepare the raw milk samples, we used 2 mL of the milk and 1/2 mL of phosphate buffer as the dilution solution. The raw milk were centrifuged for 10 min at 15000 rpm, and the milky skin (fatty) was filtered out of the solution the filtration process was repeated 4 times. Then spiked tetracycline to raw milk sample at two distinct concentration levels (1.7×10^{-5} and 2.5×10^{-5} mol L^{-1}), further the addition of 10 mg of both mag-MIP and mag-NIP material (in separate 2 mL flasks), with shaking for 120 min, followed by filtration through a 0.45 m polyester membrane[185].

A 10 mL centrifuge tube with 10 mL of phosphate buffer (0.01 mol L^{-1} and pH 7) was filled with a 500 mg egg sample and by vigorously squeezing it with our hands, we were able to get the egg's texture to a uniform state. A 10-minute ultrasonic bath was used after which the mixture was centrifuged at 15000 rpm for 5 minutes and 4-times filtered via filter paper. The tetracycline was spiked at two different concentration levels (1.7×10^{-5} and 2.5×10^{-5} mol L^{-1}) to egg samples. Then the analysis proceeds using 10 mg of mag-MIP and mag-NIP in the volume of 2 mL solutions.

3.4. Synthesis of magnetic molecular imprinted polymer for electrochemical sensor

The core (Fe_3O_4@SiO_2-MPS) of this material was synthesized in accordance with the section 3.3. To the shell (MIP) the polymerization was carried out using tetracycline as analyte (2.5×10^{-4} mol) and acrylic acid (AA) as the functional monomer (3.0×10^{-3} mol) in an ethanol/methanol solvent mixture at a 30% v/v ratio, respectively.

Previously, in order to obtain the optimal interaction between the functional monomer (AA) and the template molecule, computational studies were carried out using density functional theory (DFT), as previously reported in the literature[185].

The AA + TC mixture was reacting for 24 hours. This reaction system was kept at room temperature with constant agitation. The reaction solution was stirred for the first six hours while 3.0×10^{-2} mol of EGDMA, which is a crosslinking agent, and 0.050 mmol of ABIN, which is a radical initiator, were added in an atmosphere of N_2, followed by the addition of 200 mg of modified Fe_3O_4@SiO_2-MPS nanoparticles. It took 24 hours of reaction time at 60 ^oC to get the final product. The final representation of the synthesis of this material (mag-MIP) is showing below in **Figure 6.**[138]

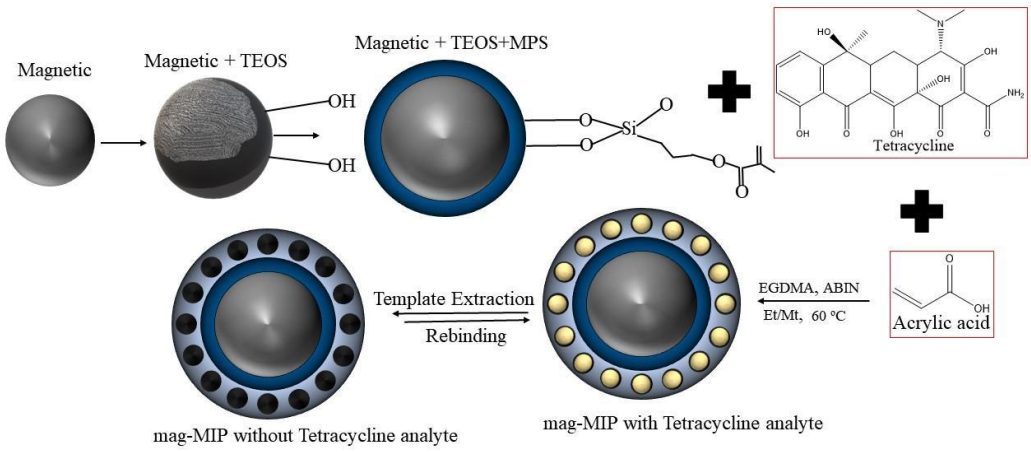

Figure 6. A detailed illustration of the production process for mag -MIP (Fe_3O_4@MIP)

Source: As per the policy of Elsevier article`s author no need to get permission[138].

To generate cavities and eliminate any unreacted chemicals, the final products were washed for five days in a 9:1 (v/v) methanol: acetic acid solution **(Figure 7).**

The mag- polymer materials (final material) was dried in an oven at 60 ºC. Similar methods were used to create the magnetic non-molecularly imprinted polymer without tetracycline.

Figure 7. Soxhlet system for removal of analyte from mag-MIP Source: Author

3.4.1. Modified carbon paste-MIP electrode construction

To ensure a uniform mixture, 15 mg of mag-MIP or 15 mg of mag-NIP, and 85 mg of graphite powder were consistently mixed using 1 mL of deionized water. To dehydrate the paste, it was left at room temperature for 12 hours after being mixed properly for approximately 20 minutes using spatula. In order to create the working paste (carbon paste electrode), a quantity of 80 µL of mineral oil was dripped into the mixture drop-by-drop.

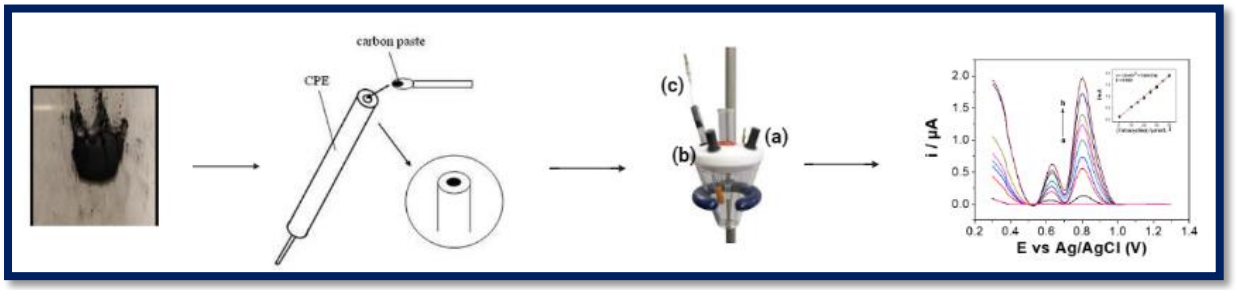

Figure 8. Depicts a carbon paste electrode in conjunction with mag-MIP carbon paste in glass reactor (a) carbon paste mag-MIP (b) Counter electrode (c) Reference electrode. Source: Author

The synthesized materials were named mag-MIP carbon paste electrode and mag-NIP carbon paste electrode. The sensor was fine-tuned in accordance with the author's published work[186]. The electrochemical sensor setup presents in **Figure 8.**

3.4.2. Electrochemical Analysis

To make the stock solution of tetracycline, we used 75% deionized water (Milli-Q Direct-0.3 Millipore), and mixed it with 25% ethanol in a 100 mL flask. The final concentration was 1.0×10^{-3} mol L^{-1}. Sonication of the solution continued for a further ten minutes.

All measurements were done in a conventional three-electrodes of 10 mL electrochemical cell, using as reference electrode a Ag/AgCl/KClsat, a platinum wire was utilized as an auxiliary electrode, and modified carbon paste was used as a working electrode in the electrochemical cell (**Figure 9)**.

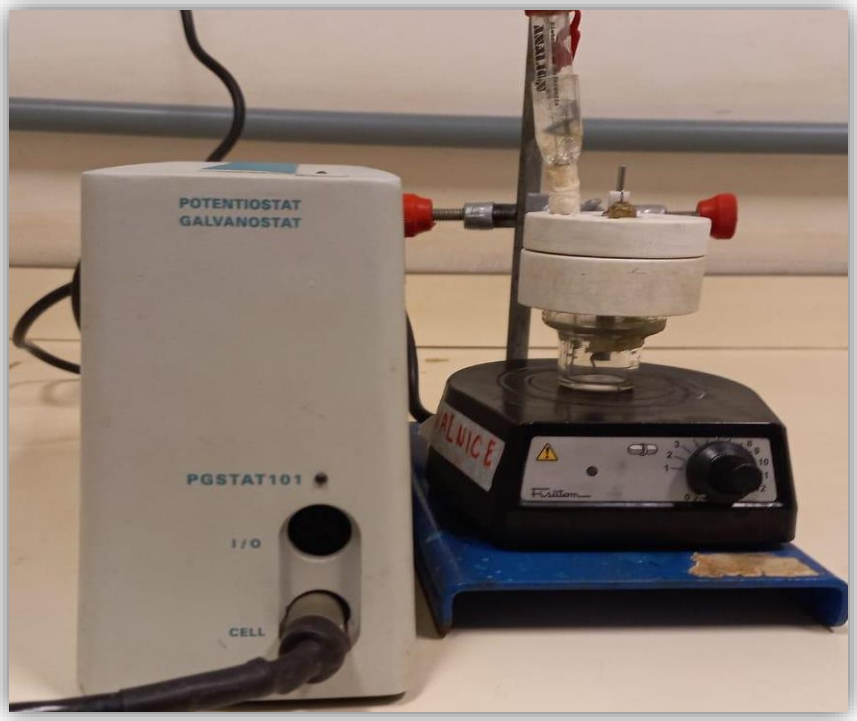

Figure 9. The photography depicts the batch electrochemical measurements that carried in electrochemical cell, which include typical three electrodes setup as well Source: Author

The voltammetric measurements were controlled by the NOVA 2.2 software and performed with an Autolab® potentiostat model (Autolab type III, Autolab/Eco Chemie). The electrochemical parameters that were used, after optimization, are listed in **Table 4.**

Table 4 Electrochemical parameters optimized to tetracycline measurements.

Parameters	Optimized values
Step potential (mV)	0.005 mV
Modulation amplitude (mV)	0.075 mV
Frequency (Hz)	10 Hz
Applied potential range (V)	0.2-1.4 V

Source: Electrochemical parameters used by author in research work.

3.4.3. Sensor Interference studies

Several antibiotics were evaluated with a tetracycline solution to determine which ones caused the most interference, including penicillin, hydrochlorothiazide, metronidazole, uric acid, captopril, minocycline, and doxycycline **(Table 5)**, at a molar ratio of 1:1 (for each concentration of 1.5×10^{-5} mol L^{-1} tetracycline).

Table 5. Structure and molar mass of non-related compounds used in the analysis of selectivity.

Nº	Structure of compounds	Molar Mass (g mol^{-1})
1	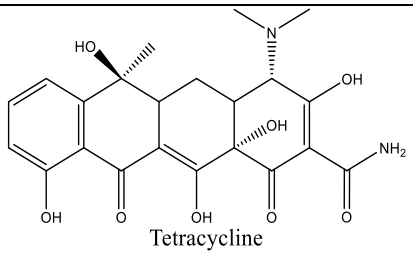 Tetracycline	444.435
2	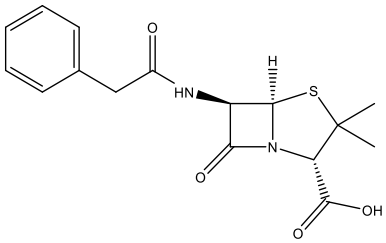 Penicillin	334.4
3	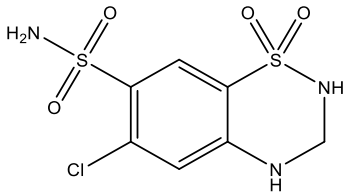 Hydrochlorothiazide	297.741
4	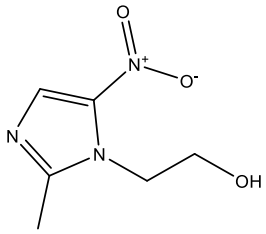 Metronidazole	171.16
5	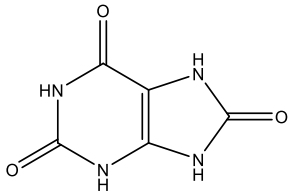 uric acid	168.11
6	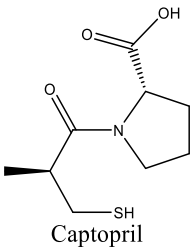 Captopril	217.29

7	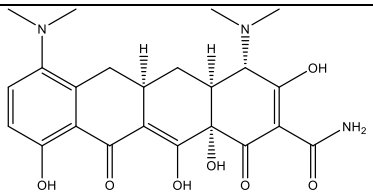 Minocycline	457.47
8	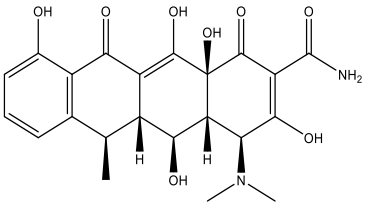 Doxycycline	444.4
9	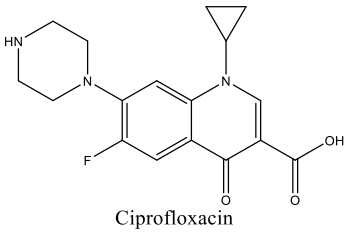 Ciprofloxacin	331.346
10	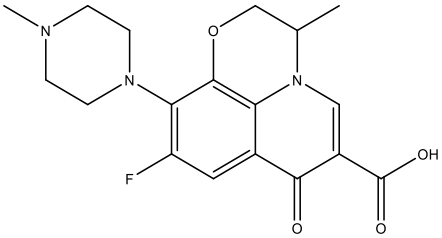 Ofloxacin	361.368

Source: All compounds were used in experiments by author.

3.4.4. Preparation of the real sample for the conduct of analysis using the sensor

Evaluation of the magnetic polymer materials was done using samples of skimmed, whole, and raw milk. The actual milk samples were made by centrifuging 4.5 mL of milk at 15000 rpm for 10 minutes. Two layers formed as a result: a heavy fat layer and a liquid layer. A micropipette was used to collect the milk's liquid layer, which was then filtered through a 0.45 µm polyester membrane. 0.1 mol L^{-1} phosphate buffer pH 7 was used to prepare tetracycline solutions 2.0 $\times 10^{-5}$ and 5.0×10^{-6} mol L^{-1} and then added to the filtered milk.

3.5. Characterizations

In the characterization section, the synthesized materials were evaluated via various techniques like scanning electron microscopy (SEM), infrared spectroscopy with Fourier transform (FTIR), and transmission electron microscopy (TEM). These techniques give information about the structure of materials, size, and functional groups which were used in the preparation of materials. The transmission electron microscopy evaluated the formation about the core@shell material. The instrumental analysis is also discussed in the followed sections.

It is essential to note that despite the fact that this section is described here, as well as Chapter 4 and Chapter 5, the findings achieved with the mag-MIP that was synthesized will be presented before those chapters.

3.5.1. Scanning electron microscopy

SEM creates images by scanning a concentrated beam of electrons across a surface. Electrons from the beam strike the material, generating signals display the surface's structure and composition. Scanning electron microscopy (Model: JSM-7500F) was used to examine the surface morphologies of changed materials (mag-MIP and mag-NIP). Gold was used in (SEM) to cover the analysed materials (mag-MIP and NIP), and a 2.0 kV accelerating voltage was applied during microscopy.

3.5.2. Infrared spectroscopy (Fourier transform)

Solid, liquid, and gaseous samples can all be investigated via infrared spectrum using the Fourier transform infrared spectroscopy (FTIR) method. The FTIR–Vertex 70 spectrometer by Bruker Shimadzu (Japan) with a spectrum range of 4000 to 400 cm^{-1} was used to analyse

the different functional groups of the prepared materials. The pellets were manufactured using a Perkin-Elmer press (7 tons), and diluting the sample of interest in KBr, in the proportion of 1:100.

3.5.3. Transmission electron microscopy

High-resolution transmission electron microscopy (TEM) reveals the structure, size distribution, and shape of nanoparticles composed of fatty acids and proteins, in addition to the hard nanoparticles formed of metallic particles, carbon, or plastics. The high-resolution transmission electron microscope HR-TEM (Philips-model CM200 super twin with a resolution of 1.9 A) was used for the TEM study.

Chapter 4

4. Results and Discussions

4.1 Adsorption study of mag-MIP

In this Chapter, will be discuss about the application of the magnetic molecular imprinted polymers (mag-MIP) synthesized in the **section 3.3** (Chapter 3), which were evaluated using HPLC and fluoresce spectroscopy.

This chapter have also, presented the surface structure, information about core@shell magnetic materials and the functional groups which were employed in the synthesis of materials.

4.2. Characterization studies

Scanning electron microscopy (SEM) was used to examine the surface morphologies of mag-MIP and mag-NIP and demonstrated differences between the two materials. The images from the micrographs indicated that the mag-MIP was composed of sphere-shaped particles **(Figure 10 (A-B))**, it has a greater porosity when contrasted with the mag-NIP.

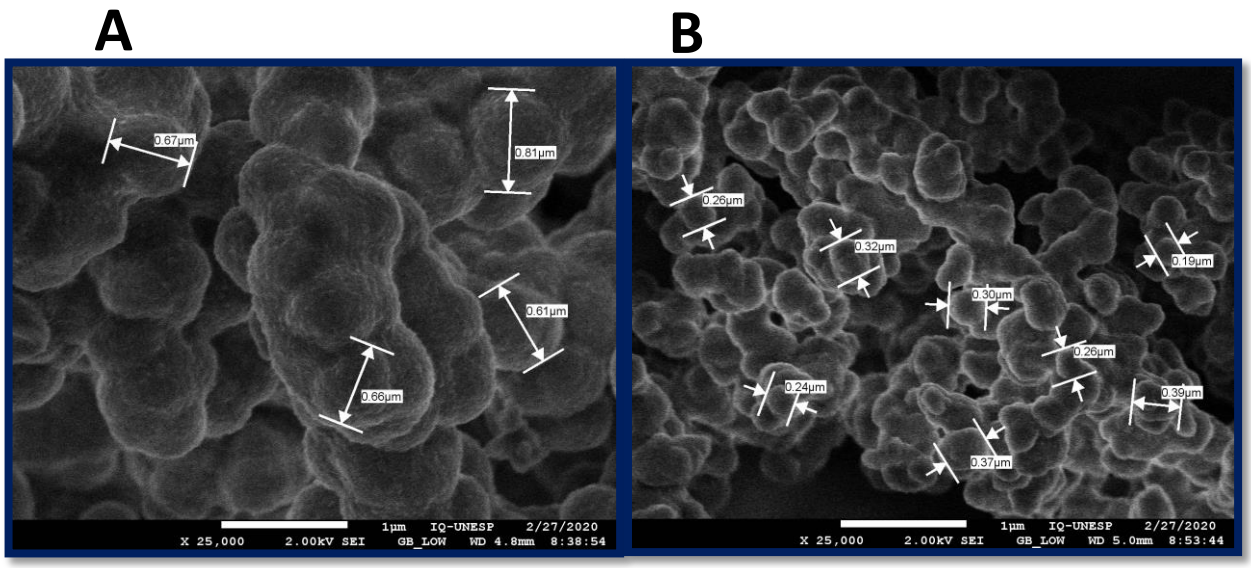

Figure 10. (A-B) SEM image (A) mag-MIP and (B) mag-NIP. Source: Author

According to the amplification of 30,000 times, it was found that the mag-NIP particles were significantly smaller in size when compared to the mag-MIP particles. The surface of the produced mag-MIP displayed improved sites and a unique structure with a micro-spherical shape for the recognition of the target compound. The mag-MIP and the NIP both exhibit particles that are homogenous[187]. In addition, the surface had a rougher texture, which provided a greater surface area. The imprinted materials capture target molecules via selective recognition sites in rebinding studies because of better analyte removal from mag-MIP.

Additionally, TEM analysis revealed magnetic nanoparticles to be spherical in shape, with a diameter of about 20 nm. **Figure 11 (A-B)** clearly shows that the core-shell structure of mag-MIPs was effectively fabricated (various resolution), as shown.

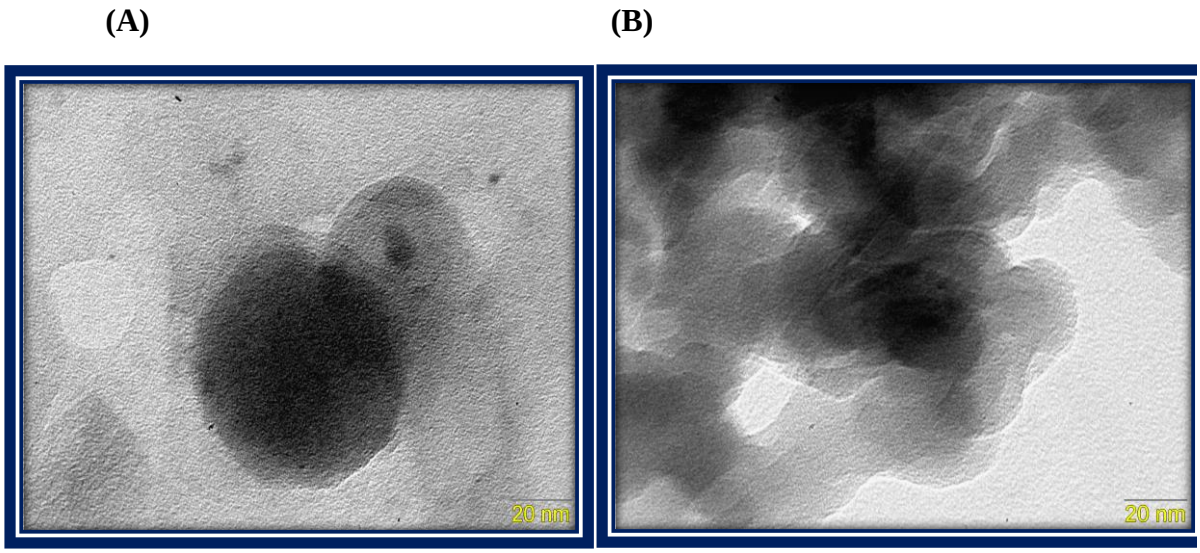

Figure 11. TEM images of the modified (A) mag-MIP, (B) mag-NIP Source: Author

Since the SiO_2-MIP shell uniformly coats the Fe_3O_4 dark core as present in the above image. The large active area of the target molecule was aided by their compact size, which allowed for more recognition sites and a better adsorption capacity. Transmission

electron micrographs of mag-NIPs show aggregates of nanoparticles **(Figure 11B)**, from which it is possible to clearly distinguish a relatively large mesosphere of aggregates, which is the evidence of core@shell shape of mag-NIP.

Mag-MIP, mag-NIP, ethylene-glycol-dimethacrylate (EGDMA), and tetracycline were all polymerized using different functional groups, as illustrated in **Figures 12**. Red (mag-MIP) and blue (mag-NIP) 540 cm^{-1} spectra show the Fe-O group's characteristics, which are pertinent to the Fe_3O_4 magnetic nanoparticles.

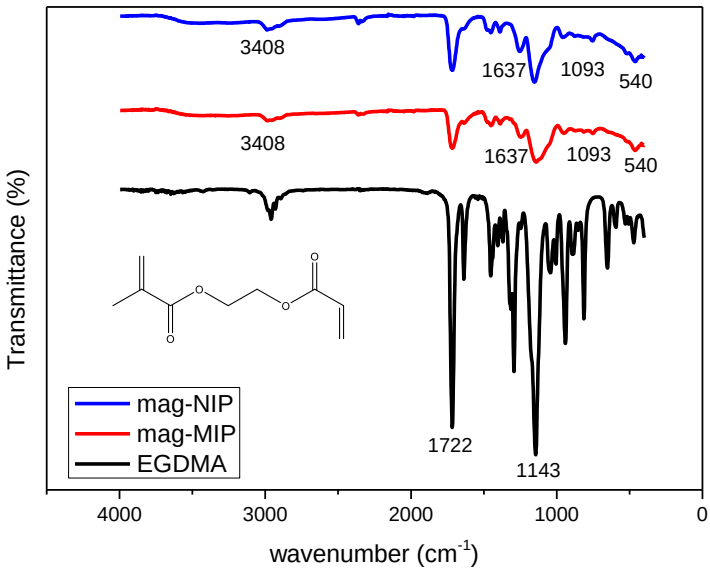

Figure 12. FTIR spectra of (red): mag-MIP, (blue): mag-NIP, and (black): EGDMA (black)
Source: Author of the work.

The peak at 1093 cm^{-1} is assigned to the Si-O-Si group and indicates that silanization has proceeded. The 3408 cm^{-1} bands can be associated with the TEOS used in the production of the magnetic nano-scale materials, which represents the Si-OH group. The EGDMA cross-linker agent's spectra are also shown in **Figure 12** (Black). When the FTIR method is applied, both the mag-MIP and the mag-NIP are distinguished by the presence of the cross-linker EGDMA, which exhibits itself as two significant peaks. The characteristic bands of the ester group at 1722 and 1143 cm^{-1}, which are related to the carbonyl stretch (C=O) and the

(CO-) bond, respectively, can be seen in the EGDMA spectrum, providing conclusive evidence that both the mag-MIP and mag-NIP are composed by this structural monomer.[159] In synthesized mag-MIPs, the C=C signal is found to be weaker at 1637 cm^{-1}, indicating that the EGDMA atoms are polymerized and cross-linked

4.3. Quantification of tetracycline using HPLC instrument

4.3.1. Construction of the analytical curve

Initially, the analytical curves from HPLC were plotted in the TC standard solutions at different concentrations, between 1.0 $\times 10^{-5}$ to 8.0 $\times 10^{-5}$ mol L^{-1}). The samples were collected in vials made of glass, and they were analysed using high-performance liquid chromatography (HPLC) at wavelengths of 350 nm. The profile of analytical curve present in **Figure 13.**

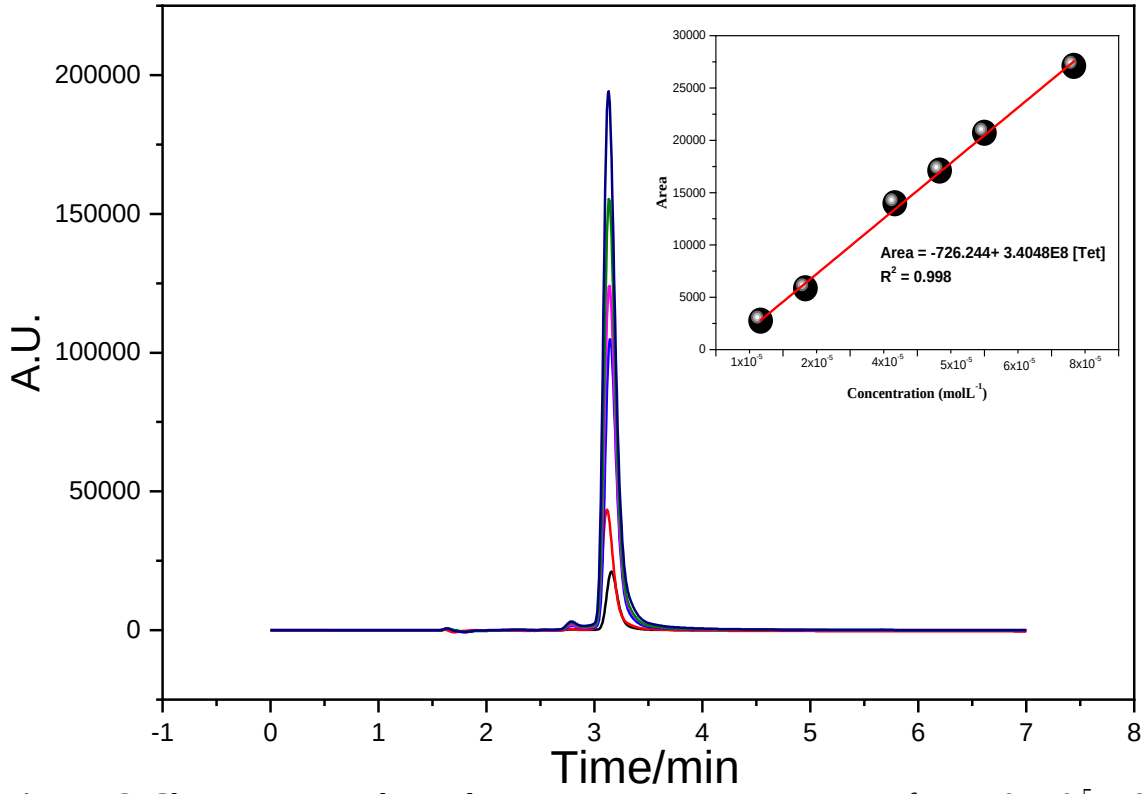

Figure 13. Chromatograms obtained to various concentrations ranges from 1.0 $\times 10^{-5}$ to 8.0 $\times 10^{-5}$ mol L^{-1}. Solvent: phosphate buffer (0.01 mol L^{-1}, pH = 7). Conditions: mobile phase was a mixture of methanol, oxalic acid (0.01 mol L^{-1}), and acetonitrile (10:70:20 v/v, respectively) with a flow rate of 1.0 mL per minute. Inset: Shows the corresponding analytical curve. Source: Author of the work.

The time were graphed against the concentrations (mol L^{-1}), and insert in **Figure 13**. A linear plot was obtained using the concentration range, and it had a coefficient of determination (R^2) of 0.998, a slope of 3.40×10^{8}, and an intercept of -728.244.

4.3.2. Effect of mass dosage on adsorption of mag-MIP and mag-NIP

Mag-MIP or mag-NIP masses of 2, 4, 6, 8, 10, and 12 mg were tested to see how they affected the adsorption of tetracycline from the solution. **Figure 14** shows that when the polymer mass grew from 2 to 12 mg, adsorption increased initially. After an 8 mg dosage of mag-MIP, the removal (%) of tetracycline antibiotics is constant because the surface adsorbent has become saturated and the mag-polymer can no longer capture the analyte from the solution.

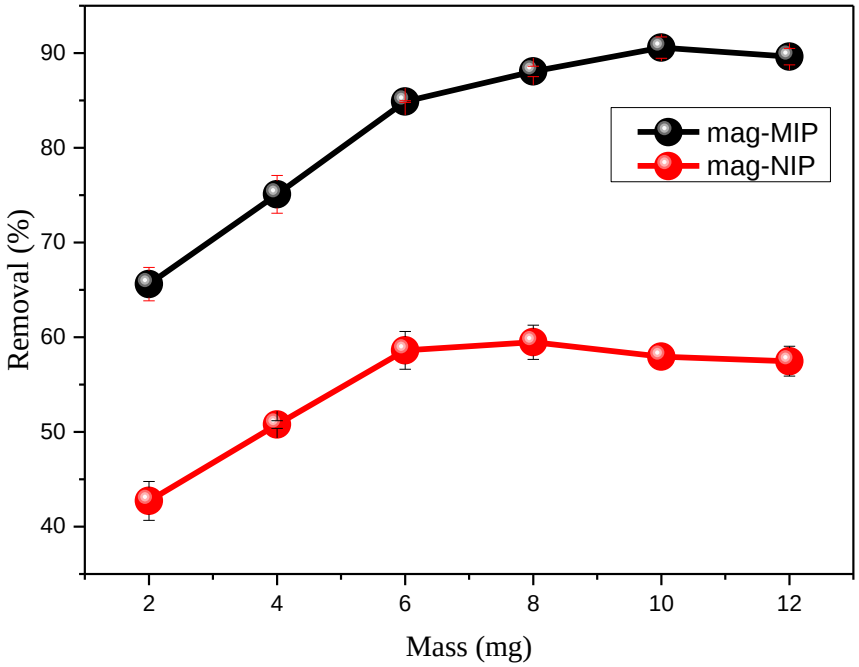

Figure 14. Mass of adsorbent affects tetracycline adsorption. Conditions: volume: 2.0 mL, solvent: phosphate buffer (0.01 mol L^{-1}, pH = 7), Time of adsorption: 5 h. Concentration: 1.0×10^{-5} mol L^{-1}, n= 2, Source: Author of the work

As can be seen from the differences in the tetracycline removal (%) between the imprinted (mag-MIP) and control polymers (mag-NIP), evaluate the imprinting ability and the specificity of the prepared imprinted particles. The polymer dosage was maintained throughout

the remaining studies at 10 mg. Although, employing this quantity yielded the highest removal (%), which was observed to be 90 (%) in 5 hours.

4.3.3. Time effect on tetracycline

The study examined how the time of contact affected the amount of tetracycline that was adsorbed. **Figure 15** illustrates the evolution of adsorption with time. Adsorption was rapid for the first 120 minutes, then progressed steadily. According to the graph, the quantity of tetracycline that can be adsorbed onto mag-MIP in 5 minutes is 0.61 mg g^{-1}, while the amount that can be adsorbed onto mag-NIP is just 0.05 mg g^{-1}. As the control polymers (mag-NIP) do not have a stronger affinity for the tetracycline molecules, the magnetic-NIP is unable to absorb the target compound in comparison to mag-MIP.

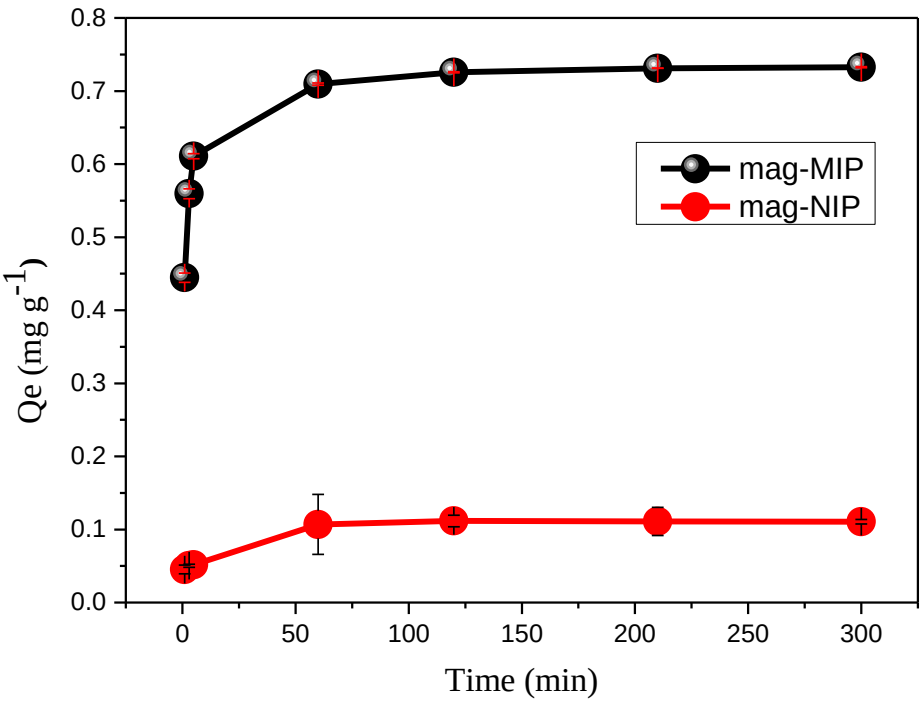

Figure 15. Adsorption capacity vs Time (min) on mag-MIP and mag-NIP, Conditions: mass: 10 mg, volume: 2.0 mL, solvent: phosphate buffer (0.01 mol L^{-1}, pH = 7), concentration (1×10^{-5} mol L^{-1}). n = 2 Source: Author of the work.

Tetracycline's quick intake from solution (up to 120 minutes) due to exposed more binding sites of materials, while the slower sorption phase was likely due to interior binding sites. After 120 minutes the adsorption process is not proceeded properly, and almost it become constant, because there are no more cavities left on the surface of synthesized materials for the tetracycline molecules, as the adsorption proceeds, the sites get saturated and the adsorption rate reduces. The tetracycline adsorption capacity of mag-MIPs is greater than that of mag-NIPs because of their more cavities on the surface area.

4.3.4. Adsorption kinetic

The pseudo-second-order equations were used to analyse the kinetic of tetracycline adsorption on mag-MIP and mag-NIP[182]

The pseudo-second-order equation is shows in Eq. (4.1):

$$\frac{t}{qt} = \frac{1}{k2qe2} + \frac{1}{qe}\, t \ldots\ldots\ldots (4.1)$$

The value of q_e (mg g^{-1}) or $Q_{120\ min}$ **(Figure 15)** is the maximum amount of tetracycline adsorbed on the mag-MIP and time (min) respectively. 1.0×10^{-5} mol L^{-1} concentration was used to investigate the adsorption of tetracycline. k_2 is the pseudo-second-order adsorption equilibrium rate constant (mg g^{-1} min^{-1}). The pseudo-second-order kinetics model is depicted in **Figure 16**.

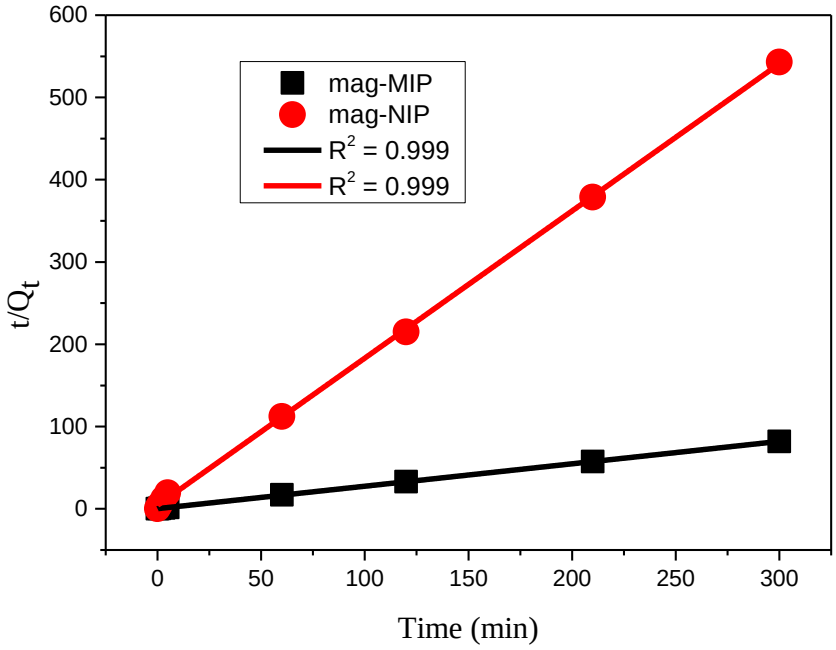

Figure 16. Pseudo 2nd order kinetic model employed for the tetracycline adsorption on mag-MIP and mag-NIP, Conditions: mass: 10 mg, volume: 2.0 mL, solvent: phosphate buffer (0.01 mol L^{-1}, pH = 7). Concentration: 1.0×10^{-5} mol L^{-1}. Source: Author

The plot of t/Q_t against t was used to determine the values of k_2 and q_e. The rate constant (k_2), and correlation coefficients (R^2) values were calculated for the mag-MIP and mag–NIP, while the theoretical value of maximum adsorption capacity Q_e was calculated using the Pseudo 2nd order kinetic equation **(Table 6)**. The theoretical value of maximum adsorption capacity Q_e (mag-MIP: 0.734 mg g^{-1}) is close to the value obtained from experimental data Q_e (mag-MIP: 0.732 mg g^{-1}), presented above **(Figure 16)**.

Table 6 Pseudo-2nd order kinetic model obtained through experimental values

	Slope	R^2	Q_e (mg g^{-1})	K_2 (mg g^{-1} min^{-1})
mag-MIP	0.2724	0.999	0.734	0.422
mag-NIP	1.7887	0.999	0.112	3.69×10^{-04}

Source: Author of the work

4.3.5. Concentration effect of TC in the adsorption on mag-MIP

Mag-MIP and mag-NIP adsorption was studied by conducting experiments with a fixed adsorbent dosage of 10 mg at various initial concentrations (Ci). It is possible to see in **Figure 17**, that when tetracycline concentration rises, the adsorption increases because there are many sites available on the surface. However, after that, the sorption capacity falls slightly because of saturation of the adsorption sites with tetracycline molecules

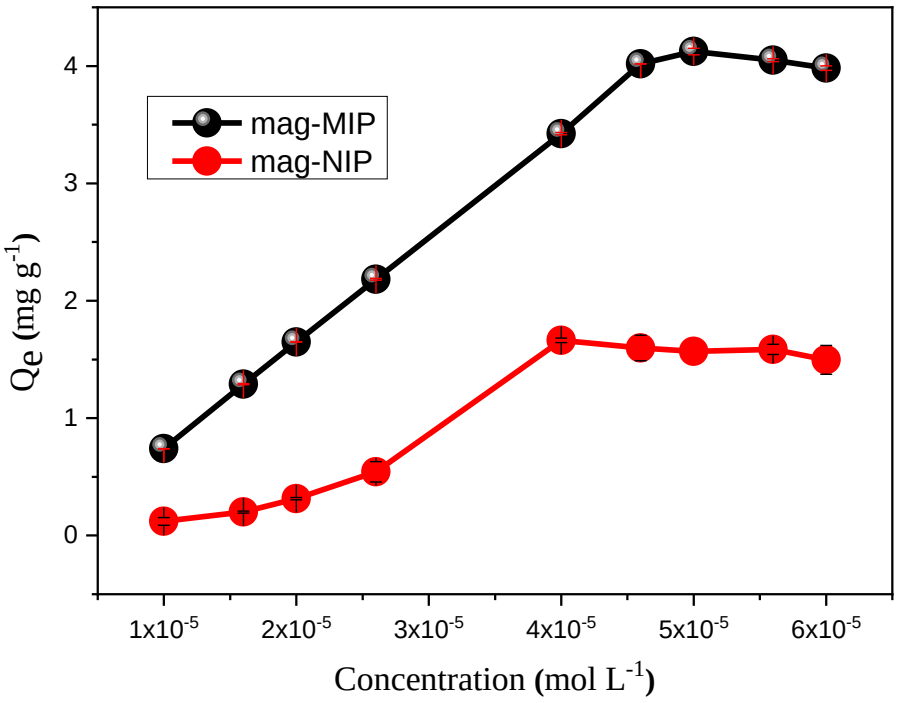

Figure 17. Tetracycline binding ability to mag-MIP and mag-NIP at various initial concentrations (1.0×10^{-5} – 6.0×10^{-5} mol L^{-1}). Conditions: adsorbent mass: 10 mg, volume: 2.0 mL, solvent: phosphate buffer (0.01 mol L^{-1} pH = 7), adsorption time: 120 minutes.
Source Author of the work

At a concentration of 5.0×10^{-5} mol L^{-1}, mag-MIP achieves its maximum adsorption capacity of (Q_e = 4.123 mg g^{-1}). Mag-MIP adsorbed a greater amount of tetracycline than the mag-NIP, indicating that imprinted cavities shaped as a result of the satisfactory reaction between functional monomer and template (TC). Eq (4.2) is used to calculate the binding capacity:

$$Qe = \frac{(Ci - Co)V}{m} \ldots\ldots\ldots\ldots\ldots (4.2)$$

In equation, Q_e is the equilibrium adsorption amount (mg g^{-1}), C_i = initial different concentrations of tetracycline (mol L^{-1}), C_e is the final (at equilibrium) concentration (mol L^{-1}) of tetracycline in remaining solutions, V (mL) is the total volume used in the D-SPE experiment, and m (mg) is the weight of mag-MIP and mag-NIP used in the D-SPE experiments.

The determination of the adsorption isotherm profile plays an important role in the process of developing the nature of an adsorption system. The linearized Langmuir model (Eq. 4.3) was using in order to analyse the experimental data obtained.

$$\frac{Ce}{qe} = \frac{1}{K_1\, Q_{max}} + \frac{C_e}{Q_e} \ldots\ldots\ldots\ldots\ldots\ldots\ldots (4.3)$$

In **equation (10)**, C_e is the equilibrium concentration tetracycline (mg L^{-1}), q_e is the quantity (mg g^{-1}) of tetracycline adsorbed, Q_{max} (mg g^{-1}) is adsorption capacity, and K_1 is Langmuir constants, reflecting adsorption capacity (mg g^{-1}) [188]. **Figure 18** shows C_e/q_e plotted against C_e. A linear plot reveals a slope of 117857.24, a value for the intercept of 0.033, and a coefficient of determination (R^2) value of 0.995.

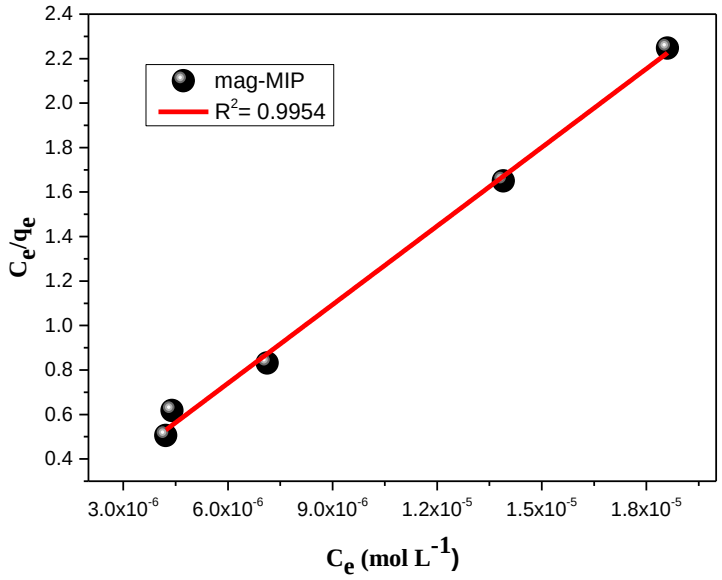

Figure 18. Tetracycline adsorption onto mag-MIP materials is predicted by the Langmuir model. Source: Author of the work

Assuming that a monolayer forms on the adsorbent's surface, as Langmuir's model does, one tetracycline molecule can be adsorbed per adsorption site, and the intermolecular forces diminish with increasing distance. The following **equation (4.4)** describes the key aspects of the Langmuir isotherm in terms of a dimensionless constant called separation factor (RL)[189]

$$RL = {}^{1}/_{1 + K1Co} \ldots\ldots\ldots\ldots\ldots (4.4)$$

Above in **equation (4.4)** C_o (mol L^{-1}) is the initial concentration of the analyte, and K1 is the Langmuir constant ($L.mg^{-1}$) associated with adsorption capacity. The value of separation factor RL represents the Isotherms can have an unfavourable (RL > 1), linear (RL = 1), favourable (0 < RL > 1), or irreversible (RL = 0) shape. The current experimental findings, which were computed using the aforementioned **equation (4.4)**, reveal that (Separation factor (RL) = 1.00), indicating linear nature of the isotherm. Isotherm data were successfully fitted with the Langmuir model, as depicted in **Figure 18.**

Figure 19, shows the isotherm of mag-NIP linear plot, the slope of linear curve is 339405.08 and intercept is 0.306 and coefficient of determination (R^2) value of 0.991. All calculated values from the slopes and intercepts of the plots, are shown in **Table 7.**

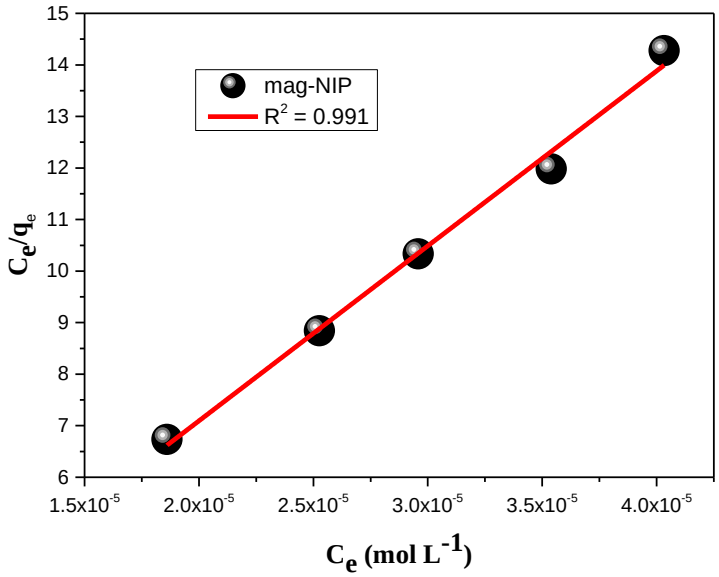

Figure 19. Tetracycline adsorption onto mag-NIP materials is predicted by the Langmuir model. Source: Author of the work

Table 7 displays the results **(mag-MIP)** and **(mag-NIP)** of calculating the Langmuir: maximum adsorption capacity Q_{max} (mg g^{-1}) = 30.303 for mag-MIP and 3.27 for mag-NIP, RL = 1.00 value same for both mag-MIP and control polymer, where it was determined that the K1 (L mg^{-1}) for mag-MIP is 0.0002, whereas the K1 for mag-NIP is 2.95×10^{-6}.

Table 7. Experimental results were based on Langmuir isotherm models.

	Slope	R_L	Q_{max} (mg g^{-1})	K_1 (L mg^{-1})
mag-MIP	117857.24	1.00	30.303	0.0002
mag-NIP	339405.08	1.00	3.27	2.95×10^{-6}

Source: Author of the work

4.3.6. Temkin Isotherm

Due to adsorbate-adsorbent interactions, the Temkin isotherm equation predicts that the heat of adsorption for all molecules in a layer will drop linearly with coverage, assuming that the bond energies in the adsorption are distributed uniformly up to a maximum binding energy[190]. A mathematical expression for the Temkin isotherm is:

$$qe = BlnA + BlnC_e \ldots\ldots\ldots\ldots\ldots\ldots (4.5)$$

Where B = RT/b represent heat of adsorption, T is the absolute temperature in kelvin, R is universal constant 1/b represents the adsorption capacity of the adsorbent and kt (L/mg) is the binding constant at equilibrium with the maximum binding energy. Isotherm constants kt and B can be calculated from a plot of qe vs ln Ce.

The Temkin isotherm model of the mag-MIP is depicted in **Figure 20**, There is a linear relationship between the ln(C_e) and the adsorption capacity (qe). The slope of the linear graph is 3.736 and the intercept is -1.17617.

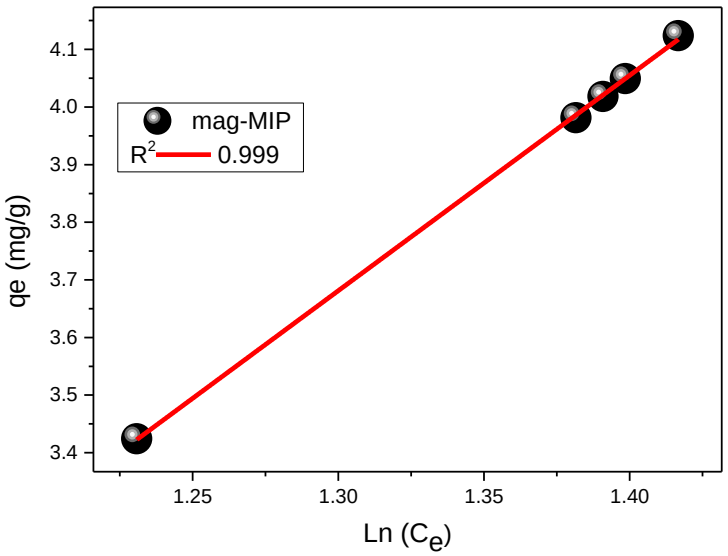

Figure 20. Tetracycline adsorption onto mag-MIP is predicted by Temkin isotherm

Figure 21 shows the Temkin isotherm model of the mag-NIP in materials. There is a linear relationship between the ln(C_e) and the adsorption capacity (qe). The slope of the linear graph is 15.499 and the intercept is -26.548.

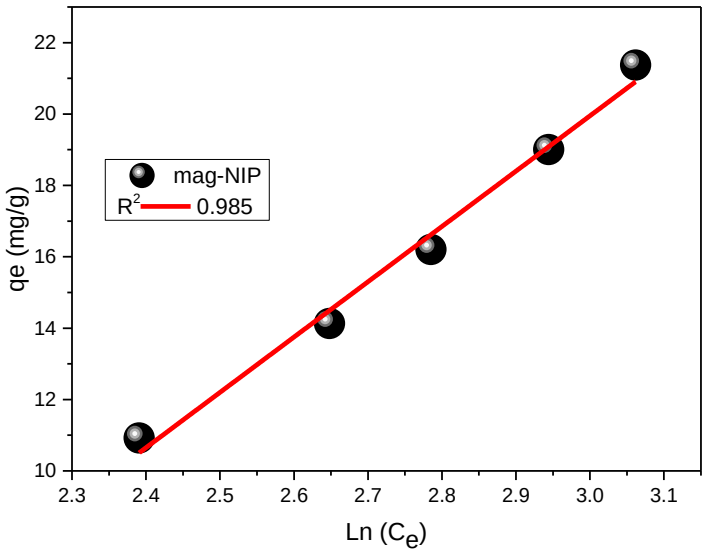

Figure 21. Tetracycline adsorption onto mag-NIP is predicted by Temkin isotherm

Table 8 Theoretical results were based on Temkin isotherm of mag-MIP and NIP

	Slope	Intercept	B_T (J mol^{-1})	K_T (L mg^{-1})
Mag-MIP	3.73648	-1.17617	3.73648	0.7299493
Mag-NIP	15.4993	-26.5482	15.4993	0.180348

Source: Author of the work

From the **Table 8**, values were estimated: K_T (equilibrium binding constant) = mag-MIP = 0.7299493, mag-NIP = 0.180348 L mg^{-1}, B_T (Temkin constant corresponding to the heat of adsorption) = mag-MIP 3.73648, and mag-NIP = 15.4993 J mol^{-1} signifying a physical adsorption process as indicated by the heat of sorption.

4.3.7. Interference Study

Competitive adsorption studies were conducted in the presence of additional molecules with similar and different structures of the tetracycline antibiotics in order to verify the formation of selective cavities on the mag-MIP surface. Antibiotics were the compounds that were utilized in such experiments as captopril, ciprofloxacin, doxycycline, metronidazole, and ofloxacin, their structure presents in above **section 3.4.3 (Table 5)**. **Figure 22** illustrates the data that were achieved from the experiment.

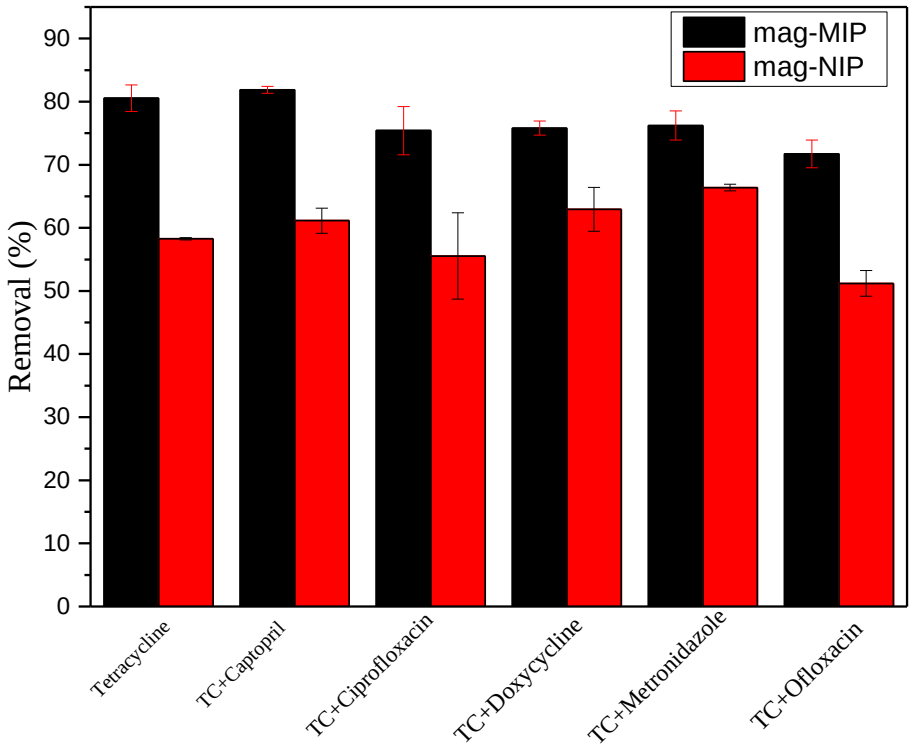

Figure 22. Profiles of the retention of several antibiotics (Con: 1.0×10^{-5} mol L^{-1}) on the mag-MIP and mag- NIP, using phosphate buffer (0.01 mol L-1) as a solvent medium (pH = 7), Time: 120 minutes. Source: Author of the work

The interference parameter was studied in the molar ratio of 1:1 (for each concentration of 1.0×10^{-5} mol L^{-1} of tetracycline). When the proposed imprinted polymer was evaluated in

the presence of several compounds with chemical structures similar to tetracycline, the proposed mag-MIP materials showed good selectivity. Adding interfering substances did not have any effect on the removal (%), as shown by these results, indicating that the magnetic imprinted materials had excellent selectivity. Doxycycline, being a member of the tetracycline class, has a strong affinity for mag-MIP without interfering with its function. However, when compared to mag-MIP, mag-NIP has a lower rate of elimination (%). For the reason that the mag-surface NIP's voids make them structurally unlike the mag-MIP, due to the unpresented cavities. Consequently, mag-NIP is not particularly selective and has little affinity for its intended targets.

4.4. Studies carried out used fluorescence spectrometry like a quantification method of TC

The fluorescence analysis to quantify the tetracycline in the adsorption experiments through D-SPE was carried out since this antibiotic has fluorescence characteristics. This section described the experiments and their responses using this analytical technique using parameters previously optimized in the section 4.2.

4.4.1. Construction of the analytical curve

Optimized parameters, such as wavelength (λ = 350 nm) and 0.01 mol L^{-1} phosphate buffer (pH = 7), were used to construct the fluorescence analytical curve shown in **Figure 24.** The linear plot was created using the concentration range of 1.0×10^{-5} to 8.0×10^{-5} mol L^{-1}. **(Figure 23)**

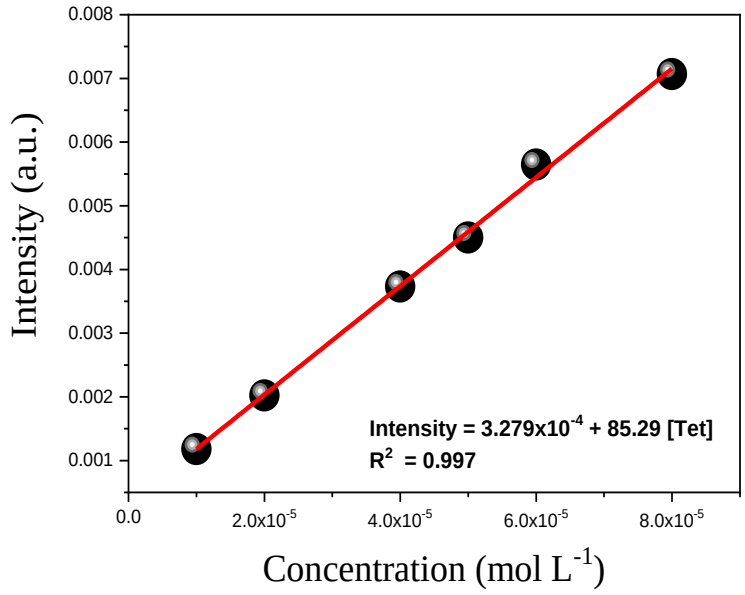

Figure 23. Fluorescence analytical curve obtained in 0.01 mol L^{-1} phosphate buffer (pH = 7), tetracycline concentrations range from 1.0 × 10^{-5} to 8.0 × 10^{-5} mol L^{-1}, ($\lambda_{excitation}$ = 350 nm, $\lambda_{emission}$ = 550 nm), wavelength range of 400-650 nm. Source: Author of the work

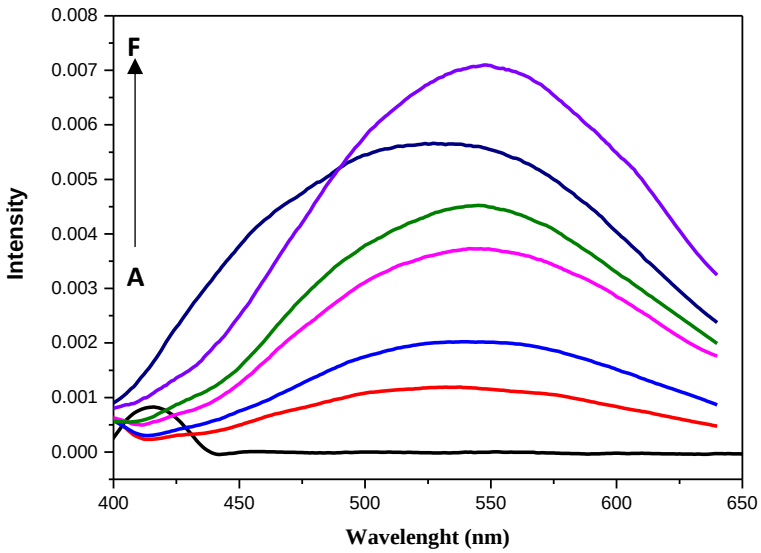

Figure 24 Fluorescence spectra obtained in 0.01 mol L^{-1} phosphate buffer (pH = 7), tetracycline concentrations range from (A) Blank, (B) 1.0 × 10^{-5} to (F) 8.0 × 10^{-5} mol L^{-1}, ($\lambda_{excitation}$ = 350, $\lambda_{emission}$ = 550), wavelength range of 400-650 nm. Source: Author

The signal intensity of the fluorescence enhances as the concentration of tetracycline increases from 1.0 × 10^{-5} to 8.0 × 10^{-5} mol L^{-1} **(Figure 23)**. The concentration range yielded a linear plot with a coefficient of determination (R^2) of 0.997. The spectra were recorded in the

wavelength range of 400-650 nm with maximum wavelength emission 550 nm **(Figure 24)**. When the concentration is raised, there is a corresponding rise in the fluorescence intensity. To optimize the maximum excitation wavelength (nm), an Agilent Cary 60 spectrophotometer was used to take spectrophotometric (UV-vis) readings. Maximum excitation wavelength was found at 350 nm. At pH 7, a buffer solution of 0.01 mol L^{-1} was utilized at the same concentration (1×10^{-5} mol L^{-1}) for the optimization. Antibiotic tetracycline is an example of a traditional intrinsic auto-fluorescent antibiotic, in the process of auto-fluorescence (AF), light in the UV-visible, near-IR spectral range is emitted by compound after being activated by light of an appropriate wavelength[191].

4.4.2. Concentration effect of TC in the adsorption on mag-MIP and mag-NIP

A fixed adsorbent dosage of 10 mg was used to evaluate the effect of the different tetracycline concentrations on the fluorescence intensity at different initial concentrations. As can be observed in Figure 25, a rise in the initial concentration of tetracycline led to an increase in the fluorescence intensity.

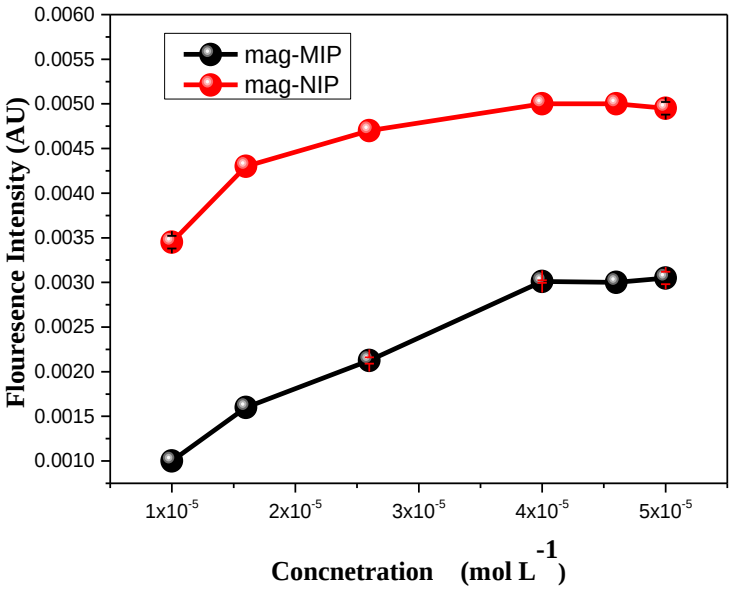

Figure 25. Effect of tetracycline elimination on fluorescence intensity using different initial concentration range (1.0×10^{-5} to 5.0×10^{-5} mol L^{-1}). Conditions: 0.01 mol L^{-1} phosphate buffer (pH = 7), adsorption time: 120 minutes, ($\lambda_{excitation}$ =350nm, $\lambda_{emission}$ =550 nm, wavelength range of 400-650 nm. Source: Author of the work.

As the concentration of tetracycline grows, the adsorption increases and the florescence intensity decreases; this is because mag-MIP has a large number of sorption sites. However, after a concentration of 3×10^{-5} mol L^{-1}, the sorption capacity diminishes and the removal process of florescence intensity slows because the sites are completely occupied by tetracycline molecules. Mag-MIP adsorbed more than mag-NIP, which suggested that imprinted sites were reshaped due to the reaction of imprinting and crosslinking, and this is clearly evident. This also suggests that the initial concentrations of tetracycline are a significant factor in the adsorption process, and due to that the intensity beginning a high value, is possible diminish the initial concentration in the D-SPE experiments, such as expecting, since the fluorescence is more sensible than UV-vis detection (used in the HPLC).

4.4.3. Application of the mag-MIP using food samples

Honey, egg, and cow milk were used to test the proposed polymer materials' (mag-MIP) capacity for selective adsorption of tetracycline. The recoveries were in the range 73.20-106.40% **(Table 8).**

Table 8. Tetracycline determination in food samples used HPLC and Fluorescence measures

Samples	Added (mol L^{-1})	Founded × 10^{-5}		Recovery[a] (%)	
		HPLC	Fluorometry	HPLC	Fluorometric
Honey	1.7×10^{-5}	1.290 (± 0.001)	1.538 (± 0.001)	75.88	90.47
Milk		1.250 (± 0.001)	1.600 (± 0.002)	73.53	94.11
EGG		1.310 (± 0.001)	1.620 (± 0.001)	77.06	95.29
Honey	2.5×10^{-5}	2.130 (± 0.003)	2.510 (± 0.001)	85.20	100.40
Milk		1.830 (± 0.003)	2.460 (± 0.003)	73.20	98.40
EGG		2.090 (± 0.001)	2.570 (± 0.002)	83,60	102.8

(a) Recovery percentage = (Founded/Added) x 100Standard deviation corresponds to triplicates. N = 3, Source: Author of the work

The various food samples were spiked at two different concentration levels, and then they were analysed using the HPLC technique as well as a fluorometric method to comparison. The matrix interference was minimal, as demonstrated by these findings. The results that were obtained suggest that the synthetic polymer materials (mag-MIP) that were developed have the potential to be utilized as an analytical tool for the purpose of quantifying tetracycline in actual samples.

Chapter 5

5. Results and Discussion obtained in the development of an electrochemical sensor based on a carbon paste modified with a magnetic molecular imprinted polymer

In this Chapter 5, will be show the results obtained in the development of a proposed non-conventional-electrochemical sensor, including details about the characterization of the magnetic material used to fabricate the sensor, its optimization in the preparation and the parameters to make the analysis, and the successfully application in real samples.

5.1. Characterization of the magnetic materials

5.1.1. Morphological Characterization

The findings of the surface morphology and topographical analysis of mag-MIP and mag-NIP (control material) are shown in **Figure 26 (A-D)** SEM micrographic investigation revealed the structure of the mag-MIP (Fe_3O_4@SiO_2–C=C-MIP) in **Figure 26A**.

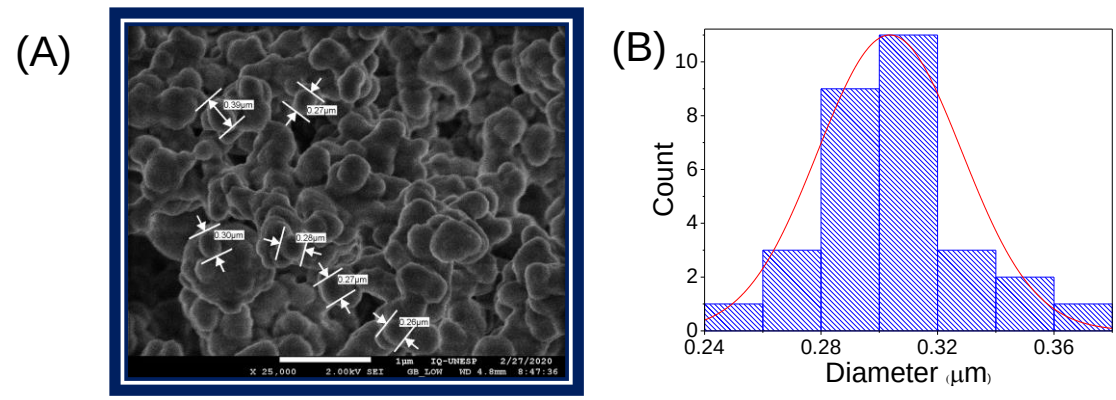

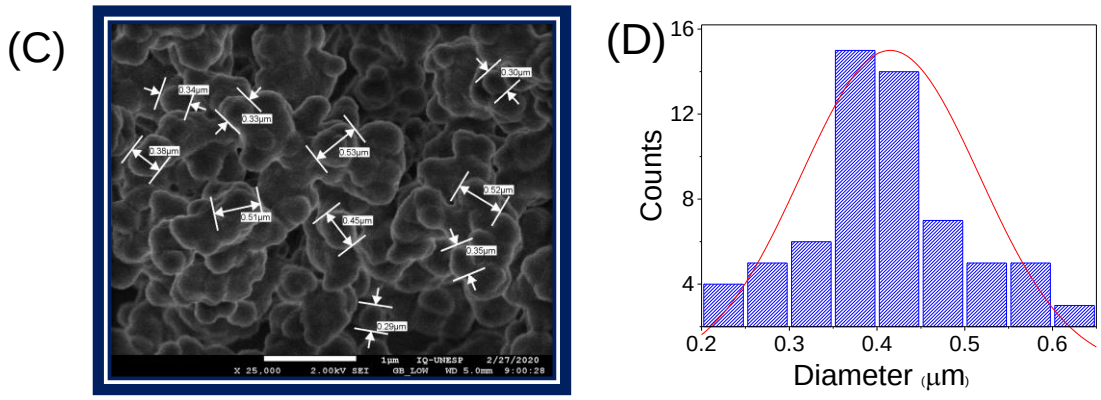

Figure 26. SEM images (A) mag-MIP and (B) mag-NIP, Histogram graph: (B) mag-MIP and (D) mag-NIP. Source: Ref [138]

MIP exhibits a more spherical shape and is uniformly distributed on the surface of the magnetic nanoparticles after being coupled with the modified magnetic nanoparticles ($Fe_3O4@SiO_2$-C=C). The magnetic nanomaterials with stability are provided by the use of silica (TEOS), and this helps prevent the agglomeration of the magnetic nanoparticles in the liquid. Magnetic nanoparticles ($Fe_3O_4@SiO_2$) modified with silanes, which are composed of multiple bonds (-C=C-), also facilitate polymerization. The image of the mag-NIP is shown in **Figure 26C**; the synthetic material that was not imprinted is exactly equivalent to the mag-MIP except that it does not contain the analyte. By examining the image in **Figure 26 (A)** one can surmise that the mag-MIP profile is identical in shape to the mag-NIP profile **(Figure 26 C)**. The magnetic imprinted polymer had an average size of 0.29 µm, while the non-imprinted polymer had a size of 0.42 µm. **Figures 26B and 26D** show homogenous dispersion of particles in terms of particle size and distribution. The spherical and homogeneous dispersion of the mag-MIP helps to the sensor's excellent repeatability by ensuring that it has a consistent output.

High-resolution transmission electron microscopy (HRTEM) is a technique that allows for the investigation of solid materials and their crystalline structure, as well as the determination of their morphology and content. Both the molecularly imprinted and non-imprinted polymers can be seen under a TEM in the images in **Figures 27A and 27B**. After

polymerization using magnetic nanoparticles, the compositions of both polymers were determined to be identical.

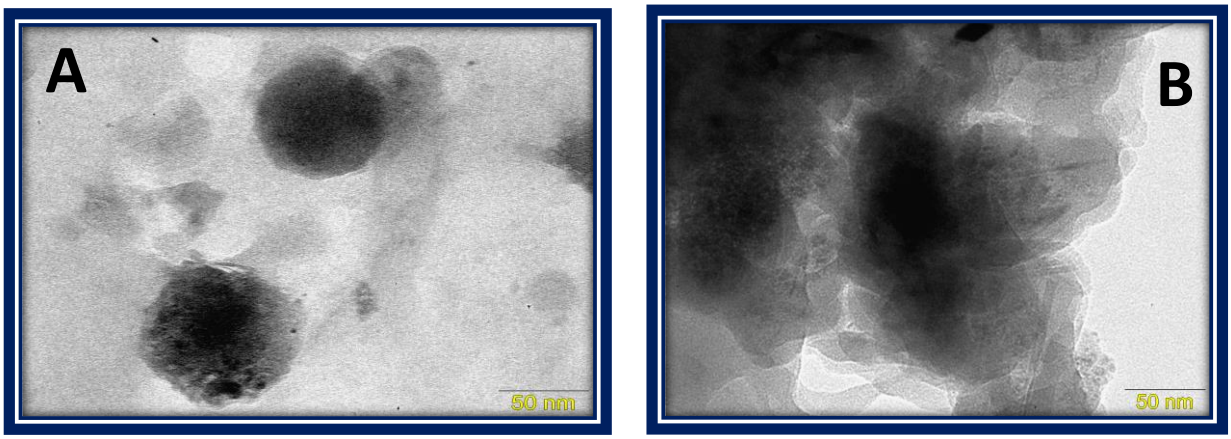

Figure 27. TEM images (A) mag-MIP and (B) mag-NIP. Source: Author of work

Figures 27(A-B) show that the cloudy sphere (light sphere) and the dark sphere form two circles. Magnetic nanoparticles have been shown to be associated with a foggy sphere of imprinted polymer (SiO_2-MIP) shell that is uniformly placed on a dark core (dark sphere) (Fe_3O_4). SiO_2-MIP showed a similar polymerization process to that of the control polymer on the core@shell of the magnetic nanoparticles. The high active area of the mag-MIP's spherical size leads to the production of more recognition sites.

5.1.2. Structural characterization using FTIR

Figure 28, shows the results of analysing the different functional groups used in the ethylene-glycol-dimethacrylate (EGDMA) and in the polymerization of mag-MIP, mag-NIP and structural monomer (cross-linker).

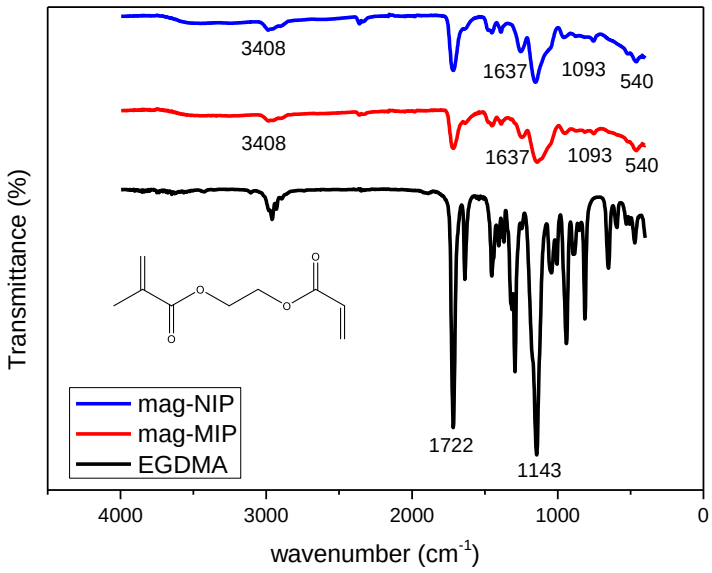

Figure 28. FTIR spectra of mag-MIP, mag-NIP, and EGDMA. Source: Ref [138]

Figure 28, depicts the Fe-O group's properties at 540 cm^{-1} in red (mag-MIP) and blue (mag-NIP), which reveal important details regarding Fe_3O_4 magnetic nanoparticles. Silanization may be seen at 1093 cm^{-1}, which is linked to the Si-O-Si group. The 3408 cm^{-1} bands can be attributed to the TEOS used in the fabrication of the magnetic nanoparticles, which represents the Si-OH group. **Figure 28 (Black)** also depicts the bands of the cross-linker agent EGDMA. It was revealed that both the mag-MIP and the mag-NIP were found to have the cross-linker EGDMA, the two significant peaks of mag-MIP and mag-NIP (1143 and 1722 cm^{-1}); the two dominant bands at 1143 and 1722 cm^{-1}, respectively, of the mag-MIP and mag-NIP; these peaks are usually associated with carbonyl (C=O, CO-) stretch.[182]. The strength of the C=C signal can be observed to be considerably less at 1637 cm^{-1}, which means that the EGDMA atoms in the synthesized mag-MIPs have been cross-linked during polymerization, as demonstrated by the results.

5.2. Optimization of the electrochemical sensor

5.2.1. Electrochemical behaviour of the analyte

Tetracycline has a phenolic diketone group in its structure. A study by Dang et al.[192] demonstrated that the phenol group can be oxidized in the presence of two anodic peaks. Two oxidation peaks at 0.63 V and 0.83 V were examined in this study. Tetracycline oxidation has previously been connected to two oxidation pathways based on the oxidation of phenol to phenoxy group in the literature[193]. Phenol undergoes one-electron and one-proton loss during oxidation at a pH of 7.0[193]. When the pH is lower than 4, one electron is lost, resulting in the creation of protonated quinonic molecules. The two-step process by which tetracycline is oxidized involves the loss of two protons. At pH 7.0, we have investigated the presence of oxidation.

5.2.2. Effect to the recognized mass in the sensor response

The amount of mag-MIP in the carbon paste was initially examined at various mass levels (1, 2, 5, 10, 15, and 20 mg) under the same concentration of tetracycline (1.5×10^{-5} mol L^{-1}). It was found that 15 mg of mag-MIP in carbon paste provided the best electrical signal **(Figure 29).**

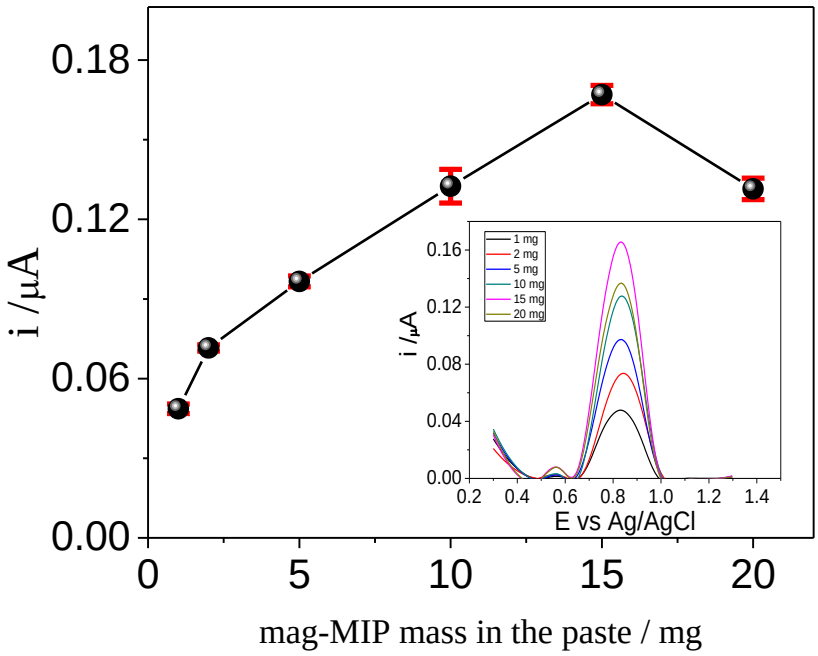

Figure 29: Impact on the efficiency of the mag-MIP caused by the use of varying mass values (1, 2, 5, 10, 15, and 20 mg) sensor in 0.1 mol L^{-1} phosphate buffer (pH 7.0), with tetracycline concentration of 1.5x10-5 mol L^{-1}. Optimized electrochemical conditions: f =10 Hz, amp = 0.075 mV, step = 0.005 mV, E (initial) = 0.2 V, E (final) = 1.4 V. Insert: Electrochemical Voltammograms of mass. Source: Ref [138]

Notably, the polymer was an important factor in the electrochemical signal's enhancement. When 20 mg of mag-MIP is added to the carbon paste, the electrochemical signal weakens abruptly. Polymer is a non-conductive material, and as a result, the bigger the amount of polymer applied, the lower the signal intensity becomes. Further trials were therefore carried out using carbon paste containing 15 mg of mag-MIP.

5.2.3. Electrochemical sensor performance as a function of pH

Tetracycline has three pKa values, according to Stephen et al[194]., (3.3, 7.6, and 9.3). Its functional groups include dimethylammonium, phenolic diketone, and tricarbonylamide and are all found in the tetracycline molecule's structure. Protonation and deprotonation are carried out by these functional groups. Tetracycline's surface carries a variety of charges that are affected by the pH of the solution [195]. Cations (TCH_3^+) of tetracycline can be observed in an acidic solution with a pH value up to 5.5[195], due to the protonation of the dimethylamine group of the antibiotic **(Figure 30).**

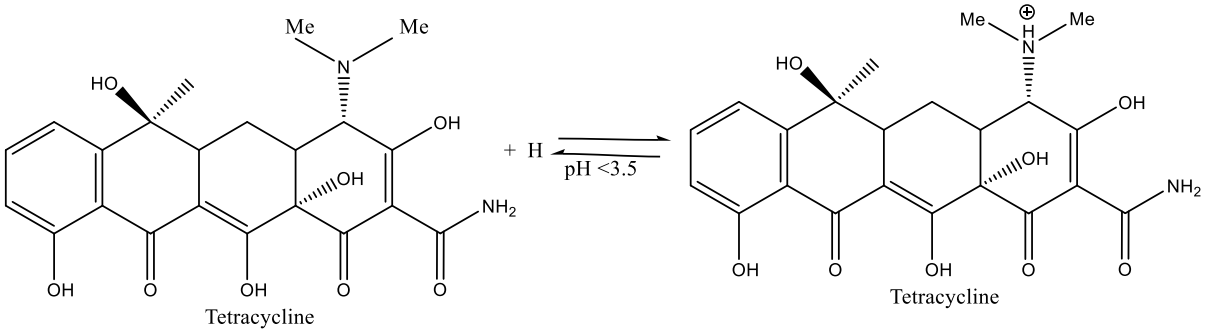

Figure 30. Tetracycline's structure in solution below a pH of 3.5 Source: Ref [138]

The deprotonation of a phenolic diketone molecule at pH levels between 5.5 and 7.5 causes the creation of zwitterions (TCH_2^0). Increasing the pH above 7.5 causes a proton loss from the tricarbonylamide and phenolic diketone groups; as can be seen in the reactions described in **Figure 31** [196], the tetracycline now has a negative charge.

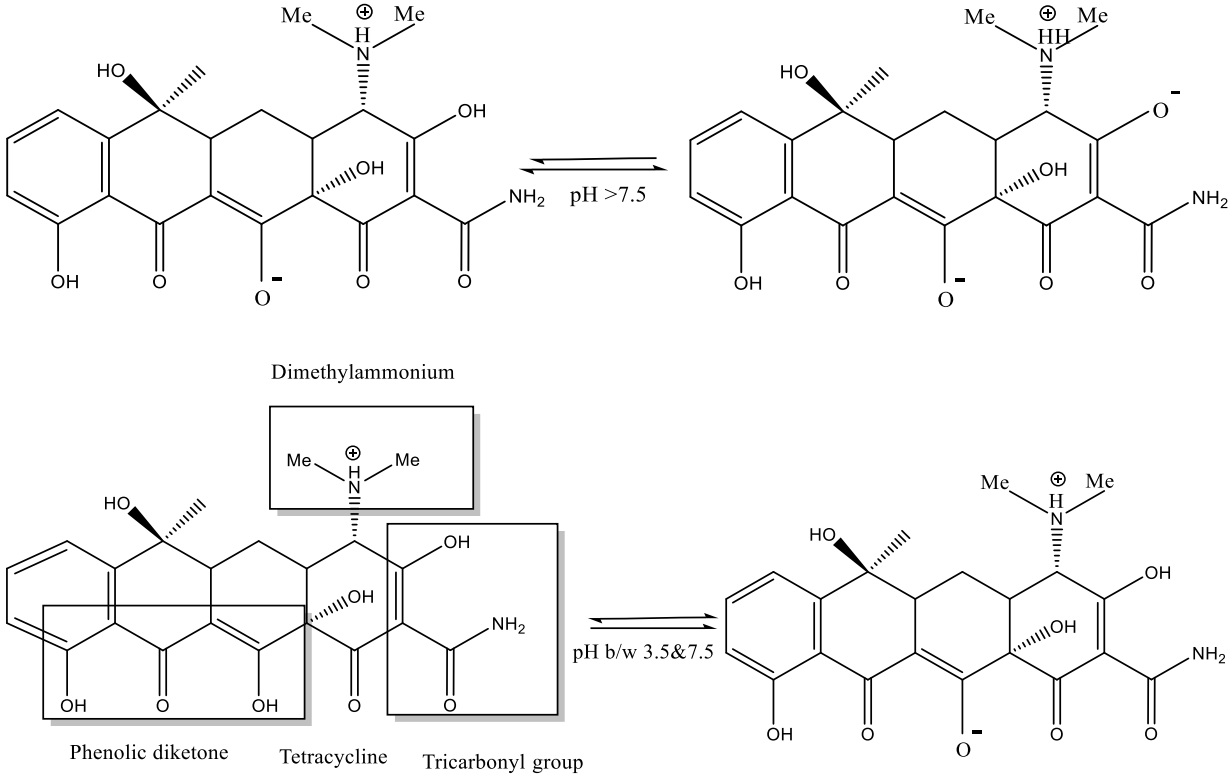

Figure 31. Tetracycline's pH-dependent chemical structure in solutions: pH > 3.5. Top: Between 3.5 and 7.5; Bottom: pH > 7.5. Source: Ref [138]

At a pH of 7.0, the tetracycline has the best possible interaction with the cavities of the polymer matrix, in case where the analyte is in its zwitter- ionic form, as demonstrated in **Figure 32**. Since the polymer's selective cavity is tailor-made to accommodate the analyte, the system can reliably detect and isolate the target molecule.

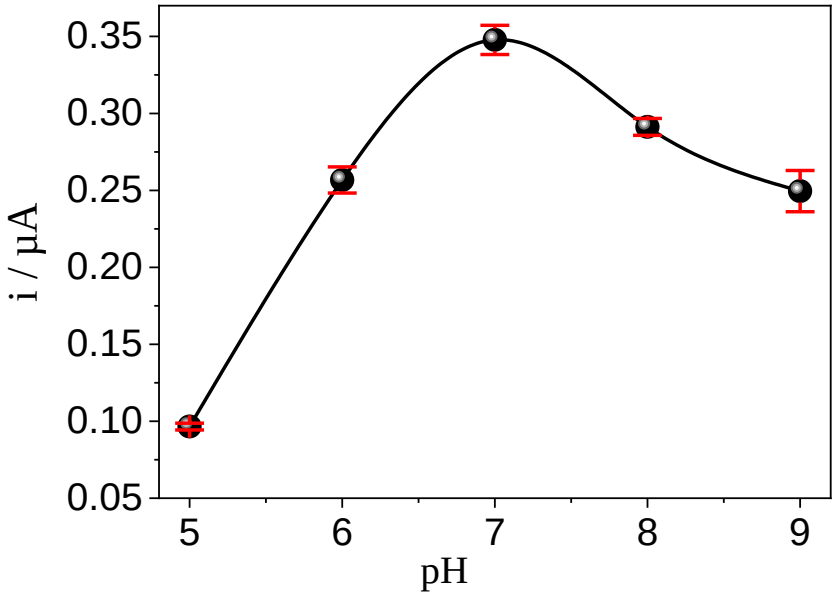

Figure 32. Electrochemical sensor efficiency as function of pH applied in 0.1 mol L^{-1} buffer solutions. Target molecule concentration were used in pH study: 1.5×10^{-5} mol L^{-1}. Optimized electrochemical conditions: f =10 Hz, amp = 0.075 mV, step = 0.005 mV, E(initial) = 0.2 V, E(final) = 1. 4 V. Bars error for n = 3. Source: Ref [138]

5.2.4. Effect of incubation time on the sensor efficiency

A study was conducted to determine the influence of varying incubation times (10, 20, 30, 40, 50, 60, 70, 80, and 90 s) on the sensor response. The findings of this investigation are given in **Figure 33**. The highest signal response was attained at 80 s whereas a little lower current response, a time of 90 s. As a direct consequence of this, a higher signal was obtained, as well as improved reproducibility; consequently, this time was utilized in each and every subsequent electrochemical experiment.

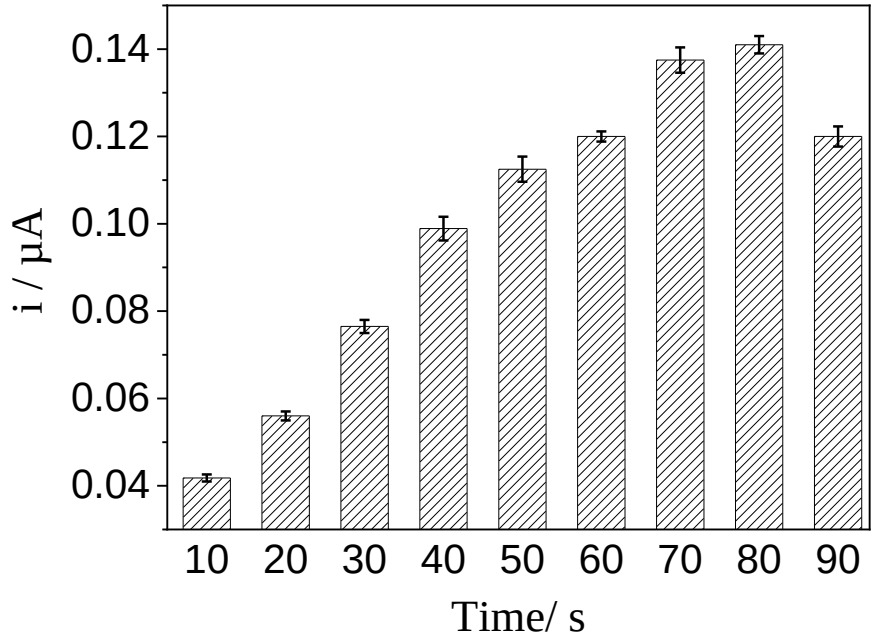

Figure 33. Conductivity measurement as function of time incubation using mag-MIP (15 mg) sensor in 0.1 mol L^{-1} phosphate buffer at pH 7.0, target molecule concentration of 1.5×10^{-5} mol L^{-1}. Optimized electrochemical conditions: f =10 Hz, amp = 0.075 mV, step = 0.005 mV, applied potential: $E_{(initial)}$ = 0.2 V, $E_{(final)}$ = 1.4 V. Error bars: n = 3. Peaks were obtained at 0.6 V and 0.8 V. Source: Ref [138]

Using the applied potential of 0.8 V, the highest analytical signal was obtained in 80 s, as shown in the graph. The mag-MIP's adsorption of tetracycline contributes to the high analytical signal observed at this time. For this reason, the preceding experiments will be conducted for a duration of 80 s.

5.2.5 Comparison studies obtained with carbon pastes modified with mag-MIP and mag-NIP, and unmodified

Two concentrations of tetracycline (5.0×10^{-7} mol L^{-1}) and 1.5×10^{-5} mol L^{-1} were used to evaluate the efficacy of sensors fabricated from magnetic molecularly imprinted polymer (mag-MIP), magnetic non-imprinted polymer (mag-NIP), and unmodified carbon paste electrode (CPE). **Figure 34**, shows the results of the investigation, which was conducted with the optimal dosage (15 % w/w for mag-MIP and mag-NIP, and 100 mg of graphite).

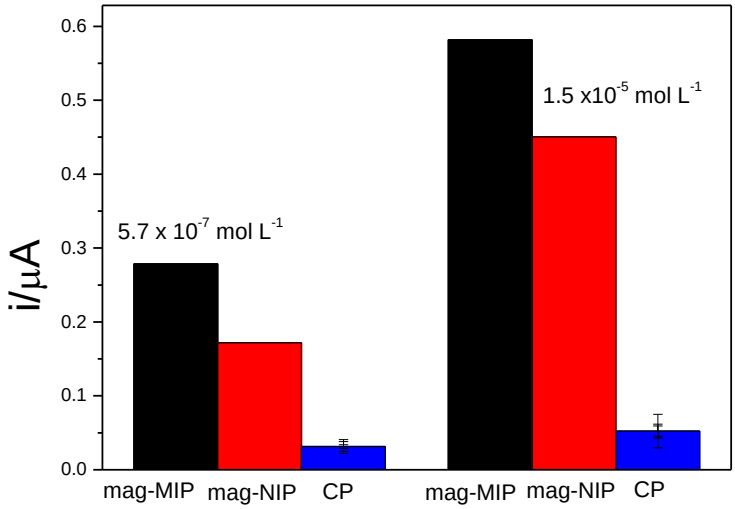

Figure 34. Two concentrations of tetracycline (5.0×10^{-7} mol L^{-1} and 1.5×10^{-5} mol L^{-1}) are used to relate the profile information of magnetic molecularly imprinted polymer (mag-MIP), magnetic non-imprinted polymer (mag-NIP), and unmodified carbon paste sensors in 0. 1 mol L^{-1} phosphate buffer at pH 7.0. Optimized electrochemical conditions: f =10 Hz, amp = 0.075 mV, step = 0.005 mV, $E_{(initial)}$ = 0.2 V, $E_{(final)}$ = 1.4 V. Source: Ref [138]

Although the polymer-based magnetic sensor displayed exceptional performance, this remarkable performance is related to the optimal interaction between cavities and analyte. It was expected that the control polymer magnetic sensor (mag-NIP), as well as an unmodified carbon paste electrode (CPE), were less efficient than the selective polymer magnetic (mag-MIP) sensor; this result is due to the low adsorption of the analyte.

5.2.6. Analytical profile of the proposed selective polymer-based sensor

All of the optimized parameters were used to generate the voltammograms. The relevant voltammograms obtained from the application of the proposed sensor are depicted in **Figure 35.** The strength of the electrochemical analytical signal rises with increasing

concentration. This is because there are cavities on the surface of the mag-MIP that are available to be filled.

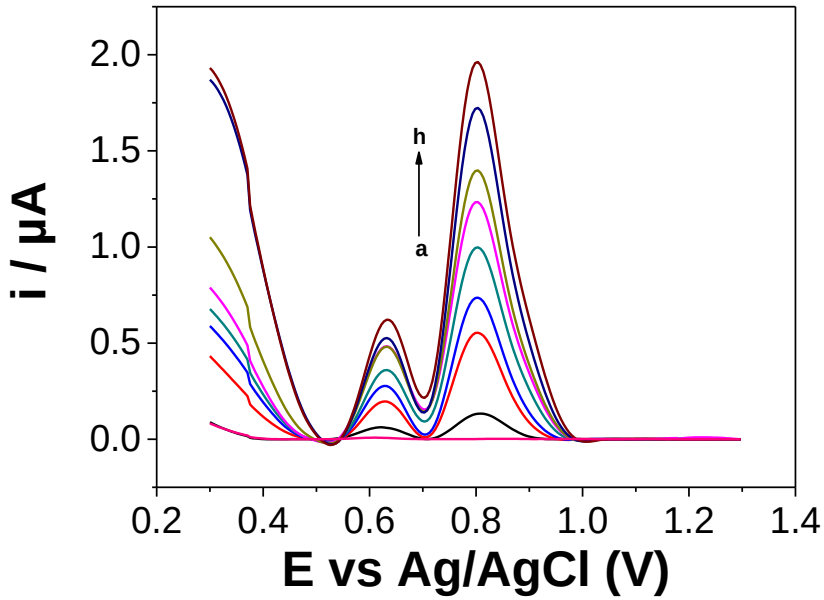

Figure 35. Voltammograms obtained with the proposed sensor in 0.1 mol L^{-1} phosphate buffer (pH 7.0) obtained at different tetracycline concentrations from 5.0×10^{-7} to 4.0×10^{-5} molL^{-1}. E (initial) = 0.2 V, E (final) = 1.4 V. Source: Ref [138]

The linear plot (**Figure 36**) was created with a co-efficient of determination (R^2) of 0.9993, slope of the curve is 0.045 and intercept is 1.03×10^{-7}. The linearity of the curve was achieved in the concentration range of 5.0×10^{-7} to $4.0\ 10^{-5}$ mol L^{-1}. The limit of detection was 0.15 µmol L^{-1}.

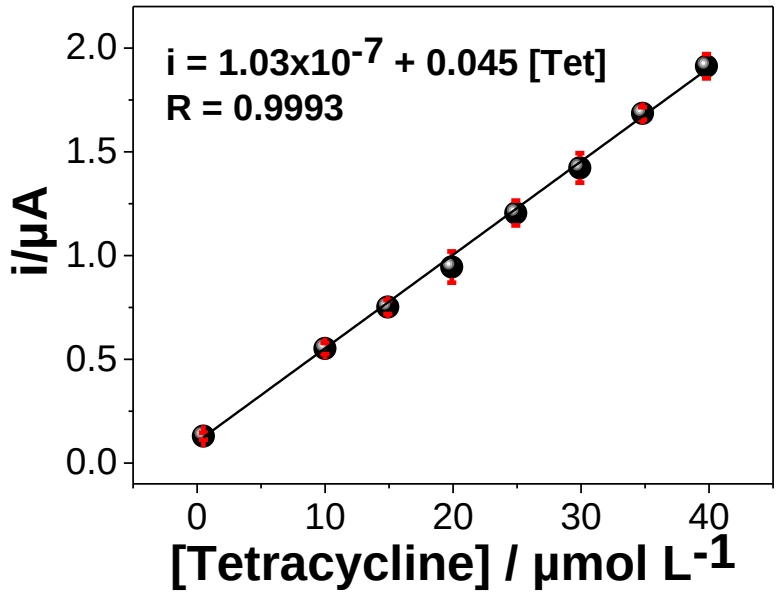

Figure 36. Analytical curve constructed from electrochemical voltammograms obtained with mag-MIP electrode. Source: Ref [138]

5.2.7. Repeatability of the mag-MIP sensor

The optimal sensor preparation consisted of 15 mg mag-MIP and 85 mg graphite, and the study was carried out with a tetracycline concentration of 1.5×10^{-5} mol L^{-1}. The repeatability of the mag-MIP sensor was determined. According to the results of a 10-period analysis, as shown in **Figure 37** below, the repeatability of the sensor was assessed.

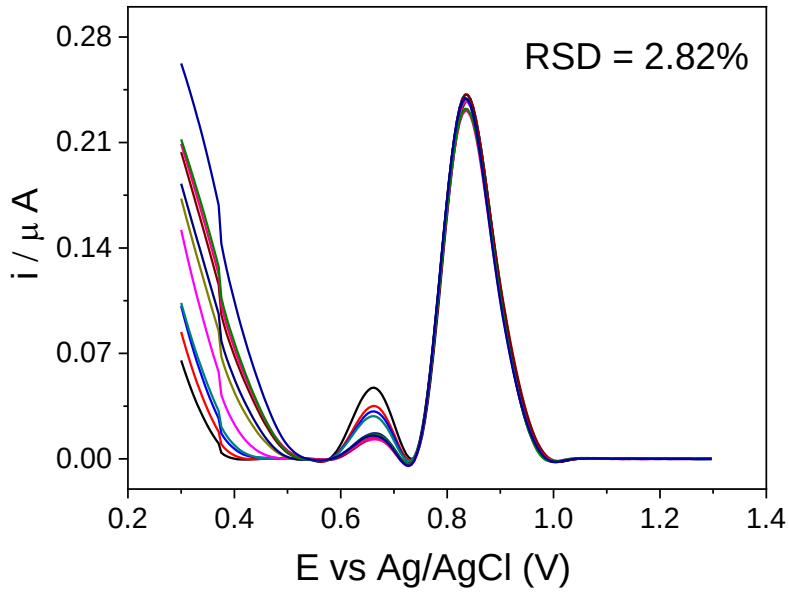

Figure 37. Analyses of repeatability were conducted in a phosphate buffer solution (0.1 mol L^{-1}) with a pH of 7.0 and a concentration of 1.5×10^{-5} mol L^{-1} of tetracycline. Electrochemical values are optimal: f = 10 Hz, A = 0.075 V, E = 0.005 V, E(initial) = 0.2 V, and E(final) = 1.4 V. Source: Ref [138]

The analytical signal's relative standard deviation (RSD) was calculated came out to be 2.82 %. Mag-MIP sensors have a low RSD, which suggests strong repeatability and stability in terms of tetracycline observations.

5.2.8 Interference

When the suggested electro-chemical (mag-MIP) sensor was evaluated in the presence of a variety of chemicals with chemical structures that were comparable to the structure of tetracycline, interference had no effect on the tetracycline concentration. The results obtained are shown in **Figure 38.**

Also were evaluated the effect of the minocycline and doxycycline, two other compounds, with structure analogous to the tetracycline **Figure 39 (A-B).**

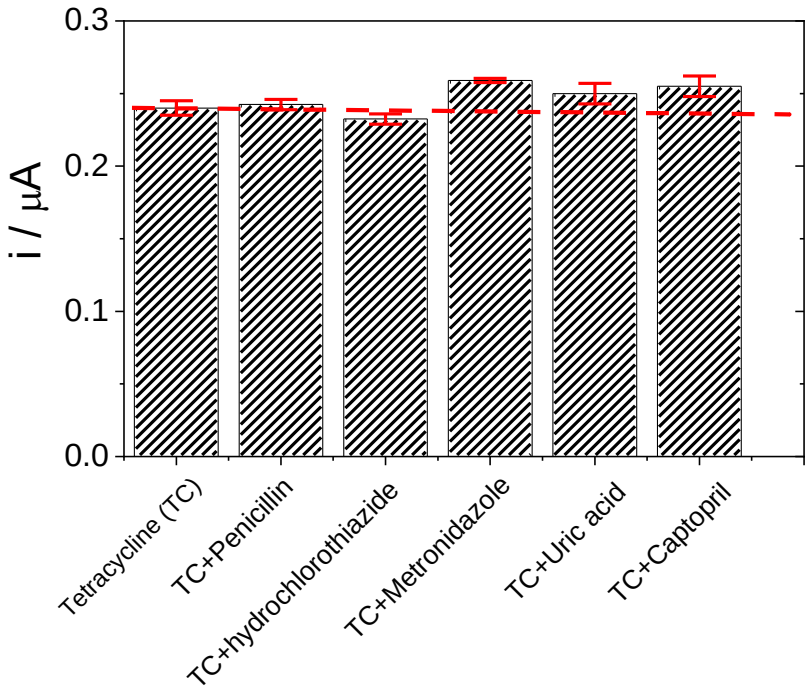

Figure 38. Analysis of interference on the mag-MIP sensor with a phosphate buffer solution of 0.1 mol L^{-1} at pH 7.0 and 1.5 $\times 10^{-5}$ mol L^{-1} of each interfering concentration. Optimized electrochemical conditions: f =10 Hz, amp = 0.075 mV, step = 0.005 V, $E_{(initial)}$ = 0.2 V, $E_{(final)}$ = 1.4 V. Source: Ref [138]

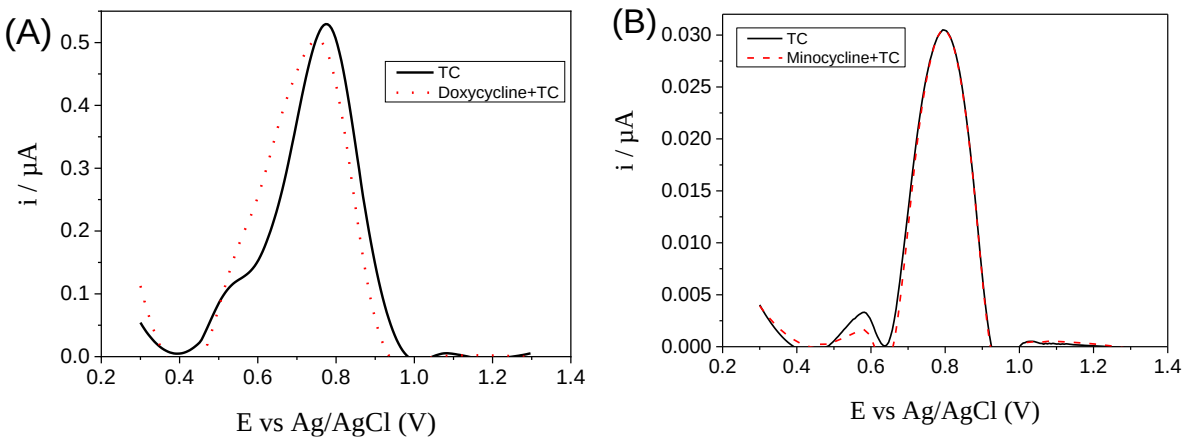

Figure 39 (A-B). Interfering effect of other compounds with similar chemical structure. Source: Ref [138]

Since tetracycline and doxycycline have the same structure analyte, the tetracycline blocked the cavities which present on the surface of the mag-MIP, and since the electrode

surface was not polished/clean well, the reaction on the surface was not totally proceeded, as shown in **Figure 39 (B**), which contrasts with **Figure 39 (A)**.

Based on this investigation, the addition of the interfering chemicals had no effect on the sensor's electrochemical signal. As can be shown, the polymer-based sensor with magnetic molecular imprinting exhibits good symmetrical signal. This result is analogous like those obtained in experiment using D-SPE.

5.2.9. Application of the proposed sensor in quantification of TC in milk samples

Three actual milk samples were spiked with tetracycline at five different concentrations (2.0×10^{-5}, 5.0×10^{-6}, 4.0×10^{-7}, 1.0×10^{-7} and 2.0×10^{-7} mol L^{-1}) to evaluate the sensor's efficacy. **Table 10** shows the sensor's response to the food samples.

Table 9 Application of electrochemical sensor in milk samples[138]

Samples	Tetracycline concentration (mol L^{-1})		Recovery[a] (%)
	Spiked	Found	
Skimmed Milk	2.0×10^{-5}	$(2.04\pm0.03) \times 10^{-5}$	102
Whole Milk	2.0×10^{-5}	$(2.06\pm0.04) \times 10^{-5}$	103
Raw Milk	2.0×10^{-5}	$(1.95\pm0.05) \times 10^{-5}$	97.5
Skimmed Milk	5.0×10^{-6}	$(5.11\pm0.18) \times 10^{-6}$	102
Whole Milk	5.0×10^{-6}	$(4.64\pm0.04) \times 10^{-6}$	93
Raw Milk	5.0×10^{-6}	$(4.85\pm0.08) \times 10^{-6}$	96
Skimmed Milk	4.0×10^{-7}	$(3.82\pm0.01) \times 10^{-7}$	95.6
Whole Milk	4.0×10^{-7}	$(3.74\pm0.03) \times 10^{-7}$	93.5
Raw Milk	4.0×10^{-7}	$(3.63\pm0.04) \times 10^{-7}$	91

Recovery percentage = (Founded/Added) x100, Standard deviation corresponds to triplicates. Source: Author of the work

The proposed sensor's recovery percentages ranged from 91% to 103% when applied to milk samples containing tetracycline. Analyte spiked with milk samples showed no influence on the detection process. In the absence of any pre-treatment, the milk samples were treated with tetracycline at concentrations of 1, 2, and 5×10^{-1} mol L^{-1}. Results demonstrated that tetracycline could not be identified under the conditions of 1.0 and 2.0 $\times10^{-7}$ mol L^{-1} tetracycline concentrations, respectively, when the model analyte was used. This is due to the concentrations being so close to the detection limit and could not identify. In the case of a tetracycline concentration of 4.0×10^{-7} mol L^{-1}, the recovery value that was obtained was found to be within the permissible acceptable range. These results demonstrate that the electrochemical sensor that has been presented is capable of accurately identifying tetracycline in liquid matrices.

5.2.10. Analysis of the current study with regard to previously published data

The proposed electrochemical sensor's efficiency was compared to that of other sensors previously described in the literature; the results of the comparison may be found in **Table 11**. The current fabricated sensor, when compared to other electrochemical sensors, performed better in terms of sensitivity, cost, and selectivity, according to the results of the comparative analysis. The suggested sensor has the added benefit of reusability because of the fact that the electrode's surface can be easily wiped down with white paper and used again in subsequent research (10 times).

In contrast to our suggested sensor, several of the approaches used in the published studies are difficult and costly to synthesize (for instance, they require functional groups to change the electrodes or two/three modifying materials), making them undesirable and often

difficult to execute. In addition to being faster than existing methods, the suggested sensing material (mag-MIP) is simple and easy to utilize.

Table 10. Analysis of the suggested CPE-mag-MIP sensor in relation to other sensors described in the literature[138]

Electrode	LOD (μmol L^{-1})	Method	Sample	Ref
Platinum nanoparticles on carbon	14.3	DPV	Urine	169
MIOPPy-AuNP/SPCE	0.65	DPV	Shrimp	170
UV-DNA/GCE	0.27	CV	Pharmaceutical and market milk	171
Gold-Screen printed	0.96	CV	Drugs and Chicken	172
Graphite-Polyurethane	2.80	DPV	Natural Water	173
CPE-mag-MIP	0.15	SWV	Market and Natural milk	This study

SPCE=Screen-printed carbon electrode; MIOPPy = Moleculary imprinted polypyrrole; AuNP = Gold; nanoparticle; CPE = Carbon paste electrode; UV= UV-Irradiated DNA; GCE = Glassy Carbon Electrode; Mag = Magnetic nanoparticles; MIP = molecularly imprinted polymer.

Source: Comparison of data with author research work

Chapter 6

6. Conclusion

The present Thesis showed the wide potential of magnetic molecularly imprinted polymers as selective receptors in real applications. The key goal was to develop a MIP capable of efficiently capturing target molecules in a very complicated and adverse environment. Second, due to its magnetic nature, mag-MIP could be easily isolated from the complex medium. A comprehensive investigation was conducted in order to synthesize magnetic selective materials to tetracycline antibiotics.

In first part (Chapter 4), where the mag-MIP (Fe_3O_4@SiO_2 -MIP) was prepared using acrylonitrile (ACN) as solvent, methacrylic acid as the functional monomer, ethylene glycol dimethacrylate (EGDMA) as the cross-linking agent, and benzoyl peroxide as the radical initiator. In tetracycline solution, the synthesized mag-MIP demonstrated, Langmuir isotherm and rapid adsorption kinetics and specific recognition affinity. For the evaluation of the synthesized material, recovery studies were carried out in spiked samples at two distinct concentration levels (1.7×10^{-5} and 2.5×10^{-5} mol L^{-1}) and the obtained values for honey, cow milk, and egg were in the range of 73.20-87.33% (HPLC) and 90.53–103.17% (Spectro-fluorometer**)**, respectively.

In Chapter 5, discussed how use a carbon paste modified magnetic molecularly imprinted polymer to develop an electrochemical sensor for detecting tetracycline concentrations in solution. The MIP was synthesized using acrylic acid (functional monomer), ethylene-glycol-dimethacrylate (cross-linker), and 2, 2 azobisisobutyronitrile (radical initiator). In terms of mechanical stability and sensitivity, the CPE-mag-MIP sensor performed admirably. The proposed biomimetic sensor was evaluated for its ability to detect tetracycline

and was determined to be appropriate due to its low operational costs, excellent repeatability, and low detection limit. The absence of interference from other chemicals in the detection of tetracycline effectively indicates the sensor's selectivity.

The innovative component of the study was the utilization of three techniques (HPLC, fluorescence spectroscopy, and an electrochemical sensor) to examine the performance of the mag-MIP in different food samples, the mag- MIP used in this investigation to determine the concentration of tetracycline in food samples stands it apart from previous research. The advantages of a fabricated electrochemical sensor were demonstrated to be substantial over other techniques, including require less time and less amount of reagents, detect low concentration, rapid monitoring, and great selectivity.

References

1. Yeom, J.-R.;Yoon, S.-U. & Kim, C.-G. Quantification of residual antibiotics in cow manure being spread over agricultural land and assessment of their behavioral effects on antibiotic resistant bacteria. **Chemosphere**, v.**182**, p.771–780, 2017.

2. Erian, I. & Phillips, C. Public Understanding and Attitudes towards Meat Chicken Production and Relations to Consumption. **Animals**, v.**7**, p.20, 2017.

3. Zhang, Y.;Geißen, S.-U. & Gal, C. Carbamazepine and diclofenac: Removal in wastewater treatment plants and occurrence in water bodies. **Chemosphere**, v.**73**, p.1151–1161, 2008.

4. Uslu, M. O.;Jasim, S.;Arvai, A.;Bewtra, J. & Biswas, N. A Survey of Occurrence and Risk Assessment of Pharmaceutical Substances in the Great Lakes Basin. **Ozone: Science & Engineering**, v.**35**, p.249–262, 2013.

5. Ishaq, M. S. *et al.* In Vitro Phytochemical, Antibacterial, and Antifungal Activities of Leaf, Stem, and Root Extracts of Adiantum capillus veneris. **The Scientific World Journal**, v.**2014**, p.1–7, 2014.

6. Sarmah, A. K.;Meyer, M. T. & Boxall, A. B. A. A global perspective on the use, sales, exposure pathways, occurrence, fate and effects of veterinary antibiotics (VAs) in the environment. **Chemosphere**, v.**65**, p.725–759, 2006.

7. Neumann, C.;Harris, D. M. & Rogers, L. M. Contribution of animal source foods in improving diet quality and function in children in the developing world. **Nutrition Research**, v.**22**, p.193–220, 2002.

8. Liu, Z.;Moate, P.;Ezerniks, V.;Cocks, B. G. & Rochfort, S. Identification and quantification of triacylglycerols containing n-3 long-chain polyunsaturated fatty acids

in bovine milk. **Journal of Dairy Science**, v.**98**, p.8473–8485, 2015.

9. Antman, K. H. Introduction: The History of Arsenic Trioxide in Cancer Therapy. **The Oncologist**, v.**6**, p.1–2, 2001.

10. Tan, S. & Tatsumura, Y. Alexander Fleming (1881–1955): Discoverer of penicillin. **Singapore Medical Journal**, v.**56**, p.366–367, 2015.

11. Ling, L. L. *et al.* A new antibiotic kills pathogens without detectable resistance. **Nature**, v.**517**, p.455–459, 2015.

12. Munoz-Davila, M. Role of Old Antibiotics in the Era of Antibiotic Resistance. Highlighted Nitrofurantoin for the Treatment of Lower Urinary Tract Infections. **Antibiotics**, v.**3**, p.39–48, 2014.

13. Bassett, E. J.;Keith, M. S.;Armelagos, G. J.;Martin, D. L. & Villanueva, A. R. Tetracycline-Labeled Human Bone from Ancient Sudanese Nubia (A.D. 350). **Science**, v.**209**, p.1532–1534, 1980.

14. Katz, L. & Baltz, R. H. Natural product discovery: past, present, and future. **Journal of Industrial Microbiology and Biotechnology**, v.**43**, p.155–176, 2016.

15. Prescott, J. F. The resistance tsunami, antimicrobial stewardship, and the golden age of microbiology. **Veterinary Microbiology**, v.**171**, p.273–278, 2014.

16. Doyle, M. P.;Loneragan, G. H.;Scott, H. M. & Singer, R. S. Antimicrobial Resistance: Challenges and Perspectives. **Comprehensive Reviews in Food Science and Food Safety**, v.**12**, p.234–248, 2013.

17. Hutchings, M. I.;Truman, A. W. & Wilkinson, B. Antibiotics: past, present and future. **Current Opinion in Microbiology**, v.**51**, p.72–80, 2019.

18. Richardson, B. J.;Lam, P. K. S. & Martin, M. Emerging chemicals of concern: Pharmaceuticals and personal care products (PPCPs) in Asia, with particular reference to Southern China. **Marine Pollution Bulletin**, v.**50**, p.913–920, 2005.

19. Samal, K.;Mahapatra, S. & Hibzur Ali, M. Pharmaceutical wastewater as Emerging Contaminants (EC): Treatment technologies, impact on environment and human health. **Energy Nexus**, v.**6**, p.100076, 2022.

20. Hou, J. *et al.* Simultaneous removal of antibiotics and antibiotic resistance genes from pharmaceutical wastewater using the combinations of up-flow anaerobic sludge bed, anoxic-oxic tank, and advanced oxidation technologies. **Water Research**, v.**159**, p.511–520, 2019.

21. Landrigan, P. J. *et al.* Human Health and Ocean Pollution. **Annals of Global Health**, v.**86**, p.151, 2020.

22. Andersson, D. I. & Hughes, D. Microbiological effects of sublethal levels of antibiotics. **Nature Reviews Microbiology**, v.**12**, p.465–478, 2014.

23. Crini, G. & Lichtfouse, E. Advantages and disadvantages of techniques used for wastewater treatment. **Environmental Chemistry Letters**, v.**17**, p.145–155, 2019.

24. Borghi, A. A. & Palma, M. S. A. Tetracycline: production, waste treatment and environmental impact assessment. **Brazilian Journal of Pharmaceutical Sciences**, v.**50**, p.25–40, 2014.

25. Khan, S. J. & Ongerth, J. E. Modelling of pharmaceutical residues in Australian sewage by quantities of use and fugacity calculations. **Chemosphere**, v.**54**, p.355–367, 2004.

26. Rivas, J.;Encinas, Á.;Beltrán, F. & Graham, N. Application of advanced oxidation

processes to doxycycline and norfloxacin removal from water. **Journal of Environmental Science and Health, Part A**, v.**46**, p.944–951, 2011.

27. Kemper, N. Veterinary antibiotics in the aquatic and terrestrial environment. **Ecological Indicators**, v.**8**, p.1–13, 2008.

28. Hao, C.;Clement, R. & Yang, P. Liquid chromatography–tandem mass spectrometry of bioactive pharmaceutical compounds in the aquatic environment—a decade's activities. **Analytical and Bioanalytical Chemistry**, v.**387**, p.1247–1257, 2007.

29. Goossens, H. Antibiotic consumption and link to resistance. **Clinical Microbiology and Infection**, v.**15**, p.12–15, 2009.

30. van den Bogaard, A. Epidemiology of resistance to antibiotics Links between animals and humans. **International Journal of Antimicrobial Agents**, v.**14**, p.327–335, 2000.

31. Swartz, M. N. Human Diseases Caused by Foodborne Pathogens of Animal Origin. **Clinical Infectious Diseases**, v.**34**, p.S111–S122, 2002.

32. Diwan, V. *et al.* Antibiotics and antibiotic-resistant bacteria in waters associated with a hospital in Ujjain, India. **BMC Public Health**, v.**10**, p.414, 2010.

33. Fatta-Kassinos, D.;Meric, S. & Nikolaou, A. Pharmaceutical residues in environmental waters and wastewater: current state of knowledge and future research. **Analytical and Bioanalytical Chemistry**, v.**399**, p.251–275, 2011.

34. Ding, C. & He, J. Effect of antibiotics in the environment on microbial populations. **Applied Microbiology and Biotechnology**, v.**87**, p.925–941, 2010.

35. Kümmerer, K. Antibiotics in the aquatic environment – A review – Part I. **Chemosphere**, v.**75**, p.417–434, 2009.

36. Phoon, B. L. *et al.* Conventional and emerging technologies for removal of antibiotics from wastewater. **Journal of Hazardous Materials**, v.**400**, p.122961, 2020.

37. Carusso, S.;Juárez, A. B.;Moretton, J. & Magdaleno, A. Effects of three veterinary antibiotics and their binary mixtures on two green alga species. **Chemosphere**, v.**194**, p.821–827, 2018.

38. Gullberg, E. *et al.* Selection of Resistant Bacteria at Very Low Antibiotic Concentrations. **PLoS Pathogens**, v.**7**, p.e1002158, 2011.

39. Bush, K. *et al.* Tackling antibiotic resistance. **Nature Reviews Microbiology**, v.**9**, p.894–896, 2011.

40. Huang, Z.;Ong, S. L. & Ng, H. Y. Submerged anaerobic membrane bioreactor for low-strength wastewater treatment: Effect of HRT and SRT on treatment performance and membrane fouling. **Water Research**, v.**45**, p.705–713, 2011.

41. Van Boeckel, T. P. *et al.* Global trends in antimicrobial resistance in animals in low- and middle-income countries. **Science**, v.**365**, 2019.

42. Povolo, V. R. & Ackermann, M. Disseminating antibiotic resistance during treatment. **Science**, v.**364**, p.737–738, 2019.

43. MacLean, R. C. & San Millan, A. The evolution of antibiotic resistance. **Science**, v.**365**, p.1082–1083, 2019.

44. Andersson, D. I. & Hughes, D. Antibiotic resistance and its cost: is it possible to reverse resistance? **Nature Reviews Microbiology**, v.**8**, p.260–271, 2010.

45. French, G. L. The continuing crisis in antibiotic resistance. **International Journal of Antimicrobial Agents**, v.**36**, p.S3–S7, 2010.

46. Finch, R. & Sharland, M. 18 November and beyond: observations on the EU Antibiotic Awareness Day. **Journal of Antimicrobial Chemotherapy**, v.**63**, p.633–635, 2009.

47. Ashley, E. A.;Lubell, Y.;White, N. J. & Turner, P. Antimicrobial susceptibility of bacterial isolates from community acquired infections in Sub-Saharan Africa and Asian low and middle income countries. **Tropical Medicine & International Health**, v.**16**, p.1167–1179, 2011.

48. Pereira-Maia, E. C. *et al.* Tetraciclinas e glicilciclinas: uma visão geral. **Química Nova**, v.**33**, p.700–706, 2010.

49. Ongas, M. *et al.* Liquid chromatography–tandem mass spectrometry for the simultaneous quantitation of ceftriaxone, metronidazole and hydroxymetronidazole in plasma from seriously ill, severely malnourished children. **Wellcome Open Research**, v.**2**, p.43, 2018.

50. Wongchang, T. *et al.* Determination of ceftriaxone in human plasma using liquid chromatography–tandem mass spectrometry. **Wellcome Open Research**, v.**4**, p.47, 2019.

51. Jeffery, J.;Vincent, Z. J.;Ayling, R. M. & Lewis, S. J. Development and validation of a liquid chromatography tandem mass spectrometry assay for the measurement of faecal metronidazole. **Clinical Biochemistry**, v.**50**, p.323–330, 2017.

52. Aranda, P. R.;Pacheco, P. H.;Olsina, R. A.;Martinez, L. D. & Gil, R. A. Total and inorganic mercury determination in biodiesel by emulsion sample introduction and FI-CV-AFS after multivariate optimization. **Journal of Analytical Atomic Spectrometry**, v.**24**, p.1441, 2009.

53. Ashoka, S.;Peake, B. M.;Bremner, G.;Hageman, K. J. & Reid, M. R. Comparison of digestion methods for ICP-MS determination of trace elements in fish tissues. **Analytica Chimica Acta**, v.**653**, p.191–199, 2009.

54. Braun, T. & Schubert, A. Journal of Radioanalytical and Nuclear Chemistry, 2005–2009: a citation-based bibliography and impact analysis using Hirsch-type statistics. **Journal of Radioanalytical and Nuclear Chemistry**, v.**285**, p.1–168, 2010.

55. Ilangovan, R.;Daniel, D.;Krastanov, A.;Zachariah, C. & Elizabeth, R. Enzyme based Biosensor for Heavy Metal Ions Determination. **Biotechnology & Biotechnological Equipment**, v.**20**, p.184–189, 2006.

56. Mahmoudpour, M.;Torbati, M.;Mousavi, M.-M.;de la Guardia, M. & Ezzati Nazhad Dolatabadi, J. Nanomaterial-based molecularly imprinted polymers for pesticides detection: Recent trends and future prospects. **TrAC Trends in Analytical Chemistry**, v.**129**, p.115943, 2020.

57. Farghaly, O. A.;Abdel Hameed, R. S. & Abu-Nawwas, A. A. H. Analytical application using modern electrochemical techniques. **International Journal of Electrochemical Science**, v.**9**, p.3287–3318, 2014.

58. Stradiotto, N. R.;Yamanaka, H. & Zanoni, M. V. B. Electrochemical sensors: a powerful tool in analytical chemistry. **Journal of the Brazilian Chemical Society**, v.**14**, p.159–173, 2003.

59. Leech, D. Analytical Applications of Polymer-Modified Electrodes. in *Electroactive Polymer Electrochemistry* p.269–296, (Springer US, 1996). doi:10.1007/978-1-4899-1715-7_6.

60. Snell, K. D. & Keenan, A. G. Surface modified electrodes. **Chemical Society**

Reviews, v.**8**, p.259, 1979.

61. Fatibello-Filho, O.;Dockal, E. R.;Marcolino-Junior, L. H. & Teixeira, M. F. S. Electrochemical Modified Electrodes Based on Metal-Salen Complexes. **Analytical Letters**, v.**40**, p.1825–1852, 2007.

62. Chen, L.;Wang, X.;Lu, W.;Wu, X. & Li, J. Molecular imprinting: perspectives and applications. **Chemical Society Reviews**, v.**45**, p.2137–2211, 2016.

63. Wang, J.;Tian, B. & Rogers, K. R. Thick-Film Electrochemical Immunosensor Based on Stripping Potentiometric Detection of a Metal Ion Label. **Analytical Chemistry**, v.**70**, p.1682–1685, 1998.

64. Wang, J. Modified electrodes for electrochemical sensors. **Electroanalysis**, v.**3**, p.255–259, 1991.

65. Zen, J.-M.;Senthil Kumar, A. & Tsai, D.-M. Recent Updates of Chemically Modified Electrodes in Analytical Chemistry. **Electroanalysis**, v.**15**, p.1073–1087, 2003.

66. Kalcher, K. Chemically modified carbon paste electrodes in voltammetric analysis. **Electroanalysis**, v.**2**, p.419–433, 1990.

67. Lowinsohn, D. & Bertotti, M. Sensores eletroquímicos: considerações sobre mecanismos de funcionamento e aplicações no monitoramento de espécies químicas em ambientes microscópicos. **Química Nova**, v.**29**, p.1318–1325, 2006.

68. Kutner, W.;Wang, J.;L'her, M. & Buck, R. P. Analytical aspects of chemically modified electrodes: Classification, critical evaluation and recommendations (IUPAC Recommendations 1998). **Pure and Applied Chemistry**, v.**70**, p.1301–1318, 1998.

69. Fernandes-Junior, W. S. *et al.* Electrochemical Sensor Based on Nanodiamonds and Manioc Starch for Detection of Tetracycline. **Journal of Sensors**, v.**2021**, p.1–10,

2021.

70. Osteryoung, J. G. & Schreiner, M. M. Recent Advances in Pulse Voltammetry. **C R C Critical Reviews in Analytical Chemistry**, v.**19**, p.S1–S27, 1988.

71. Evans, D. H.;O'Connell, K. M.;Petersen, R. A. & Kelly, M. J. Cyclic voltammetry. **Journal of Chemical Education**, v.**60**, p.290, 1983.

72. Guo, G.;Zhao, F.;Xiao, F. & Zeng, B. Voltammetric determination of tetracycline by using multi-wall carbon nanotube - ionic liquid film coated glassy carbon electrode. **International Journal of Electrochemical Science**, v.**4**, p.1365–1372, 2009.

73. Mirceski, V. *et al.* Square-Wave Voltammetry: A Review on the Recent Progress. **Electroanalysis**, v.**25**, p.2411–2422, 2013.

74. Karimi-Maleh, H. *et al.* Carbon Paste Modified Electrode as Powerful Sensor Approach Determination of Food Contaminants, Drug Ingredients, and Environmental Pollutants: A Review. **Current Analytical Chemistry**, v.**15**, p.410–422, 2019.

75. Rubianes, M. D. & Rivas, G. A. Carbon nanotubes paste electrode. **Electrochemistry Communications**, v.**5**, p.689–694, 2003.

76. Musameh, M.;Wang, J.;Merkoci, A. & Lin, Y. Low-potential stable NADH detection at carbon-nanotube-modified glassy carbon electrodes. **Electrochemistry Communications**, v.**4**, p.743–746, 2002.

77. Šljukić, B.;Banks, C. E. & Compton, R. G. Iron Oxide Particles Are the Active Sites for Hydrogen Peroxide Sensing at Multiwalled Carbon Nanotube Modified Electrodes. **Nano Letters**, v.**6**, p.1556–1558, 2006.

78. Karimi-Maleh, H.;Bananezhad, A.;Ganjali, M. R. & Norouzi, P. Electrochemical nanostructure platform for the analysis of glutathione in the presence of uric acid and

tryptophan. **Analytical Methods**, v.**9**, p.6228–6234, 2017.

79. Karimi-Maleh, H.;Ganjali, M. R.;Norouzi, P. & Bananezhad, A. Amplified nanostructure electrochemical sensor for simultaneous determination of captopril, acetaminophen, tyrosine and hydrochlorothiazide. **Materials Science and Engineering: C**, v.**73**, p.472–477, 2017.

80. Musameh, M. & Wang, J. Sensitive and stable amperometric measurements at ionic liquid–carbon paste microelectrodes. **Analytica Chimica Acta**, v.**606**, p.45–49, 2008.

81. Sheikhshoaie, M.;Karimi-Maleh, H.;Sheikhshoaie, I. & Ranjbar, M. Voltammetric amplified sensor employing RuO 2 nano-road and room temperature ionic liquid for amaranth analysis in food samples. **Journal of Molecular Liquids**, v.**229**, p.489–494, 2017.

82. Arabali, V.;Ebrahimi, M. & Karimi-Maleh, H. Highly sensitive determination of promazine in pharmaceutical and biological samples using a ZnO nanoparticle-modified ionic liquid carbon paste electrode. **Chinese Chemical Letters**, v.**27**, p.779–782, 2016.

83. Karimi-Maleh, H. *et al.* Simultaneous determination of 6-mercaptopruine, 6-thioguanine and dasatinib as three important anticancer drugs using nanostructure voltammetric sensor employing Pt/MWCNTs and 1-butyl-3-methylimidazolium hexafluoro phosphate. **Biosensors and Bioelectronics**, v.**86**, p.879–884, 2016.

84. Karimi-Maleh, H.;Salehi, M. & Faghani, F. Application of novel Ni(II) complex and ZrO 2 nanoparticle as mediators for electrocatalytic determination of N -acetylcysteine in drug samples. **Journal of Food and Drug Analysis**, v.**25**, p.1000–1007, 2017.

85. Bananezhad, A. Fabrication of Amplified Nanostructure Based Sensor for Analysis of

N-Acetylcysteine in Presence of High Concentration Folic Acid. **International Journal of Electrochemical Science**, p.8045–8058, 2017. doi:10.20964/2017.09.34.

86. Karimi-Maleh, H. *et al.* A Novel DNA Biosensor Based on a Pencil Graphite Electrode Modified with Polypyrrole/Functionalized Multiwalled Carbon Nanotubes for Determination of 6-Mercaptopurine Anticancer Drug. **Industrial & Engineering Chemistry Research**, v.**54**, p.3634–3639, 2015.

87. Bavandpour, R. *et al.* Liquid phase determination of adrenaline uses a voltammetric sensor employing CuFe2O4 nanoparticles and room temperature ionic liquids. **Journal of Molecular Liquids**, v.**213**, p.369–373, 2016.

88. Karimi-Maleh, H.;Rostami, S.;Gupta, V. K. & Fouladgar, M. Evaluation of ZnO nanoparticle ionic liquid composite as a voltammetric sensing of isoprenaline in the presence of aspirin for liquid phase determination. **Journal of Molecular Liquids**, v.**201**, p.102–107, 2015.

89. Ferancová, A.;Korgová, E.;Mikó, R. & Labuda, J. Determination of tricyclic antidepressants using a carbon paste electrode modified with β-cyclodextrin. **Journal of Electroanalytical Chemistry**, v.**492**, p.74–77, 2000.

90. Gupta, V. K.;Rostami, Saeed, Hassan Karimi-Male, F. K.;Keyvanfard, M. & Saleh, T. A. Square Wave Voltammetric Analysis of Carbidopa Based on Carbon Paste Electrode Modified with ZnO/CNTs Nanocomposite and n-hexyl-3-methylimidazolium Hexafluoro Phosphate Ionic Liquid. **Int. J. Electrochem. Sci.,** v.**10**, p.1517–1528,.

91. Baranwal, J.;Barse, B.;Gatto, G.;Broncova, G. & Kumar, A. Electrochemical Sensors and Their Applications: A Review. **Chemosensors**, v.**10**, p.363, 2022.

92. Rashid, J. I. A. & Yusof, N. A. The strategies of DNA immobilization and hybridization detection mechanism in the construction of electrochemical DNA sensor: A review. **Sensing and Bio-Sensing Research**, v.**16**, p.19–31, 2017.

93. Herrera-Chacón, A.;Cetó, X. & del Valle, M. Molecularly imprinted polymers - towards electrochemical sensors and electronic tongues. **Analytical and Bioanalytical Chemistry**, v.**413**, p.6117–6140, 2021.

94. Zhang, S.;Geryak, R.;Geldmeier, J.;Kim, S. & Tsukruk, V. V. Synthesis, Assembly, and Applications of Hybrid Nanostructures for Biosensing. **Chemical Reviews**, v.**117**, p.12942–13038, 2017.

95. Baig, N.;Sajid, M. & Saleh, T. A. Recent trends in nanomaterial-modified electrodes for electroanalytical applications. **TrAC Trends in Analytical Chemistry**, v.**111**, p.47–61, 2019.

96. Zhu, Y. *et al.* Structural Engineering of 2D Nanomaterials for Energy Storage and Catalysis. **Advanced Materials**, v.**30**, p.1706347, 2018.

97. Sun, H.;Zhang, Y.;Zhang, J.;Sun, X. & Peng, H. Energy harvesting and storage in 1D devices. **Nature Reviews Materials**, v.**2**, p.17023, 2017.

98. Kinnear, C.;Moore, T. L.;Rodriguez-Lorenzo, L.;Rothen-Rutishauser, B. & Petri-Fink, A. Form Follows Function: Nanoparticle Shape and Its Implications for Nanomedicine. **Chemical Reviews**, v.**117**, p.11476–11521, 2017.

99. Vankayala, R. & Hwang, K. C. Near-Infrared-Light-Activatable Nanomaterial-Mediated Phototheranostic Nanomedicines: An Emerging Paradigm for Cancer Treatment. **Advanced Materials**, v.**30**, p.1706320, 2018.

100. Cai, Z. *et al.* Application of nanotechnologies for removing pharmaceutically active

compounds from water: development and future trends. **Environmental Science: Nano**, v.**5**, p.27–47, 2018.

101. Walekar, L. *et al.* Functionalized fluorescent nanomaterials for sensing pollutants in the environment: A critical review. **TrAC Trends in Analytical Chemistry**, v.**97**, p.458–467, 2017.

102. Wang, H.;Chen, L.;Feng, Y. & Chen, H. Exploiting Core–Shell Synergy for Nanosynthesis and Mechanistic Investigation. **Accounts of Chemical Research**, v.**46**, p.1636–1646, 2013.

103. Inan, H. *et al.* Photonic crystals: emerging biosensors and their promise for point-of-care applications. **Chemical Society Reviews**, v.**46**, p.366–388, 2017.

104. Gawande, M. B. *et al.* Core–shell nanoparticles: synthesis and applications in catalysis and electrocatalysis. **Chemical Society Reviews**, v.**44**, p.7540–7590, 2015.

105. Silva, R. & Asefa, T. Noble Metal-Free Oxidative Electrocatalysts: Polyaniline and Co(II)-Polyaniline Nanostructures Hosted in Nanoporous Silica. **Advanced Materials**, v.**24**, p.1878–1883, 2012.

106. Silva, R.;Voiry, D.;Chhowalla, M. & Asefa, T. Efficient Metal-Free Electrocatalysts for Oxygen Reduction: Polyaniline-Derived N- and O-Doped Mesoporous Carbons. **Journal of the American Chemical Society**, v.**135**, p.7823–7826, 2013.

107. Stöber, W.;Fink, A. & Bohn, E. Controlled growth of monodisperse silica spheres in the micron size range. **Journal of Colloid and Interface Science**, v.**26**, p.62–69, 1968.

108. Liu, Y. & Tang, Z. Multifunctional Nanoparticle@MOF Core-Shell Nanostructures. **Advanced Materials**, v.**25**, p.5819–5825, 2013.

109. Moon, H. R.;Lim, D.-W. & Suh, M. P. Fabrication of metal nanoparticles in metal–organic frameworks. **Chem. Soc. Rev.**, v.**42**, p.1807–1824, 2013.

110. Sugikawa, K.;Furukawa, Y. & Sada, K. SERS-Active Metal–Organic Frameworks Embedding Gold Nanorods. **Chemistry of Materials**, v.**23**, p.3132–3134, 2011.

111. He, L. *et al.* Core-Shell Noble-Metal@Metal-Organic-Framework Nanoparticles with Highly Selective Sensing Property. **Angewandte Chemie**, v.**125**, p.3829–3833, 2013.

112. Della Rocca, J.;Liu, D. & Lin, W. Nanoscale Metal–Organic Frameworks for Biomedical Imaging and Drug Delivery. **Accounts of Chemical Research**, v.**44**, p.957–968, 2011.

113. Zhu, C.;Yang, G.;Li, H.;Du, D. & Lin, Y. Electrochemical Sensors and Biosensors Based on Nanomaterials and Nanostructures. **Analytical Chemistry**, v.**87**, p.230–249, 2015.

114. Kalambate, P. K.;Li, Y.;Shen, Y. & Huang, Y. Mesoporous Pd@Pt core–shell nanoparticles supported on multi-walled carbon nanotubes as a sensing platform: application in simultaneous electrochemical detection of anticancer drugs doxorubicin and dasatinib. **Analytical Methods**, v.**11**, p.443–453, 2019.

115. Jiwanti, P. K.;Wardhana, B. Y.;Sutanto, L. G. & Chanif, M. F. A Review on Carbon-based Electrodes for Electrochemical Sensor of Quinolone Antibiotics. **ChemistrySelect**, v.**7**, 2022.

116. Zhang, Z. *et al.* Fe(III)-based metal–organic framework-derived core–shell nanostructure: Sensitive electrochemical platform for high trace determination of heavy metal ions. **Biosensors and Bioelectronics**, v.**94**, p.358–364, 2017.

117. He, L. *et al.* Novel electrochemical biosensor based on core-shell nanostructured

composite of hollow carbon spheres and polyaniline for sensitively detecting malathion. **Sensors and Actuators B: Chemical**, v.**258**, p.813–821, 2018.

118. Askim, J. R.;Mahmoudi, M. & Suslick, K. S. Optical sensor arrays for chemical sensing: the optoelectronic nose. **Chemical Society Reviews**, v.**42**, p.8649, 2013.

119. Yan, X.;Li, H. & Su, X. Review of optical sensors for pesticides. **TrAC Trends in Analytical Chemistry**, v.**103**, p.1–20, 2018.

120. Liu, X. *et al.* A novel "modularized" optical sensor for pH monitoring in biological matrixes. **Biosensors and Bioelectronics**, v.**109**, p.150–155, 2018.

121. Mahmoud, W. E. Synthesis and characterization of 2A-3SHPA decorated ZnS@CdS core–shell heterostructure nanowires as a fluorescence probe for antimony ions detection. **Sensors and Actuators B: Chemical**, v.**238**, p.1001–1007, 2017.

122. Pauling, L. A Theory of the Structure and Process of Formation of Antibodies. **Journal of the American Chemical Society**, v.**62**, p.2643–2657, 1940.

123. WULFF, G. The use of polymers with enzyme-analogous structures for the resolution of racemates. **Angrew. Chem. Internat. Edit.**, v.**11**, p.341, 1972.

124. Hu, X.;Hu, Y. & Li, G. Development of novel molecularly imprinted solid-phase microextraction fiber and its application for the determination of triazines in complicated samples coupled with high-performance liquid chromatography. **Journal of Chromatography A**, v.**1147**, p.1–9, 2007.

125. Piletsky, S. .;Panasyuk, T. .;Piletskaya, E. .;Nicholls, I. . & Ulbricht, M. Receptor and transport properties of imprinted polymer membranes – a review. **Journal of Membrane Science**, v.**157**, p.263–278, 1999.

126. Martín-Esteban, A. Molecularly-imprinted polymers as a versatile, highly selective

tool in sample preparation. **TrAC Trends in Analytical Chemistry**, v.**45**, p.169–181, 2013.

127. Meier, F.;Schott, B.;Riedel, D. & Mizaikoff, B. Computational and experimental study on the influence of the porogen on the selectivity of 4-nitrophenol molecularly imprinted polymers. **Analytica Chimica Acta**, v.**744**, p.68–74, 2012.

128. Yan, M. . & RAMSTRÖM. *Molecularly imprinted materials-science and technology*. (New York: Marcel Dekker., 2005).

129. Yilmaz, E.;Mosbach, K. & Haupt, K. Influence of functional and cross-linking monomers and the amount of template on the performance of molecularly imprinted polymers in binding assays. **Analytical Communications**, v.**36**, p.167–170, 1999.

130. Xie, L.;Guo, J.;Zhang, Y. & Shi, S. Efficient Determination of Protocatechuic Acid in Fruit Juices by Selective and Rapid Magnetic Molecular Imprinted Solid Phase Extraction Coupled with HPLC. **Journal of Agricultural and Food Chemistry**, v.**62**, p.8221–8228, 2014.

131. Lu, F. *et al.* Flow injection chemiluminescence sensor based on core–shell magnetic molecularly imprinted nanoparticles for determination of chrysoidine in food samples. **Sensors and Actuators B: Chemical**, v.**173**, p.591–598, 2012.

132. Płotka-Wasylka, J.;Szczepańska, N.;de la Guardia, M. & Namieśnik, J. Modern trends in solid phase extraction: New sorbent media. **TrAC Trends in Analytical Chemistry**, v.**77**, p.23–43, 2016.

133. Liu, Y. *et al.* Preparation of monodispersed macroporous core–shell molecularly imprinted particles and their application in the determination of 2,4-dichlorophenoxyacetic acid. **Journal of Chromatography A**, v.**1323**, p.11–17, 2014.

134. Kan, X. *et al*. Preparation and Recognition Properties of Bovine Hemoglobin Magnetic Molecularly Imprinted Polymers. **The Journal of Physical Chemistry B**, v.**114**, p.3999–4004, 2010.

135. Uzuriaga-Sánchez, R. J. *et al*. Magnetically separable polymer (Mag-MIP) for selective analysis of biotin in food samples. **Food Chemistry**, v.**190**, p.460–467, 2016.

136. Khan, S. *et al*. Synthesis and characterization of magnetic-molecularly imprinted polymers for the HPLC-UV analysis of ametryn. **Reactive and Functional Polymers**, v.**122**, p.175–182, 2018.

137. Garcia, S. M.;Wong, A.;Khan, S. & Sotomayor, M. D. P. T. A simple, sensitive and efficient electrochemical platform based on carbon paste electrode modified with Fe3O4@MIP and graphene oxide for folic acid determination in different matrices. **Talanta**, v.**229**, p.122258, 2021.

138. Zeb, S.;Wong, A.;Khan, S.;Hussain, S. & Sotomayor, M. D. P. T. Using magnetic nanoparticles/MIP-based electrochemical sensor for quantification of tetracycline in milk samples. **Journal of Electroanalytical Chemistry**, v.**900**, p.115713, 2021.

139. Figueiredo, L.;Erny, G. L.;Santos, L. & Alves, A. Applications of molecularly imprinted polymers to the analysis and removal of personal care products: A review. **Talanta**, v.**146**, p.754–765, 2016.

140. Xiao, D. *et al.* Magnetic solid-phase extraction based on Fe 3 O 4 nanoparticle retrieval of chitosan for the determination of flavonoids in biological samples coupled with high performance liquid chromatography. **RSC Adv.**, v.**4**, p.64843–64854, 2014.

141. Sposito G. *The surface chemistry of natural particles*. (Oxford Univ. Press, 2004).

142. Ip, A. W. M.;Barford, J. P. & McKay, G. Reactive Black dye adsorption/desorption

onto different adsorbents: Effect of salt, surface chemistry, pore size and surface area. **Journal of Colloid and Interface Science**, v.**337**, p.32–38, 2009.

143. ZAMPORI, L.;GALLOSTAMPINO, P. & DOTELLI, G. Adsorption of nitrobenzene and orthochlorophenol on dimethyl ditallowyl montmorillonite: A microstructural and thermodynamic study. **Applied Clay Science**, v.**42**, p.605–610, 2009.

144. Xin, X. *et al.* Removal of o -nitrobenzoic acid by adsorption on to a new organoclay: montmorillonite modified with HDTMA microemulsion. **Environmental Technology**, v.**32**, p.447–454, 2011.

145. Fuller, M.;Smith, J. A. & Burns, S. E. Sorption of nonionic organic solutes from water to tetraalkylammonium bentonites: Mechanistic considerations and application of the Polanyi–Manes potential theory. **Journal of Colloid and Interface Science**, v.**313**, p.405–413, 2007.

146. Vasanth Kumar, K. & Sivanesan, S. Sorption isotherm for safranin onto rice husk: Comparison of linear and non-linear methods. **Dyes and Pigments**, v.**72**, p.130–133, 2007.

147. Hussain, S.;Khan, S.;Gul, S.;Pividori, M. I. & Del Pilar Taboada Sotomayor, M. A novel core@shell magnetic molecular imprinted nanoparticles for selective determination of folic acid in different food samples. **Reactive and Functional Polymers**, v.**106**, p.51–56, 2016.

148. Abidi, S. L. High-performance liquid chromatography of phosphatidic acids and related polar lipids. **Journal of Chromatography A**, v.**587**, p.193–203, 1991.

149. Li, P.;Rao, D.;Wang, Y. & Hu, X. Adsorption characteristics of polythiophene for tetracyclines and determination of tetracyclines in fish and chicken manure by solid

phase extraction-HPLC method. **Microchemical Journal**, v.**173**, p.106935, 2022.

150. Zergiebel, S.;Ueberschaar, N. & Seeling, A. Development and optimization of an ultra-fast microextraction followed by HPLC-UV of tetracycline residues in milk products. **Food Chemistry**, v.**402**, p.134270, 2023.

151. O. Schmitt, M. & Schneider, S. Spectroscopic investigation of complexation between various tetracyclines and Mg2+ or Ca2+. **PhysChemComm**, v.**3**, p.42, 2000.

152. Rodríguez, N.;Ortiz, M. C.;Herrero, A. & Sarabia, L. A. Performance characteristics according to Commission Decision 2002/657/EC in the fluorimetric determination of tetracycline in the absence and in the presence of magnesium. **Luminescence**, v.**22**, p.518–526, 2007.

153. Villa, J. E. L.;Khan, S.;Neres, L. C. S. & Sotomayor, M. D. P. T. Preparation of a magnetic molecularly imprinted polymer for non-invasive determination of cortisol. **Journal of Polymer Research**, v.**28**, p.298, 2021.

154. Cantarella, M. *et al.* Molecularly imprinted polymer for selective adsorption of diclofenac from contaminated water. **Chemical Engineering Journal**, v.**367**, p.180–188, 2019.

155. Fang, L.;Miao, Y.;Wei, D.;Zhang, Y. & Zhou, Y. Efficient removal of norfloxacin in water using magnetic molecularly imprinted polymer. **Chemosphere**, v.**262**, p.128032, 2021.

156. Li, H. *et al.* Synthesis of magnetic molecularly imprinted polymer particles for selective adsorption and separation of dibenzothiophene. **Microchimica Acta**, v.**179**, p.123–130, 2012.

157. Lowdon, J. W. *et al.* MIPs for commercial application in low-cost sensors and assays –

An overview of the current status quo. **Sensors and Actuators B: Chemical**, v.**325**, p.128973, 2020.

158. Piletsky, S. A.;Parhometz, Y. P.;Lavryk, N. V.;Panasyuk, T. L. & El'skaya, A. V. Sensors for low-weight organic molecules based on molecular imprinting technique. **Sensors and Actuators B: Chemical**, v.**19**, p.629–631, 1994.

159. Zhao, X.;He, Y.;Wang, Y.;Wang, S. & Wang, J. Hollow molecularly imprinted polymer based quartz crystal microbalance sensor for rapid detection of methimazole in food samples. **Food Chemistry**, v.**309**, p.125787, 2020.

160. Dayal, H.;Ng, W. Y.;Lin, X. H. & Li, S. F. Y. Development of a hydrophilic molecularly imprinted polymer for the detection of hydrophilic targets using quartz crystal microbalance. **Sensors and Actuators B: Chemical**, v.**300**, p.127044, 2019.

161. Motia, S.;Bouchikhi, B.;Llobet, E. & El Bari, N. Synthesis and characterization of a highly sensitive and selective electrochemical sensor based on molecularly imprinted polymer with gold nanoparticles modified screen-printed electrode for glycerol determination in wastewater. **Talanta**, v.**216**, p.120953, 2020.

162. Sadriu, I. *et al.* Molecularly imprinted polymer modified glassy carbon electrodes for the electrochemical analysis of isoproturon in water. **Talanta**, v.**207**, p.120222, 2020.

163. Liu, Y.;Liang, Y.;Yang, R.;Li, J. & Qu, L. A highly sensitive and selective electrochemical sensor based on polydopamine functionalized graphene and molecularly imprinted polymer for the 2,4-dichlorophenol recognition and detection. **Talanta**, v.**195**, p.691–698, 2019.

164. Scheller, F. W.;Zhang, X.;Yarman, A.;Wollenberger, U. & Gyurcsányi, R. E. Molecularly imprinted polymer-based electrochemical sensors for biopolymers.

Current Opinion in Electrochemistry, v.**14**, p.53–59, 2019.

165. Frasco, M.;Truta, L.;Sales, M. & Moreira, F. Imprinting Technology in Electrochemical Biomimetic Sensors. **Sensors**, v.**17**, p.523, 2017.

166. Ramanaviciene, A.;Ramanavicius, A. & Finkelsteinas, A. Basic Electrochemistry Meets Nanotechnology: Electrochemical Preparation of Artificial Receptors Based on Nanostructured Conducting Polymer, Polypyrrole. **Journal of Chemical Education**, v.**83**, p.1212, 2006.

167. Ratautaite, V.;Nesladek, M.;Ramanaviciene, A.;Baleviciute, I. & Ramanavicius, A. Evaluation of Histamine Imprinted Polypyrrole Deposited on Boron Doped Nanocrystalline Diamond. **Electroanalysis**, v.**26**, p.2458–2464, 2014.

168. Zeng, G.;Liu, Y.;Ma, X. & Fan, Y. Fabrication of magnetic multi-template molecularly imprinted polymer composite for the selective and efficient removal of tetracyclines from water. **Frontiers of Environmental Science & Engineering**, v.**15**, p.107, 2021.

169. Wang, S.-X. *et al.* Specific adsorption of tetracycline from milk by using biocompatible magnetic molecular imprinting material and evaluation by ECD. **Food Chemistry**, v.**326**, p.126969, 2020.

170. Gao, W. *et al.* Preparation of Magnetic Molecularly Imprinted Polymer (MMIP) Nanoparticles (NPs) for the Selective Extraction of Tetracycline from Milk. **Analytical Letters**, v.**53**, p.1097–1112, 2020.

171. Song, J. *et al.* Novel Fe-based metal–organic framework (MOF) modified carbon nanofiber as a highly selective and sensitive electrochemical sensor for tetracycline detection. **Chemical Engineering Journal**, v.**427**, p.130913, 2022.

172. Guo, Q. *et al.* Low-cost electrochemical sensor based on montmorillonite for antibiotic tetracycline hydrochloride detection. **Journal of Materials Science: Materials in Electronics**, v.**33**, p.427–442, 2022.

173. Liu, Z. *et al.* Molecularly imprinted polymer decorated 3D-framework of functionalized multi-walled carbon nanotubes for ultrasensitive electrochemical sensing of Norfloxacin in pharmaceutical formulations and rat plasma. **Sensors and Actuators B: Chemical**, v.**288**, p.363–372, 2019.

174. Wang, H. *et al.* Preparation and application of a carbon paste electrode modified with multi-walled carbon nanotubes and boron-embedded molecularly imprinted composite membranes. **Bioelectrochemistry**, v.**121**, p.115–124, 2018.

175. Wang, Y. *et al.* CuCo2O4/N-Doped CNTs loaded with molecularly imprinted polymer for electrochemical sensor: Preparation, characterization and detection of metronidazole. **Biosensors and Bioelectronics**, v.**142**, p.111483, 2019.

176. Feier, B.;Blidar, A.;Pusta, A.;Carciuc, P. & Cristea, C. Electrochemical Sensor Based on Molecularly Imprinted Polymer for the Detection of Cefalexin. **Biosensors**, v.**9**, p.31, 2019.

177. Ma, J. *et al.* The study of core–shell molecularly imprinted polymers of 17β-estradiol on the surface of silica nanoparticles. **Biosensors and Bioelectronics**, v.**26**, p.2791–2795, 2011.

178. Bergamin, B.;Pupin, R.;Wong, A. & Sotomayor, M. A New Electrochemical Platform Based on a Polyurethane Composite Electrode Modified with Magnetic Nanoparticles Coated with Molecularly Imprinted Polymer for the Determination of Estradiol Valerate in Different Matrices. **Journal of the Brazilian Chemical Society**, 2019. doi:10.21577/0103-5053.20190142.

179. Byun, H.-S.;Youn, Y.-N.;Yun, Y.-H. & Yoon, S.-D. Selective separation of aspirin using molecularly imprinted polymers. **Separation and Purification Technology**, v.**74**, p.144–153, 2010.

180. Sachin.;Joishar, D.;Singh, N. P.;Varathan, E. & Singh, N. Sodium Docusate Surface-Modified Dispersible and Powder Zinc Peroxide Formulation: An Adsorbent for the Effective and Fast Removal of Crystal Violet Dye, an Emerging Wastewater Contaminant. **ACS Omega**, v.**6**, p.22570–22577, 2021.

181. Li, Z.;Schulz, L.;Ackley, C. & Fenske, N. Adsorption of tetracycline on kaolinite with pH-dependent surface charges. **Journal of Colloid and Interface Science**, v.**351**, p.254–260, 2010.

182. Luna Quinto, M.;Khan, S.;Picasso, G. & Taboada Sotomayor, M. D. P. Synthesis, characterization, and evaluation of a selective molecularly imprinted polymer for quantification of the textile dye acid violet 19 in real water samples. **Journal of Hazardous Materials**, v.**384**, p.121374, 2020.

183. Wang, S. *et al.* A direct competitive assay-based aptasensor for sensitive determination of tetracycline residue in Honey. **Talanta**, v.**131**, p.562–569, 2015.

184. Wang, L.-F.;Peng, J.-D. & Liu, L.-M. A reversed-phase high performance liquid chromatography coupled with resonance Rayleigh scattering detection for the determination of four tetracycline antibiotics. **Analytica Chimica Acta**, v.**630**, p.101–106, 2008.

185. Pizan-Aquino, C. *et al.* Evaluation of the performance of selective M-MIP to tetracycline using electrochemical and HPLC-UV method. **Materials Chemistry and Physics**, v.**245**, p.122777, 2020.

186. Khan, S.;Wong, A.;Zanoni, M. V. B. & Sotomayor, M. D. P. T. Electrochemical sensors based on biomimetic magnetic molecularly imprinted polymer for selective quantification of methyl green in environmental samples. **Materials Science and Engineering: C**, v.**103**, p.109825, 2019.

187. Khan, S.;Wong, A.;Rychlik, M. & Sotomayor, M. del P. T. A Novel Synthesis of a Magnetic Porous Imprinted Polymer by Polyol Method Coupled with Electrochemical Biomimetic Sensor for the Detection of Folate in Food Samples. **Chemosensors**, v.**10**, p.473, 2022.

188. Ullah, Z.;Hussain, S.;Gul, S.;Khan, S. & Bangash, F. K. Use of HCl-modified bentonite clay for the adsorption of Acid Blue 129 from aqueous solutions. **Desalination and Water Treatment**, v.**57**, p.8894–8903, 2016.

189. OFOMAJA, A. & HO, Y. Equilibrium sorption of anionic dye from aqueous solution by palm kernel fibre as sorbent. **Dyes and Pigments**, v.**74**, p.60–66, 2007.

190. Inyinbor, A. A.;Adekola, F. A. & Olatunji, G. A. Kinetics, isotherms and thermodynamic modeling of liquid phase adsorption of Rhodamine B dye onto Raphia hookerie fruit epicarp. **Water Resources and Industry**, v.**15**, p.14–27, 2016.

191. Miao, L.;Liu, W.;Qiao, Q.;Li, X. & Xu, Z. Fluorescent antibiotics for real-time tracking of pathogenic bacteria. **Journal of Pharmaceutical Analysis**, v.**10**, p.444–451, 2020.

192. Dang, X.;Hu, C.;Wei, Y.;Chen, W. & Hu, S. Sensitivity Improvement of the Oxidation of Tetracycline at Acetylene Black Electrode in the Presence of Sodium Dodecyl Sulfate. **Electroanalysis**, v.**16**, p.1949–1955, 2004.

193. Kushikawa, R. T.;Silva, M. R.;Angelo, A. C. D. & Teixeira, M. F. S. Construction of

an electrochemical sensing platform based on platinum nanoparticles supported on carbon for tetracycline determination. **Sensors and Actuators B: Chemical**, v.**228**, p.207–213, 2016.

194. Sassman, S. A. & Lee, L. S. Sorption of Three Tetracyclines by Several Soils: Assessing the Role of pH and Cation Exchange. **Environmental Science & Technology**, v.**39**, p.7452–7459, 2005.

195. Zhang, G.;Liu, X.;Sun, K.;Zhao, Y. & Lin, C. Sorption of tetracycline to sediments and soils: assessing the roles of pH, the presence of cadmium and properties of sediments and soils. **Frontiers of Environmental Science & Engineering in China**, v.**4**, p.421–429, 2010.

196. Wang, Y.-J.;Jia, D.-A.;Sun, R.-J.;Zhu, H.-W. & Zhou, D.-M. Adsorption and Cosorption of Tetracycline and Copper(II) on Montmorillonite as Affected by Solution pH. **Environmental Science & Technology**, v.**42**, p.3254–3259, 2008.